Neutron Capture Cross Sections of the Krypton Isotopes and the s-Process Branching at ^{79}Se

G. Walter, B. Leugers, F. Käppeler, Z. Y. Bao, D. Erbe,
G. Rupp, G. Reffo, F. Fabbri
Institut für Kernphysik

Kernforschungszentrum Karlsruhe

NEUTRON CAPTURE CROSS SECTIONS OF THE KRYPTON ISOTOPES AND THE s-PROCESS BRANCHING AT ^{79}Se

G. Walter, B. Leugers, F. Käppeler, Z.Y. Bao[+], D. Erbe, G. Rupp, G. Reffo[++], F. Fabbri[++]

[+] on leave from the Institute of Atomic Energy, Academia Sinica, Peking, China

[++] E.N.E.A. Bologna, Italy

Abstract

The input data for an analysis of the s-process branching at ^{79}Se
have been significantly improved. The neutron capture cross
sections for the stable krypton isotopes (except ^{86}Kr) were
measured between 3 and 240 keV neutron energy. In addition,
statistical model calculations of the (n,γ)-cross sections for
all isotopes involved in this branching were performed. With these
data and with other experimental results from literature a re-
commended set of Maxwellian average cross sections was established
in the mass region 77<A<85. The relevant decay parameters of the
involved unstable nuclei and the parameters for the s-process
model are discussed as well. On this basis the following aspects
are investigated: the temperature during s-process, the decompo-
sition into s- and r-process contributions and the solar krypton
abundance.

Die Neutroneneinfangquerschnitte der Kryptonisotope und die
s-Prozess Verzweigung am ^{79}Se

Zusammenfassung

Die Datenbasis für die Analyse der s-Prozeß Verzweigung beim
^{79}Se wurde signifikant verbessert. Für die stabilen Krypton-
isotope (mit Ausnahme von ^{86}Kr) wurde der Neutroneneinfang-
querschnitt zwischen 3 und 240 keV gemessen. Weiterhin wurden die
(n,γ)-Querschnitte aller Isotope,die in dieser Verzweigung
eine Rolle spielen,mit dem statistischen Modell berechnet. Aus
diesen Daten und mit experimentellen Ergebnissen aus der Literatur
wurde ein empfohlener Satz von Maxwell-gemittelten Querschnitten
im Massenbereich 77<A<85 erstellt. Die für die Verzweigung
relevanten Zerfallsparameter der instabilen Kerne sowie die Para-
meter des s-Prozess Modells werden ebenfalls diskutiert. Auf
dieser Grundlage werden folgende Aspekte untersucht: die Tempe-
ratur beim s-Prozeß, Aufteilung der Häufigkeiten in s- und r-
Prozeß Anteile und die solare Kryptonhäufigkeit.

CONTENTS

1. INTRODUCTION

In this paper we discuss the s-process branching at ^{79}Se in the light of new experimental and theoretical neutron capture cross sections. This branching is best suited to yield an estimate for the s-process temperature due to the accelerated beta decay from the isomeric state at 95.7 keV in ^{79}Se. Up to now only preliminary analyses were possible due to the lack of data (Ward, Newman and Clayton, 1976).

For that reason we have measured the neutron capture cross sections of the stable krypton isotopes and have calculated the cross sections of all nuclei involved in the branching. The theoretical calculations were performed with great care including as much experimental information on the respective nuclei as possible (e.g. experimental level densities, low lying level schemes or extrapolations from neighbouring nuclei). Contrary to the usual global description of parameters we find it essential for a more accurate treatment that local parameter systematics are included. From this local behaviour it is possible to deduce even uncertainties for the calculated cross sections which are useful for estimating their impact on the resulting s-process temperature. Besides the measured and calculated cross sections we also evaluated existing cross section measurements and condensed all this information to a set of recommended Maxwellian averages for kT = 30 keV in the mass range 78<A<84.

In addition to the capture cross sections we consider the required information on s-process parameters (seed abundance, fluence distribution) as well as the decay parameters of the relevant unstable nuclei (^{79}Se and ^{80}Br).

2. EXPERIMENTS

The neutron capture cross sections of the krypton isotopes were measured relative to the standard gold cross section of ENDF/B-IV (Garber 1975). Capture events were registered by detecting the gamma-ray cascade from the deexciting compound nucleus with two C_6D_6-scintillators. Neutron energies were determined by time-of-flight (TOF). A set of six isotopic mixtures was used to determine the neutron capture cross sections of ^{78}Kr, ^{80}Kr, ^{82}Kr, ^{83}Kr, ^{84}Kr and, as a consistency check, also the capture cross sections of natural krypton. The isotopic compositions of the samples are given in Table 1.

2.1 Experimental Set-Up

The experiments were performed at the Karlsruhe 3.75 MV Van de Graaff accelerator. Important parameters of the neutron source and the accelerator are listed in Table 2. The target consisted of a metallic lithium layer of 3 µm thickness and 6 mm diameter evaporated on a 0.3 mm thick tantalum backing. As the protons are slowed down in penetrating the lithium, the target yields neutrons with a continuous energy spectrum. The target backing was cooled from the outside by a thin film of flowing water, thus increasing the neutron flux at low energies by elastic hydrogen scattering.

Elaborate background reduction and careful beam collimation resulted in the experimental set-up shown in Fig. 1. $^6Li_2CO_3$ was chosen as coating material of the inner collimator to minimize gamma background. The surrounding shielding consists of a B_4C-araldite mixture which is an effective neutron absorber due to the high ^{10}B density. The 478 keV gamma line from neutron capture in ^{10}B is suppressed by the 20 cm thick lead shielding of the C_6D_6-scintillators. Only a small fraction of neutrons penetrates the ^{10}B shielding and is finally absorbed by capture in the outer shielding of Li-loaded paraffin. Some of these neutrons might be captured in hydrogen, but the associated 2.2 MeV gamma-rays are suppressed by a factor 10^4 in the lead

shielding and are therefore negligible. Another background compo-
nent originating from neutron capture in the antimony admixture
to ordinary lead could be eliminated by using pure lead for the
shielding. A non-negligible fraction of the background was caused
by neutrons scattered in the sample, thermalized in the C_6D_6-
scintillators and subsequently captured in the lead shielding
or the residual hydrogen of the C_6D_6 scintillator (ratio D/H $\sim$
0.72). This background was reduced by a factor of two by coating
the scintillator volume with a 4 mm thick layer of $^6Li_2CO_3$. With
this set-up capture cross sections of the order of 1 mb have
been measured successfully (Almeida and Käppeler 1983).

Our sample cannings consisted of low mass stainless steel
spheres with an inner diameter of 20 mm and a wall thickness of
0.5 mm. The krypton gas was brought into the containers by
cooling them to liquid nitrogen temperature. The spheres could
withstand pressures of $\sim$ 500 atmospheres but were operated during
the measurements at only $\sim$ 300 atmospheres. The samples were
located at a flight path of 60.5 cm. With the overall time re-
solution of $\sim$ 1 ns obtained in these time-of-flight measure-
ments, an energy resolution of $\sim$ 0.5 keV at 30 keV neutron
energy was obtained, most of this being due to the 20 mm dia-
meter of the sample cannings.

Up to seven samples were mounted on a sample changer super-
vised by the data acquisition computer. One position was occupied
by a canning containing a 1 mm thick gold disk for measuring the
neutron flux. An empty canning and a canning filled with graphite
served for experimental background determination so that four
positions remained for the cannings filled with the various kryp-
ton isotopes. The samples were successively moved into the measu-
ring position. A full cycle was chosen to take about 1 hour; in
this way long term variations in the neutron yield affected all
samples equally. This was verified by means of an additional
neutron monitor located at 90 deg to the beam axis (see Fig. 1),
the spectrum of which was recorded for all samples separately.

2.2 Electronics and Data Acquisition

Fig. 2 shows a block diagram of the electronics. Dynode signals from the photomultipliers, E_1 and E_2, were used for pulse height analysis whereas the anode signals served to define the TOF. Capture events were stored in a two dimensional array of 16 pulse height and 1024 TOF channels for each of the two detectors. In this way, the full experimental information was recorded and pulse height weighting could be applied off line. Coincident events were stored separately in a 1024 channel TOF spectrum. These data were served for later correction of pile-up events. Another 1024 channels were used to record the neutron monitor spectrum. All these spectra were accumulated for each sample position; during a sample change the data were sequentially written to magnetic tape and, in addition, added to a sum spectrum on magnetic disc for continuous inspection throughout the measurement. Digital ratemeters allowed for a permanent control of all relevant count rates.

2.3 Data Analysis

The efficiency of the scintillation detectors is a non-linear function of the gamma-ray energy. In order to determine the number of captures independently of the multiplicity of the gamma-ray cascade, we applied the Maier-Leibnitz weighting technique (Rau 1963, Macklin and Gibbons 1967) to our spectra.

The procedure of data analysis is illustrated as follows: First, all individual, sequential spectra were read from magnetic tape, inspected by computer routines for equal neutron flux and correct time resolution, eventually normalized to equal flight path and then added to sum spectra. As an example, the summed TOF spectra for the first pulse height channel of the ^{80}Kr run are shown in Fig. 3 where the "empty" and ^{80}Kr-spectra are given for the two detectors. These spectra are shifted arbitrarily to illustrate that they agree within counting statistics.

Let now GOLD, CARBON and KRYPTON be the TOF spectra of the gold, carbon and krypton sample after subtraction of the spectrum of the empty canning. These spectra are plotted in Fig. 4. It can clearly be seen from CARBON that neutron scattering in the sample caused a time-dependent background. In turn, this effect can be corrected for just by means of this spectrum because carbon does not capture neutrons at a detectable rate. For this purpose, the CARBON spectrum is normalized in a TOF region right of the gamma peak at channel 900 which contains no genuine capture events. (The gamma peak marks the zero point of the TOF scale when the proton pulses hit the Li-target). After subtraction of the normalized CARBON spectrum from GOLD and KRYPTON the spectra of Fig. 5 are obtained which finally were subjected to the Maier-Leibnitz procedure. Then, the so corrected count rates C can be expressed by

$$C = \varepsilon \cdot N \cdot \phi \cdot \sigma \text{ with } \varepsilon = kB. \tag{1}$$

B denotes the binding energy of the captured neutron plus its kinetic energy E_n, σ is the capture cross section, ϕ the neutron flux and N the number of nuclei in the sample and k is a constant. Combining the count rates of the investigated sample and the gold sample, the unknown cross section is then given by

$$\sigma_{Kr}(E_n) = \frac{N_{Au} \, B_{Au} \, C_{Kr}(E_n)}{N_{Kr} \, B_{Kr} \, C_{Au}(E_n)} \, \sigma_{Au}(E_n) \tag{2}$$

When isotopic mixtures are used B has to be replaced by an effective value

$$B_{eff} = \frac{\sum\limits_{i} N_i \, \sigma_i \, B_i}{\sum\limits_{i} N_i \, \sigma_i} \tag{3}$$

with the sum running over all isotopes.

The final GOLD and CARBON spectra are used only for normalization; these spectra were smoothed artificially during data analysis to improve statistics. This procedure is discussed in detail by Leugers (1979) and Almeida (1982) and must, of course,

take into account that at least for the gold sample, the
smoothing is performed consistently for the experimental
spectrum and for the standard gold cross section.

Finally, corrections have been applied to the cross
sections accounting for neutron multiple scattering and self-
shielding and for gamma-ray self-absorption in the samples, for
pile-up events and for the lost fraction of low-energy gamma-
rays which were cut off by the electronic pulse-height threshold
(see Leugers 1979 and Almeida 1982 for a detailed discussion).

3. EXPERIMENTAL RESULTS AND UNCERTAINTIES

3.1 Experimental capture cross sections

The deduced cross sections are plotted as a function of neutron energy in Figs. 6, 7 and 8 for Kr-nat, ^{84}Kr and ^{80}Kr, respectively. Isotopic corrections were negligible only for ^{84}Kr. The cross sections of all other isotopes had to be determined from the cross sections measured for the various isotopic mixtures by solving the corresponding set of linear equations. In Figs. 9, 10 and 11 the respective cross sections of the mixtures, denoted by quotation marks are shown. The unfolded isotopic cross sections are given in numerical form in the appendix.

3.2 Maxwellian averaged cross sections

The neutron capture rates for a nuclear species, i, is given by

$$\frac{dN_i}{dt} = - N_i \, n_n \, v\sigma \tag{4}$$

for monoenergetic neutrons. Here N_i and n_n are the density of nuclei and neutrons, v denotes the neutron velocity and σ the capture cross section at fixed neutron energy.

During the formation of the heavy elements inside a star, however, we have to consider a non-relativistic, non-degenerate plasma.

In case of thermal equilibrium, characterized by a temperature T, the velocity v has to be replaced by v_T and σ by the Maxwellian average $\frac{<\sigma v>}{v_T}$ (Clayton 1968)

$$\frac{<\sigma v>}{v_T} = \frac{2}{\sqrt{\pi}} \; \frac{\int_0^\infty dE \; \sigma(E) \; E \; \exp(-\frac{E}{kT})}{\int_0^\infty dE \; E \; \exp(-\frac{E}{kT})} \tag{5}$$

Now v represents the relative velocity between neutrons and nuclei and v_T the most probable neutron velocity

$$v_T = \sqrt{\frac{2kT}{\mu}} \tag{6}$$

(μ reduced mass, k Boltzmann constant).

From our data we calculated $\overline{\dfrac{\langle\sigma v\rangle}{v_T}}$ between kT = 20 and 50 keV. These Maxwellian averaged cross sections are summarized in Table 3. In the following we consider only Maxwellian average cross sections and denote these by σ for simplicity.

The simultaneous measurement of the capture cross section of natural krypton provides a consistency check for our isotopic results. For kT = 30 keV we combined our individual isotopic cross sections weighted with their relative abundances and obtained a composed cross section of 67 $\pm$ 5 mb which is in good agreement with the experimental result of 63 $\pm$ 4 mb for Kr-nat.

At this point we note that the new ^{84}Kr cross section determines the isomeric ratio, IR, in ^{85}Kr which is defined as the ratio of the partial capture cross section of ^{84}Kr leading to the isomeric state in ^{85}Kr and the total capture cross section of ^{84}Kr. The partial cross section was measured for kT = 25 keV by Beer and Käppeler (1982) who report $\sigma^P(^{84}$Kr$)$ = 24 $\pm$ 3 mb. With the total capture cross section for the same thermal energy $\sigma(^{84}$Kr$)$ = 42.2 $\pm$ 4.8 mb we obtain

$$IR(^{85}\text{Kr}) = 0.57 \pm 0.10 \quad .$$

This value is an important parameter for a forthcoming analysis of the ^{85}Kr-branching by Walter et al. (1983).

3.3 Uncertainties

In this section we discuss the uncertainties related to the various steps of data analysis. Principally, there are two classes of uncertainties: those which are about equal for all isotopes (e.g. reference cross section, sample related effects) and others which are determined by the size of the respective cross sections (background, statistics). As can be seen from Figs. 3 to 5 the latter uncertainties depend also strongly on neutron energy. Here, we restrict the discussion to the uncertainties of the Maxwellian average cross section.

Note that in calculating the total uncertainty we have neglected possible correlations between individual components. All considered uncertainties are summarized in Table 4.

a)   Standard cross section: For the Maxwellian average of the ENDF/B-IV cross section of ^{197}Au we estimated an uncertainty of 3 %. Meanwhile, a new version ENDF/B-V is available, which on an average is higher by $\sim$ 2.3 % compared to ENDF/B-IV. However, this version might change as the data of Macklin et al. (1975), on which it is primarily based, have been revised recently (Macklin 1982).

b)   Gamma-ray self-absorption in the sample: This effect was investigated experimentally for a set of gold samples with different thicknesses and diameters (Wisshak, Walter and Käppeler 1983). From these results extrapolations to other sample materials could be made. These corrections which introduce an uncertainty of 1 % were not applied to our first results (Leugers 1979 and Leugers et al. 1979).

c)   Neutron multiple scattering and self-absorption: For the gold sample these correction factors were calculated by the SESH-code (Fröhner 1968). For the Krypton samples the spherical geometry implied that no correction was required for neutron multiple scattering and therefore only the self-shielding effect was corrected for.

d)   Pile-up events: Given the large solid angle of the detectors seen by the sample, there is a nonnegligible probability for two (or more) gamma-rays of the same cascade to be simultaneously detected in the same detector. These events are incorrectly weighted by the Maier-Leibnitz method. The correction is derived from the experimentally measured coincidence rate between the two C_6D_6 detectors. The resulting uncertainty is $\sim$ 1 %.

e)   Lower threshold correction: Events with a pulse height less than 90 keV fall below the electronic threshold and are lost. Because the pulse height weighting function is very small for these events, the resulting correction as also small leading to an uncertainty of 0.5 %.

f) Sample mass: The weight of the empty and filled sample cannings was determined before and after the measurements. Losses of krypton gas through leaks in the cannings were negligible in most cases. The related uncertainties are 1 % except for ^{84}Kr where 2 % had to be tolerated.

g) Time dependent background: The relative size of this correction depends on the observed signal-to-background ratio in the TOF spectra. This uncertainty is typically 1 % but 2 % for ^{84}Kr because of its smaller cross section.

h) Weighting function: The uncertainty introduced by the pulse height weighting function was checked by variation of the adopted function (Hensley 1980) within reasonable limits (30 %). The impact on the cross sections is relatively small giving rise to an uncertainty of 0.5 - 1 %.

i) Effective neutron binding energy: This uncertainty is the smaller the higher the sample is enriched. It is largest for "^{78}Kr" and "Kr-nat" (3 %) and zero for ^{84}Kr.

j) Isotopic impurities: The isotopic cross sections were determined from the experimentally investigated "mixtures" solving the corresponding set of linear equations. The related uncertainties are correlated to the enrichment of the samples. They are largest for ^{78}Kr (10 %) and again zero for ^{84}Kr.

k) Statistics: The statistical uncertainties are typically 2 % but are larger for ^{84}Kr (3 %) because of the less favourable signal-to-background ratio.

4. MODEL CALCULATIONS

Theoretical calculations of neutron capture cross sections in the keV energy range are usually based on the Hauser-Feshbach formalism. For astrophysical purposes extensive calculations of Maxwellian average cross sections for $kT = 30$ keV have been performed (Holmes et al. 1976, Woosley et al. 1978) on a variety of isotopes using global parameter systematics in order to cover a large range of atomic masses. However, such global treatments imply that local details (e.g. due to deformation or to shell effects) are not sufficiently accounted for, and the results so obtained differ from experimental cross sections by 30-50 % on the average.

The reliability of theoretical cross sections can be improved by refined techniques as they were developed for evaluation of neutron cross sections in the technological field. The idea is to use as much experimental information as is available in the literature to determine the relevant Hauser-Feshbach parameters and to build local parameter systematics for the investigated isotopes and for their neighbours as well (Reffo 1980a). In this procedure special attention was paid to achieve internal consistency of all parameter sets. The so determined parameter sets enable us to deduce the capture cross sections with typical uncertainties of ∿ 25 % even for those isotopes for which no experimental information is available at all. The capability of the local approach may be verified by comparison of theoretical data obtained by this technique (Benzi et al. 1973, Harris, 1981) and by global parametrization (Holmes et al. 1976) with experimental cross sections as quoted in the compilation of Käppeler et al. (1982). From Table 1 in this latter reference one finds average deviations from the experimental values of 20-25 % for local and 30-40 % for global parameter sets. It should be noted that the systematic treatment of parameters as well as the theoretical formalism has been improved recently in several aspects (Reffo 1980b, Reffo et al. 1982, Reffo 1981 now even allowing for calculation of capture gamma-ray spectra and isomeric ratios).

In the present investigation our interest is focused
on the mass region 78 < A < 84 and, in particular, on the
radioactive isotopes on the s-process path, ^{79}Se and ^{81}Kr,
which cannot be investigated experimentally. We also try
to quantify the uncertainties in the calculations for some
important cases in order to estimate how they affect the re-
lated astrophysical interpretations.

4.1 Outline of the Model

Our investigations are carried out with the modular system
of computer codes, IDA, (Reffo and Fabbri 1981). The present
cross section calculations were made with the module POLIFEMO
based on the Hauser-Feshbach theory including correction for
width fluctuations. It was used in the spherical optical model
approximation to calculate the neutron transmission coeffi-
cients in the entrance and exit channel. The probability for
gamma decay of the compound nucleus states of any given J and
π is then determined for each step of each possible gamma-ray
cascade.

After summation over all J and π and by considering
E1, E2 and M1 electromagnetic selection rules, the various
single step contributions are lumped together into energy
bins according to the energies of the emitted gamma rays so
that partial and total gamma-ray spectra can be obtained on
option. The code also traces gamma-ray stories which feed
some particular levels. In this way, it is possible to cal-
culate the cross sections for the population of isomeric
states and the corresponding gamma-ray spectra as well. For
the transitions between discrete levels, gamma-ray decay schemes
and branching ratios were either given as input or were in-
ternally calculated according to different options.

The gamma-decay widths of E1 transitions are estimated according to the Brink-Axel model as used by Reffo (1980a) where

$$\overline{\Gamma_\gamma}(E,J,\pi) = \frac{C}{\rho(E,J,\pi)} \; (\delta_{J_n,|J-1|} + \delta_{J_n,J\neq 0} + \delta_{J_n,J_n+1}) \\ * \delta_{\pi_n,-\pi}(E-E_n)^2 \sigma_L(E-E_n) \tag{7}$$

gives the width for gamma decay from continuum levels (E,J,π) to the nth discrete level (E_n, J_n, π_n) and

$$\Delta\overline{\Gamma_\gamma}(E,J,\pi) = \frac{C}{\rho(E,J,\pi)} \; \varepsilon^2 \; \sigma_L(\varepsilon) \sum_{J'=|J-1|}^{J+1} \rho(E-\varepsilon,J',-\pi)\Delta\varepsilon \tag{8}$$

the width for gamma decay from continuum levels (E,J,π) to continuum levels $(E-\varepsilon,J',-\pi)$.

$$\sigma_L(\varepsilon) = \sum_{R=1}^{2} \sigma_R \frac{\varepsilon^2 \; \Gamma_R^2}{(\varepsilon^2-E_R^2)^2+\varepsilon^2\Gamma_R^2} \tag{9}$$

is the adopted Lorentzian form for the splitted photon-absorption cross section and $C = 2/3 \; (\pi\hbar c)^2$.

4.2 Model Parameters

The most important quantities needed for the determination of gamma decay widths of the compound system are the level density ρ and the photon absorption cross section σ_L. In spite of many attempts, there is no level density model which may provide absolute values over a wide range of atomic masses. Therefore, we adopt the approach outlined below which offers the advantage of being characterized by only two parameters (a,U_x) both of which exhibit a well established systematic behaviour (Reffo 1980 b). For evaluation of the level density the range of accessible excitation energies is subdivided into three intervals:

(i) The region of known discrete levels where no theoretical model is needed; the respective quantum characteristics (E, J, π) are taken from Lederer and Shirley (1978)

(ii) At high excitation energies a total level density

$$\rho_2(E) = \frac{\sqrt{\pi}}{12} \frac{\exp[2\sqrt{a(E-\Delta)}]}{a^{1/4}(E-\Delta)^{5/4}\sqrt{2\pi\sigma^2(E)}} \tag{10}$$

is assumed, Δ being the pairing correction and a the level density parameter. This expression results essentially from the Fermi gas model.

The corresponding spin distribution is

$$f(E, J) = \frac{(2J+1)\exp[-(J+1/2)^2/2\sigma^2(E)]}{2\ \sigma^2(E)} \tag{11}$$

with a spin cut-off factor $\sigma^2(E) = 0.146\ \sqrt{a(E-\Delta)}\ A^{2/3}$. The level density parameter a that characterizes the level density and the spin distribution has been treated as a free parameter which was obtained at the neutron separation energy by normalization of ρ_2 to mean spacings D of s-wave neutron resonances.

(iii) In the intermediate region between the last known discrete level and the region where the Fermi gas model is valid, a semiempirical exponential form suggested by Gilbert and Cameron (1965) was used for interpolation

$$\rho_1 = \frac{1}{T}\exp[(E-E_o)/T] \tag{12}$$

Both parameters in this equation, T and E_o, can be expressed by the level density parameter a and by an effective energy $U_x = E_x - \Delta$, Δ being the pairing energy, and E_x that excitation energy where the level densities ρ_1 and ρ_2 match smoothly. Eventually, it may be helpful in ambiguous cases to consider the nuclear temperature as a supplementary information, because it exhibits a very stable behaviour with mass number (Reffo 1980a).

For the parities usually an equal distribution is assumed in the entire continuum energy range. But for certain cases specified below a distribution

$$P(\pi, E) = e^{AE+B} \tag{13}$$

is used (Reffo 1980a) in order to account for the experimental parity distribution of the discrete levels.

4.2 Evaluation of Model Parameters

The discussion of how we determined the parameters and the parameter systematics for the investigated isotopes is presented in the same order as they were introduced in the preceding section.

Optical model parameters (OMP): In the energy range considered here we know that the OMP may influence even strongly the calculated neutron capture cross sections. To reduce this uncertainty we have chosen OMP sets which reproduce s- and p-wave strength functions S_o, S_1 and the scattering radii R because these quantities completely determine the compound nucleus cross section and the shape elastic cross section, respectively, for neutron energies below 100 keV. For the Kr and Se isotopes this requirement was sufficiently satisfied by the OMPs of Wilmore and Hodgson (1964) and for the Br isotopes by those of Perey and Buck (1962). These adopted OMP sets were tested by comparison of our calculated total cross sections with experimental results.

In Table 5 the scattering radii R and strength functions S_o, S_1 which we calculated with the above OMP sets are shown together with the respective values taken from systematics and from analysis of neutron resonances. The good agreement between calculated and empirical values indicates that no significant uncertainty is to be expected in this part of the cross section calculations.

Level density parameters: The level density parameter a, that characterizes ρ_2, is usually deduced from statistical analyses of neutron resonance schemes but where no such infor-

mation is available, a can be deduced either from systematics
(Reffo 1980a) or from experimental capture cross sections,
provided that all other model parameters are sufficiently known.

For the Se and Br isotopes the existing resonance schemes are
rather poor (Mughabghab et al. 1981). Therefore, no sophisticated
resonance analysis could be performed but mean resonance spacings
D_{OBS} were deduced by simple staircase statistics and the associated
uncertainties were derived using Student's t-distribution. The
resulting values for D_{OBS} are listed in Table 6. They show sig-
nificant discrepancies compared to the values given by Mughabghab
et al. (1981) and also more conservative uncertainties.

In case of the Kr isotopes, resonance schemes were not
available except for ^{86}Kr. Therefore in our first calculations
(Leugers et al. 1979) level density parameters were deduced
from overall systematics. But with the now available experimental
cross sections the mean level spacings could be improved. In the
range of the Maxwellian energy distribution (kT = 30 keV) one
may write (Reffo 1980a)

$$\sigma_{n\gamma} = K \frac{\overline{\Gamma_\gamma}}{\overline{D}} \quad , \tag{14}$$

K being a known factor. Provided that the average radiative
width is known, D can thus be determined from the cross section.
Uncertainties were estimated via error propagation from the
uncertainties of $\sigma_{n\gamma}$ and Γ_γ as given in Table 6.

The results for a are plotted in the upper part of Fig. 12
for all investigated isotopes, and members of the individual
families are connected by eye guide curves. Two features can
be distinguished in this plot which justify the local treatment
of a: There is a significant difference in a for even-even
and non even-even target nuclei (open and black symbols) and
there appears to be a displacement between the even Se and Kr
isotopes as well. However, in this particular case the uncertainties

are too large to allow for a conclusive statement and so the effect of different proton numbers was neglected here. This is in accord with Reffo (1980a) who finds that this effect starts to be sizeable only for A > 100. Assuming a smooth dependence of $\underline{a}$ on neutron number, the scatter of the $\underline{a}$ values deduced from experimental data could be used to estimate the uncertainty of the systematics. In view of the large uncertainties, especially for the Se isotopes, we assumed $\Delta\underline{a} \sim 0.5$ MeV^{-1} as being realistic. The finally adopted level density parameters are listed in Table 9; values interpolated from the systematics are marked by an asterisk.

In the intermediate energy range the level schemes of all compound nuclei (Lederer and Shirley 1978) were considered to deduce the parameters U_x and T. For some examples Fig. 13 shows the cumulated number of the known discrete levels (staircase plots) and the respective fits (solid lines). The inserts give the spin distributions of the known levels which have been fitted by the maximum likelihood method to obtain the spin cut-off factors σ^2. The resulting values for U_x and σ^2 are also shown in Table 9. As one may see from Fig. 13, sometimes there is no good agreement between the experimental and the fitted spin distribution. In these cases two values for σ^2 are given in Table 9, the first being derived from the theoretical and the second from the experimental distribution, and the adopted value is marked (§). The differences between theoretical and experimental σ^2-results are assumed as an estimate for the uncertainty in the spin distribution.

The continuum approximation for the level density, ρ_1, was used above the excitation energy E_{cut} which is indicated by arrows in Fig. 13. The position of E_{cut} is determined either by the energy of the first level of unknown J,π or where the fitted curve starts to deviate from the staircase plot due to missing levels. The results for E_{cut} are given in Table 9.

In the mid part of Fig. 12 the matching energy U_x is plotted versus neutron number for all investigated isotopes. The smooth behaviour of U_x provides not only information for those cases where only poor level schemes are available but can also be used as a test for the analyzed level schemes and for the respective values of $\underline{a}$. If, for a particular isotope, U_x does not fit in the systematics of Fig. 12, this would indicate ambiguities and would require reconsideration of the entire parameter set. Overall, the consistent systematics for $\underline{a}$ and U_x as shown in Fig. 12 ensure the reliability of the basic experimental information and of the analysis as well.

For calculation of the isomeric ratio

$$IR = \frac{\text{partial capture cross section to the isomer}}{\text{total capture cross section}}$$

for ^{79}Se the gamma decay scheme and branching ratio in the compound nucleus are also required as input. This information was taken from Lederer and Shirley (1978). Gaps in these data were filled by the assumption that E1, M1 single particle transitions dominate. The finally adopted level scheme with all spectroscopic information is summarized in Table 7.

Radiative Widths: The giant resonance parameters (GRP) for the calculation of the radiative widths are taken from the systematics of Reffo (1980a). The corresponding nuclear deformations ß were determined from the tentative systematics at the bottom of Fig. 12. The deformation parameters used for the systematics are taken from Stelson and Grodzins (1965) or are deduced from quadrupole moments (Fuller and Cohen 1969). The adopted GRP and deformations are listed in Table 9.

Table 8 shows the radiative widths for s- and p-wave resonances calculated with the above parameters in comparison to experimental values. In general, the agreement is remarkably good, at least in view of the experimental uncertainties.

4.3 Results and Discussion

Our calculated neutron capture cross section are summarized in Table 10. The astrophysically important Maxwellian averaged cross sections for kT = 30 keV are listed in Table 11 together with the experimental values. This table provides also results from other calculations and the experimental data from the literature.

Before entering in a detailed discussion it should be noted that a comparison of our previous calculations (Leugers et al. 1979) with the present results illustrates the amendments which were achieved by improving the OMP sets and the systematics for the level density parameter $\underline{a}$. Major changes occured for the odd isotopes ^{81}Kr and ^{83}Kr but also for ^{78}Kr, mainly because the new experimental data allowed for a refined evaluation of $\underline{a}$ in this mass region, including odd-even effects. For a few important cross sections, especially for ^{79}Se , we tried to estimate the uncertainties of our calculations. Neglecting the uncertainties due to the OMP sets (as justified above) we traced the propagation of the uncertainties from the radiative decay width Γ_γ and from the level spacing D. The radiative decay width depends on the level density parameter $\underline{a}$, the nuclear temperature T (through U_x), the spin distribution (through σ^2) and on the parity distribution $P(\pi)$. As D also depends on $\underline{a}$, one obtains

$$\sigma_{n\gamma}(\Gamma_\gamma, D) = \sigma_{n\gamma}(\underline{a}, U_x, \sigma^2, \beta, P(\pi)). \tag{15}$$

Although $\underline{a}$ and U_x are correlated for a particular isotope the correlation becomes negligible when these parameters are taken from systematics. Therefore, in our analysis we assumed these parameters to be independent of each other. The uncertainties of $\underline{a}$, U_x and β were estimated from the scatter of the points in Fig. 12. The difference between the experimental and theoretical spin distributions was assumed as the uncertainty of the spin cut-off factor σ^2.

Finally, we have neglected the uncertainty from $P(\pi)$, because an extrapolation of the equal distribution for the two parities from the discrete levels to the whole energy range seemed reasonable. With this procedure uncertainties of 20 and 23 % are estimated for ^{78}Se and ^{79}Se, respectively.

Comparison of the present results with other calculations exhibits reasonable agreement for the Se and Br isotopes but with three exceptions: the ^{78}Se value of Holmes et al. (1976) and the ^{79}Se and ^{81}Br values of Harris (1981) are discrepant from the other data by almost a factor 2.

For the Kr isotopes the discrepancies are more severe, in particular if one compares the entire sequence of cross sections rather than a single isotope. There seems to be a general trend to underestimate the cross sections of the even, neutron-poor isotopes but also the results for ^{84}Kr are highly discrepant. This shows clearly the virtue of the local parameter systematics which provides a consistent set of parameters for each of the investigated isotopes. This seems to be the more important close to magic neutron numbers.

The good agreement between our calculation and the experimental data is illustrated in Fig. 14 for all investigated isotopes. The fact that the relevant radioactive nuclei ^{79}Se and ^{81}Kr have always two stable neighbours makes it possible to deduce their parameters from our systematics by <u>inter</u>polation. Therefore we are confident that our approach yielded reliable values for these cross sections.

In addition to the cross sections we have also calculated the isomeric ratio IR and the average gamma cascade multiplicity $\bar{m}$ for ^{79}Se. This case was considered only for completeness because the population of the isomeric state in ^{79}Se by neutron capture is not important for the s-process (it decays almost exclusively to the ground with a half life much shorter than the neutron capture time scale). At 30 keV neutron energy we get IR $(^{79}$Se$) = 0.52$. In the calculation of the isomeric ratio we found that a maximum cascade multiplicity m=4 was sufficient to account for 97 % of the cross section; the average multiplicity was $\bar{m} = 2.7$.

5. ASTROPHYSICAL INTERPRETATION

5.1 s-Process model and the ^{79}Se-branching

We adopted the phenomenological s-process model of Clayton et al. (1961) which assumes a rather weak neutron flux and an exponential distribution of neutron exposures τ

$$\rho(\tau) = \frac{f_1 N_{56}}{\tau_{01}} \exp(-\tau/\tau_{01}) + \frac{f_2 N_{56}}{\tau_{02}} \exp(-\tau/\tau_{02}) \tag{16}$$

$f_{1,2}$ are the fractions of the solar ^{56}Fe abundance N_{56} which act as seed for the s-process and $\tau_{01,2}$ are mean fluences in (mb^{-1}). While the second term accounts for the bulk of s-process abundances the first term in eq.(16) is required to reproduce the enhanced s-process contributions in the region $56 < A \underset{\sim}{<} 90$. In the following we accept the fluence distribution determined recently by Käppeler et al. (1982) who derived the parameters f and τ_0 by a best fit of the calculated products $\sigma N_s(A)$ to the empirical values for s-only isotopes. These normalizing points were determined from evaluated experimental cross sections which are folded with the Maxwellian neutron energy distribution and from the solar abundances $N_\odot$ quoted by Cameron (1982). We note at this point, that the adopted model and also the fluence distribution should be considered as an approximation. Modifications to that simple picture could for instance be that the two terms of the fluence distribution might be characterized by different neutron densities and temperatures - and both these effects would have significant impact on our branching analyses. We will come back to this problem in the following sections.

In this model the characteristic product σN_s can be calculated as a function of mass number by the relation

$$\sigma N_s(A) = \frac{f_1 N_{56}}{\tau_{01}} \prod_{i=56}^{A} \left(1 + \frac{1}{\sigma_i \tau_{01}}\right)^{-1}$$

$$+ \frac{f_2 N_{56}}{\tau_{02}} \prod_{i=56}^{A} \left(1 + \frac{1}{\sigma_i \tau_{02}}\right)^{-1} \tag{17}$$

For convenience the factors $(1 + \frac{1}{\sigma_i \tau_{ox}})^{-1}$ are abbreviated by $\zeta^x(^A Z)$ for isotope A of element Z.

From equation (17) it can be seen that σN_s is a smooth function of A which is determined by the product $\sigma_i \tau_0$. For large cross sections or $\sigma_i \tau_0 \gtrsim 1$, σN_s depends only weakly on A as it is the case in the Se, Br, Kr-region.

The specific situation for the ^{79}Se branching is illustrated in Fig. 15. The branching points ^{79}Se and ^{80}Br are shaded and the s-only isotopes ^{80}Kr and ^{82}Kr are marked by double boxes. The involved isotopes are linked by the s-process mass flow as it is considered in our calculations.

That there is certainly a significant branching at ^{79}Se is obvious from the isotopic abundances of s-only ^{80}Kr and ^{82}Kr, because ^{80}Kr would be bypassed completely otherwise. For a quantitative treatment one must consider the product σN_s rather than the abundances. A similar although less pronounced observation is to be expected for the σN_s-values of ^{78}Se and ^{80}Se as both these isotopes are also produced significantly by the s-process. A third possibility to investigate the branching at ^{79}Se is provided by the comparison of σN_s for ^{80}Se and ^{80}Kr. All these cases will be considered below.

The branching at ^{79}Se can be expressed in terms of the beta decay rate $\lambda_{\beta^-} = \ln2/t_{1/2}$ and of the neutron capture rate $\lambda_n = n_n v_T \sigma$ where $t_{1/2}$ is the effective half live of ^{79}Se at s-process temperatures T_s and n_n is the corresponding neutron density; $v_T = \sqrt{\frac{2kT}{\mu}}$ is the average thermal velocity with μ being the reduced neutron mass. Then the branching ratio B_n reads

$$B_{\beta^-}(^{79}Se) = \frac{\lambda_{\beta^-}(^{79}Se)}{\lambda_{\beta^-}(^{79}Se) + \lambda_n(^{79}Se)} \tag{18}$$

The beta decay rate λ_{β^-} is expected to be temperature dependent and can be determined from the analysis of the branching. For the neutron capture rate λ_n one needs the cross section of ^{79}Se and the neutron density n_n.

The (minor) branching at ^{80}Br occurs because of the two decay modes of this nucleus, whereas neutron capture can be neglected due to the short half lives. In this case one obtains

$$B_{\beta^-}(^{80}Br) = \frac{\lambda_{\beta^-}(^{80}Br)}{\lambda_{\beta^-}(^{80}Br) + \lambda_{EC}(^{80}Br)} \tag{19}$$

The problem with this branching is that the ratio of the two decay rates in ^{80}Br depends also on temperature. In section 5.3 the parameters required in eqs. (18, 19) are discussed in detail.

With these definitions the products σN_s can be evaluated for the isotopic pairs (^{80}Kr, ^{82}Kr), (^{78}Se, ^{80}Se) and (^{80}Kr, ^{80}Se). The first pair is certainly the most promising case because both isotopes are of pure s-process origin. The corresponding σN_s values can be expressed as

$$\sigma N_s(^{80}Kr) = \sum_{x=1}^{2} \sigma N_s^x(^{78}Se) \frac{B_{\beta^-}(^{79}Se)}{1-B_{\beta^-}(^{79}Se)} \zeta_m^x(^{79}Se) \; \zeta^x(^{79}Br) B_{\beta^-}(^{80}Br)$$

$$\zeta^x(^{80}Kr) \tag{20}$$

and

$$\sigma N_s(^{82}Kr) = \sum_{x=1}^{2} \sigma N_s^x(^{78}Se) \left| \frac{B_{\beta^-}(^{79}Se)}{1-B_{\beta^-}(^{79}Se)} \zeta_m^x(^{79}Se) \; \zeta^x(^{79}Br) \right.$$

$$B_{\beta^-}(^{80}Br) \zeta^x(^{80}Kr) \; \zeta^x(^{81}Kr) \zeta^x(^{82}Kr)$$

$$+ \; \zeta_m^x(^{79}Se) \zeta^x(^{80}Se) \zeta^x(^{81}Br) \zeta^x(^{82}Kr)$$

$$+ \; \frac{B_{\beta^-}(^{79}Se)}{1-B_{\beta^-}(^{79}Se)} \zeta_m^x(^{79}Se) \zeta^x(^{79}Br) (1-B_{\beta^-}(^{80}Br)) \zeta^x(^{80}Se)$$

$$\left. \zeta^x(^{81}Br) \zeta^x(^{82}Kr) \right| \tag{21}$$

where ζ_m is given by

$$\zeta_m^x(^{79}Se) = \left(\frac{1}{1-B_{\beta^-}(^{79}Se)} + \frac{1}{\sigma(^{79}Se)\tau_{ox}} \right)^{-1} \tag{22}$$

According to Käppeler et al. (1982) different weight has to be given to the two components of the fluence distribution $(\sigma N_s^1(^{78}Se)/\sigma N_s^2(^{78}Se) = 0.52)$. Apart from this, the ratio $\sigma N_s(^{80}Kr)/\sigma N_s(^{82}Kr)$ is independent of any assumption on elemental abundances and is determined completely by the quantities $\zeta^x(A_z)$ and the branching ratios for ^{79}Se and ^{80}Br. The effective s-process branching ratio for ^{79}Se results from eqs.20 and 21 by inserting the empirical value for the ratio $\sigma N_s(^{80}Kr)/\sigma N_s(^{82}Kr)$. As one deals with two isotopes of pure s-process origin the associated uncertainty is caused only by the cross sections of ^{80}Kr and ^{82}Kr.

Contrary to this ideal case, the determination of $B_\beta-(^{79}Se)$ via the σN_s-value of the isotope pair $(^{78}Se, {}^{80}Se)$ is complicated because a correction must be made for the abundance contribution from the r-process. For ^{78}Se this correction can be taken from the calculated σN_s-curve of Käppeler et al. (1982) as ^{80}Se is part of the ^{79}Se branching. The required r-process contribution is determined by interpolation of the respective values for ^{76}Ge, ^{78}Se and ^{82}Se, ^{86}Kr. Another drawback comes from the fact that for ^{78}Se no experimental cross sections are available. Because ^{78}Se and ^{80}Se are the immediate neighbours of the branching point the ratio $\sigma N_s(^{80}Se)/\sigma N_s(^{78}Se)$ is influenced by fewer isotopes and the corresponding expression for $\sigma N_s(^{80}Se)$ is simpler than eq. 21 :

$$\sigma N_s(^{80}Se) = \sum_{x=1}^{2} \sigma N_s^x(^{78}Se) \left[\zeta_m^x(^{79}Se)\zeta^x(^{80}Se) \right.$$

$$\left. + \frac{B_\beta-(^{79}Se)}{1-B_\beta-(^{79}Se)} \zeta_m^x(^{79}Se)\zeta^x(^{79}Br)(1-B_\beta-(^{80}Br)) \zeta^x(^{80}Se)] \right] \quad (23)$$

The third possibility for defining $B_\beta-(^{79}Se)$ is to compare the empirical σN_s-value for ^{80}Se and ^{80}Kr. However, this procedure requires the abundance ratio of Se and Kr and therefore suffers from the large uncertainty of the krypton abundance. In principle, one can use the σN_s-curve to deduce the Kr-abundance such that $\sigma N_s(^{82}Kr)$ is normalized to the curve as it is discussed in section 5.3. But this leaves still a considerable uncertainty because the abundance ratio of Kr and Se cannot be verified by this method as long as an experimental cross section for the corresponding normalization point ^{76}Se is lacking. For complete-

ness, we also give the expression for this pair of nuclei:

$$\frac{\sigma N_s(^{80}Kr)}{\sigma N_s(^{80}Se)} =$$

$$\frac{\sum\limits_{x=1}^{2} [1-B_\beta-(^{79}Se)]^{-1} B_\beta-(^{79}Se)\zeta_m^x(^{79}Se)\zeta^x(^{79}Br) \quad B_\beta-(^{80}Br)\zeta^x(^{80}Kr)\sigma N_s^x(^{78}Se)}{\sum\limits_{x=1}^{2} \zeta_m^x(^{79}Se)\zeta^x(^{80}Se)+B_\beta-(^{79}Se)\zeta^x(^{79}Br) \quad [1-B_\beta-(^{80}Br)]\zeta^x(^{80}Se) \quad \sigma N_s^x(^{78}Se)} \qquad (24)$$

All quantities which are required to evaluate the effective branching ratio $B_\beta-(^{79}Se)$ under s-process conditions will be discussed in section 5.5.

The cross sections determined in this work can also be used to improve the respective s- and r-process abundance contributions. This decomposition can easily be done by the approximate relations

$$N_s(A) = \frac{\sigma N_s(A)}{\sigma(A)} \quad \text{and} \quad N_r(A) = N_\odot - N_s \qquad (25)$$

which are valid under the assumption that abundance contributions from other processes, (e.g. from the p-process) are negligible (see also Käppeler et al. 1982).

5.2 Decay parameters of ^{79}Se and ^{80}Br

The beta decay rate of both isotopes depends on temperature, at least in the range of interest around kT = 30 keV. Fig. 16 illustrates that this is a very strong effect for ^{79}Se. The first excited state at 96 keV is thermally polulated to $\sim$1 % (Walter and Beer 1982) at s-process temperature and undergoes allowed beta transitions to ^{79}Br with a half life of $\sim$ 20 d while the ground state decay is first forbidden with a half life of $\leq$ 6 x 10^4 yr. As thermal equilibrium is achieved on a much faster time scale than the decay, the population of the excited state is constant in time and given by

$$P_i = (2J_i+1) \exp (-E_i/kT) / Z \qquad (26)$$

where Z is the partition function, J_i the spin and E_i the energy of the excited state. The total beta decay rate λ_{β^-} is given by the sum of all partial rates

$$\lambda = P_o \lambda_o + \sum_i P_i \lambda_i \; .$$
(27)

As can be seen from Fig. 16, there are several possibilities for allowed beta transitions from excited states in ^{79}Se and even a back-decay from the 207 keV state in ^{79}Br cannot be excluded. These transitions, however, have to be weighted with the respective population probabilities and this, finally, reduces the number of effective links to the decay of the first excited state in ^{79}Se to the ground state of ^{79}Br. In Table 12 all the parameters are summarized which we considered in this respect. Unknown log ft-values were taken from Conrad (1976) and are estimates based on available values for similar transitions in neighboring nuclei. Because the high temperature leads to almost complete ionization in the mass region around A = 80 the phase space for the emitted electrons is modified compared to the terrestrial situation. The resulting effects (bound state beta decay, capture of continuum electrons, hampered electron capture from bound states etc.) have been taken into account in determining the s-process decay rate λ_i^* (Conrad 1976). The last column of Table 12 lists the decay rate of each level, leading to an overall half life of $t_{1/2}^* = 4.3$ yr at kT = 30 keV. This value is slightly longer than the 3.3 yr derived by Conrad because in the meantime the J^π assignment for the 130 keV state in ^{79}Se has been settled (Walter and Beer 1982 and references therein). The back decay from the 207 keV state in ^{79}Br turned out to be not significant under s-process conditions. It can be all the more neglected as Se is 6 times more abundant than Br (Anders and Ebihara 1982).

The temperature dependence of the half life of ^{79}Se is plotted in Fig. 17 for the range between 0 and 10^9 K. One finds a very steep slope between 1 and 3×10^8 K just where the s-process temperature is supposed. The dashed lines indicate the range of uncertainty which results from the 10 % uncertainty of the log ft-value for the decay from the 96 keV state. This state is an isomer with 3.9 m half life against gamma-decay to the ground

state. This time may be long enough that it eventually permits to measure the beta decay branch from this state directly. At present, a first attempt for such an experiment is being prepared. If it succeeds, it would provide a major improvement for determining the s-process temperature. The thin solid line in Fig. 17 represents the somewhat higher estimate of Newman (1973) and Cosner and Truran (1981) who neglected the effect of ionization.

The decay of the second radioactive isotope in the ^{79}Se-branching, ^{80}Br, also depends on temperature. In that case it is not the half life which is affected but the branching ratio $\lambda_{\beta^-}/\lambda_{EC}$, which Conrad (1976) predicts to change from the terrestrial value of 11 to 28 at kT = 30 keV for the reasons mentioned above. For simplicity, all calculations in this work will use a constant value $B_{\beta^-}(^{80}Br)$ = 0.97.

5.3 The solar krypton abundance

The observation that ^{82}Kr can be formed only by the s-process and that the total s-process flow passes through this isotope, provides a possibility to determine the solar krypton abundance by comparison of $\sigma N_s(^{82}Kr)$ with the respective value of the $\sigma N(A)$-curve. The total krypton abundance follows then from the well known isotopic ratios. A possible p-process contribution to the ^{82}Kr abundance can be neglected in this context: if one accepts the ^{78}Kr abundance as an upper limit then a possible p-process component of ^{82}Kr is $\lesssim$ 3 %. This problem will be addressed in more detail below because it is of some concern to the analysis of the ^{79}Se branching.

Adopting the σN_s - curve of Käppeler et al. (1982) with $\sigma N_s(A=82)$ = 557 mb (Si $\equiv$ 10^6) and an estimated uncertainty of $\sim$ 25 % (as obtained from Table 3 in this reference) one finds directly

$$N_s(^{82}Kr) = N^0(^{82}Kr) = \frac{\sigma N_s(A=82)}{\sigma(^{82}Kr)} = 6.6 \pm 1.7 \ (Si \equiv 10^6) \qquad (28)$$

and

$$N^0_{Kr} = N^0(^{82}Kr) \ / \ 0.116 = 57 \pm 15 \ (Si \equiv 10^6) \qquad (29)$$

The uncertainty of this krypton abundance comes mainly from the fact that for A<85 the σN_s-curve is composed of two neutron fluence components. The softer one contributes $\sim$ 30 % to $\sigma N_s(^{82}Kr)$ but cannot be accurately defined at present because of lacking experimental cross sections for the s-only isotopes ^{70}Ge, ^{76}Se in the neighborhood of ^{82}Kr.

This krypton abundance is in fair agreement with the values estimated in recent abundance compilations by interpolation between isotopes of neighboring elements (^{83}Kr between ^{81}Br and ^{85}Rb, ^{84}Kr between ^{80}Se and ^{88}Sr). In this way, Cameron (1981) obtained N_{Kr}^{o} = 41.3 while Anders and Ebihara (1982) report a value of 45.3. The latter authors assumed the 11 % difference between the ^{83}Kr and the ^{84}Kr interpolation as an estimate for the uncertainty of the Kr abundance. However, interpolation requires a smooth abundance variation with mass number which only holds for the r-process contribution. Both isotopes, ^{83}Kr and ^{84}Kr, do have sizeable abundance components from the s-process (33 and 38 %, respectively, Käppeler et al. 1982) and therefore a simple interpolation is not correct. In fact, as most of the abundances used for the interpolation are dominated by r-process contributions, this procedure determines rather the r-process component of the krypton abundance. A quite different krypton abundance N_{Kr}^{o} = 25 is given by Palme, Suess and Zeh (1981) which is derived from the composition of solar rare gas components in gas rich meteorites (Marti, Wilkening and Suess 1972).

5.4 r-Process abundances in the Se, Br, Kr region

With the branching analysis, the related capture cross sections and the σN-curve of Käppeler et al. (1982) it is possible to decompose the observed isotopic abundances into their s- and r-components. The p-process contributions are small (as is obvious for ^{80}Kr) and will be neglected in our discussion here.

Selenium: For $^{77,78}Se$ the decomposition is straightforward yielding fractional r-process contributions of 67 and 47 %. The s-process contribution to ^{80}Se follows from the branching ratios at ^{79}Se and ^{80}Br and is found to be 76 % of its observed abundance.

Bromine: Both these isotopes lie within the branching and their decomposition depends therefore on the branching ratio. Other complications are the contributions from their radioactive isobars ^{79}Se and ^{81}Kr. Nevertheless, the r-process component dominates the bromine abundance.

Krypton: ^{83,84}Kr show also a strong r-process contribution.

In Table 13 all the numerical values relevant for the separation of s- and r-process contributions are summarized including ^{75}As for comparison. For our calculated cross sections a 40 % uncertainty was assumed except for those of ^{78,79}Se which are estimated in Table 11. For the ^{77}Se cross section a somewhat larger uncertainty of 50 % was admitted. The σN_s-values from Käppeler et al. (1982) were estimated to be accurate to 25 % and for the solar abundances the uncertainties quoted by Anders and Ebihara (1982) were used. The resulting r-process abundances are plotted in Fig. 18. While the odd mass isotopes show fairly constant values for N_r, a strange pattern is found for the even isotopes. Obviously, ^{80}Se and ^{84}Kr are higher by a factor two compared to the trend of their even neighbors. This feature seems to be significant as is illustrated by the estimate of $N_r(^{80}$Se) based on a capture cross section of only 20 mb instead of the 47 mb from our calculation. Also the ^{84}Kr-value is difficult to move downwards. A reduction of the Kr-abundance would not help because then the ^{83}Kr value would go down, too. In addition, the discrepancy of the present σN-values for ^{80}Kr and ^{80}Se would be increased. In view of the unsatisfactory situation with many of the involved cross sections, better experimental data have to be awaited for a thorough discussion of these problems.

5.5 The s-process temperature

With the numerical data presented above the branching ratio
$B_{\beta}-$ at ^{79}Se can be determined:

(i) ^{80}Kr, ^{82}Kr: From the experimental cross sections and the
the accurately known isotopic abundances one finds

$$R = \frac{\sigma N_s (^{80}Kr)}{\sigma N_s (^{82}Kr)} = 0.59 \pm 0.04 \tag{30}$$

The quoted uncertainty of 7 % is somewhat smaller than one
would expect from the cross sections listed in Table 3.
But for R only the cross section ratio is needed which
means that part of the systematic uncertainties (e.g. due
to the gold standard cross section and most of the multiple
scattering and self shielding correction) cancel out. The
uncertainty in the isotopic ratio was neglected. Inserting
R into eqs. 20, 21 yields the branching ratio $B_{\beta}- = 0.50$.
It is interesting to note that the uncertainty of $B_{\beta}-$ is do-
minated by that from the cross section ratio of ^{80}Kr and
^{82}Kr. All other cross sections do not affect $B_{\beta}-$ significant-
ly. If, for instance, the calculated value of 47 mb for the
cross section of ^{80}Se is reduced by its likely uncertainty
of 30 %, $B_{\beta}-$ is changed only by 3 %. The effect of the addi-
tional branching at ^{80}Br is even smaller. If the electron
capture branch is completely neglected at this point, $B_{\beta}-$
is not changed by more than 1 %. The systematic uncertainty
introduced by the model in splitting σN into two components
is also not severe. From the work of Käppeler et al. (1982)
one may assume an uncertainty of 35 % for the quoted
ratio 33/67 for the two fluence components at A = 78.
Changing this ratio to 21/90 results in $B_{\beta} = 0.52$. Therefore,
the branching ratio at ^{79}Se as deduced from the σN-values
of ^{80}Kr and ^{82}Kr is

$$B_{\beta}- = 0.50 \pm 0.05 \tag{31}$$

with a conservatively estimated uncertainty of 10 %.

(ii) ^{78}Se, ^{80}Se: The two complications in this determination of
$B_{\beta}-$ (correction for r-process contributions and poor
cross section information) do not allow for a meaningful
analysis. If one starts from $\sigma N_s (^{78}Se) = 693$ mb (Käppeler

et al. 1982) one gets $N_s(^{78}Se) = 7.7$ and $N_r = N^{\odot}-N_s = 6.9$. The r-process abundance can be interpolated:

$$N_r(^{80}Se) = 1/2 \ (N_r(^{78}Se) + N^{\odot}(^{82}Se)) = 7.2 \qquad (32)$$

which leads to

$$N_s(^{80}Se) = N^{\odot}-N_r = 23.7. \qquad (33)$$

With these s-process abundances and the calculated cross sections one finds that $\sigma N_s(^{80}Se) > \sigma N_s(^{78}Se)$. A solution of this dilemma would require a drastic reduction of the cross section ratio $\sigma(^{80}Se)/\sigma(^{78}Se)$. Therefore, an accurate measurement of this ratio needs to be carried out. However, even then the r-process subtraction might be too uncertain to derive $B_{\beta}-$ sufficiently reliable, so that, in turn, $B_{\beta}-$ could be used to fix $N_r(80_{Se})$.

(iii) ^{80}Kr, ^{80}Se: Evaluation of equation (24) shows that this combination is also not suited for a determination of $B_{\beta}-$. An additional uncertainty due to the elemental abundance ratio krypton/selenium is added to the problems discussed under (ii) for ^{80}Se. Similar to the case above, comparison of $\sigma N(^{80}Kr)$ and $\sigma N(^{80}Se)$ may not yield an accurate value for $B_{\beta}-$, but in turn, $B_{\beta}-$ may be used to estimate the ratio $N^{\odot}_{Kr}/N^{\odot}_{Se}$. The comparison of ^{80}Kr and ^{80}Se tends to underestimate $B_{\beta}-$, probably because the calculated cross section of ^{80}Se is too high; but it seems that variation of $\sigma(^{80}Se)$ alone does not solve the problem.

In summary, we adopt

$$B_{\beta} = 0.50 \pm 0.05 \qquad (34)$$

as the present best value for the branching ratio at ^{79}Se.

In order to derive the effective β-decay rate of ^{79}Se under s-process conditions from this result, we have to evaluate the neutron capture rate $\lambda_n = n_n \ \sigma v_T$ and that means we have to find the neutron density n_n. It has been attempted repeatedly to

determine this parameter from other s-process branchings. In principle there are at least two such branchings which do not depend on temperature for $T < 5 \times 10^8 K$ (^{85}Kr, ^{185}W) and some others where the temperature effect is not very large (^{151}Sm, ^{170}Tm, ^{204}Tl). Up to now, the problem has always been that there was not enough accurate information on cross sections and/or decay schemes to allow for an accurate analysis. We do not want to digress deeply in a comparison of the existing work on the s-process neutron density, which we have listed partly in Table 14. However, some comments might be in order to explain our adopted value for n_n. Although the result of Käppeler et al. (1982) from analysis of the ^{85}Kr branching was reduced by a factor 2 (due to a new ^{86}Kr cross section and the new isomeric ratio in ^{85}Kr) this value appears too high compared to the other data in Table 14. Käppeler et al. (1982) note that their analysis could not solve for a severe overproduction either of ^{86}Kr and ^{87}Rb or of ^{86}Se and ^{87}Sr dependent on how they normalize their analysis. Therefore their value (based on the σN-product of s-only ^{86}Sr) should not be taken as final and one should keep in mind that it could also be 6×10^7 cm^{-3} if the ^{86}Kr normalization would have been used; the ^{85}Kr-branching was therefore not considered in our estimate of the neutron density. The numbers quoted from the ^{151}Sm branching are taken from a recent study of Beer et al. (1983). This work comprises a careful investigation of the temperature dependence of all involved beta decay rates. The ^{170}Tm result is taken from Beer et al. (1981). The problem with this branching and that at ^{185}W is that in both cases the neutron capture probability is very low. For that reason it is very difficult to perform a reliable analysis. In addition, all three branchings contain only one s-only isotope and must therefore be normalized to the σN-curve which is most crucial when the neutron capture part of the branching is weak.

In summary, we are left with two sets of values for the neutron density which group around 5×10^8 and 5×10^7 cm^{-3}. Recent precise cross section measurements for $^{148,150}Sm$ (Winters et al. 1983) indicate, however, that the σN-curve in the mass region $A > 140$ has to be raised by ~ 25 % which implies that the neutron

densities derived from the branchings at ^{170}Tm, ^{185}W and ^{204}Tl have to be increased significantly. For this reason we favour the larger values of the neutron density and adopt $n_n = 3 \pm 2 \times 10^8$ cm^{-3} as a reasonable estimate.

The effective beta decay rate of ^{79}Se can now be calculated

$$\lambda_\beta = \lambda_n \frac{B}{1-B} = 0.5 \pm 0.4 \text{ yr}^{-1} .$$

This leads to an associated half life of $t_{1/2} = 1.4^{-0.6}_{+5.6}$ yr (36) and with this result only a lower limit of $\sim 3 \times 10^8$ K for the mean s-process temperature can be read from Fig. 17.

The main uncertainties of this estimate are of different nature:

(i)   The nuclear physics aspects comprise the unknown beta decay rate from the isomeric state in ^{79}Se and the poorly known capture cross sections which are needed to improve the value for the neutron density. Any further improvement of the situation can be achieved only with better nuclear physics data.

(ii) The assumption that s-process nucleosynthesis can be described by the simple model used and especially by assuming that the two fluence terms are characterized by the same neutron density and temperature. In order to investigate this quantitatively, more reliable analyses in the mass region A>100 are needed to define the conditions for the second irradiation term of equation (17).

Although we find a lower limit of 3×10^8K for the mean s-process temperature, our result is not conclusive with respect to the question whether the ^{22}Ne (α,n) or the ^{13}C(α,n)-reaction was the neutron source of the s-process. These neutron sources are believed to operate at significantly different temperatures (kT>25 keV and kT>10-15 keV, respectively). We feel that the present uncertainties need to be reduced considerably for a detailed discussion (possible differences in T and n_n for the two fluence components, pulsed scenarios).

6. CONCLUSIONS

For the first time the neutron capture cross sections of the stable krypton isotopes 78,80,82,83,84 and of elemental krypton were measured between 3 and 250 keV neutron energy. The experimental uncertainties of the Maxwellian average cross sections for kT = 30 keV are typically 5 - 12 %.

The measurements were supplemented by detailed cross section calculations using the Hauser-Feshbach model. These calculations were carried out with consistent sets of model parameters which were evaluated using as much experimental information as possible.

Together with the decay parameters of ^{79}Se and ^{80}Br these data were used for a study of the s-process flow through the mass region 78<A<84 with special emphasis on the branching at ^{79}Se. Normalization of the σN-value of ^{82}Kr to the σN-curve of Käppeler et al. (1982) yields a krypton abundance of $N^{\ominus}_{(Kr)} = 57 \pm 15$ which is in fair agreement with recent abundance compilations (Cameron 1981, Anders and Ebihara 1982). The new cross sections allowed also for a decomposition of the observed abundances into their s- and r-process contributions.

The s-process branching at ^{79}Se is characterized by a very steep temperature dependence and can therefore be used to estimate the actual s-process temperature. It was found that - in spite of the new cross sections - a reliable interpretation is not possible unless more quantitative information is available for the beta decay branch of the isomeric state in ^{79}Se. Nevertheless, the present estimate tends to confirm the commonly assumed s-process temperature of $\sim 3 \times 10^{8}$K.

Table 1   Isotopic composition of the samples

| Sample | Enrichment (%) in | | | | | |
	^{78}Kr	^{80}Kr	^{82}Kr	^{83}Kr	^{84}Kr	^{86}Kr
"Kr-78"	8.8	34.8	34.8	9.5	11.8	0.3
"Kr-80"	4.1	93.8	2.1	-	-	-
"Kr-82"	0.2	20.2	75.6	3.8	0.2	-
"Kr-83"	-	-	16.0	71.4	12.6	-
"Kr-84"	-	-	-	-	100.0	-
"Kr-nat"	0.35	2.25	11.6	11.5	57.0	17.3

Table 2   Parameters of the neutron source and the
accelerator

Neutron producing reaction	$^{7}Li(p,n)^{7}Be$
reaction threshold energy	1.881 MeV
neutron spectrum	$4 < E_n < 250$ keV, continuous
proton energy	2.025 MeV
accelerator repetition rate	1 MHz
typical beam current	7 μA
pulse width	< 1 ns
long term machine stability	$< 10^{-3}$

Table 3   Maxwellian average cross sections of the measured
               Kr-isotopes as a function of kT (Reference Au
               cross section is ENDF/B-IV)

	$\langle\sigma v\rangle/v_T$ (mb)						
	kT = 20 keV	25	30	35	40	45	50
^{78}Kr	386±47	370±45	359±44	338±41	326±40	315±38	306±37
^{80}Kr	317±16	288±15	265±13	248±13	234±12	223±11	213±11
^{82}Kr	103± 7	94± 7	87± 6	82± 6	78± 6	75±5	72± 5
^{83}Kr	334±20	287±17	250±15	228±14	209±12	194±11	182±11
^{84}Kr	49.5±5.7	42.2±4.8	37.3±4.3	33.7±3.9	31.1±3.6	29.1±3.3	27.5±3.1
^{nat}Kr	81± 5	70± 4	63± 4	58±3.5	54± 3	51± 3	48± 3

Table 4   Sources and magnitudes of the experimental
           uncertainties (%).

Uncertainty originating from	Rel. contribution to the uncertainty in $\langle \sigma v \rangle / v_T$
Au standard	$\sim$ 3
gamma-ray self-absorption in the sample	$\sim$ 1
neutron scattering and self-absorption in the sample	$\sim$ 2
pile-up correction	$\sim$ 1
lower threshold correction	$\sim$ 0.5
sample mass determination	$\sim$ 1-2
time dependent background subtraction	$\sim$ 1-2
weighting function	$\sim$ 0.5-1
effective neutron binding energy	$\sim$ 2-3
isotopic impurities	$\sim$ 2-10
statistics	$\sim$ 2-3
Total	$\sim$ 5 - 12

Table 5 . Comparison of s- and p-wave strength functions and scattering radii as calculated with our OMP sets to the respective values taken from systematics or from experiment (Mughabghab and Garber 1973)

| Target Isotope | Mughabghab and Garber (1973) Systematics | | | Exp. | This work | | |
	$S_0 \times 10^4$	$S_1 \times 10^4$	R(fm)	$S_0 \times 10^4$	$S_0 \times 10^4$	$S_1 \times 10^4$	R(fm)
^{76}Se	1.6	2.2	6.8	$1.7 \pm .7$	1.5	2.2	7.1
^{78}Se	1.5	2.6	6.8	$1.2 \pm .3$	1.4	2.5	7.1
^{79}Se	1.4	2.8	6.8		1.35	2.65	7.0
^{80}Se	1.35	3.0	7.0	$1.6 \pm .6$	1.3	2.85	7.0
^{79}Br	1.4	2.8	6.8	$1.2 \pm .18^{+)}$	1.3	2.9	6.9
^{81}Br	1.3	3.2	6.8	$1.2 \pm .18^{+)}$	1.2	3.4	6.85
^{78}Kr	1.5	2.6	6.8		1.4	2.5	7.05
^{79}Kr	1.4	2.8	6.8		1.35	2.6	7.0
^{80}Kr	1.35	3.0	7.0		1.3	2.85	7.0
^{81}Kr	1.3	3.2	7.0		1.3	3.1	6.95
^{82}Kr	1.2	3.4	7.0		1.25	3.3	6.9
^{83}Kr	1.15	3.6	7.0		1.2	3.55	6.9
^{84}Kr	1.1	3.8	7.0		1.2	3.8	6.85

[+)] values deduced from an elemental sample

Table 6   Evaluation of the level density parameter $\underline{a}$ from experimental data

(average capture cross sections or neutron resonance schemes)

Target Isotope	$\sigma_{n,\gamma}^{Exp}$ *) (mb)	$\Gamma_{\gamma}^{\ell=0}$ # (meV)	D_{OBS}^{σ} (eV)	$\underline{a}^{\sigma}$ (MeV^{-1})	D_{OBS}^{RES} § (eV)	N^{RES}	$\underline{a}^{RES}$ (MeV^{-1})
^{74}Se					500 ± 250	6	$13.6 +^{1.1}_{-0.7}$
^{76}Se					760 ± 300	13	$14.2 +^{0.9}_{-0.5}$
^{77}Se					136 ± 30	23	$13.0 +^{0.3}_{-0.4}$
^{78}Se					1700 ± 500	13	$13.7 +^{0.7}_{-0.5}$
^{80}Se					3500 ± 2000	10	$13.1 +^{1.5}_{-0.8}$
^{79}Br					57 ± 23	6	$13.0 +^{0.5}_{-0.4}$
^{78}Kr	357 ± 44	$230^+ \pm 50^+$	225 ± 90	$13.9 +^{0.7}_{-0.3}$			
^{80}Kr	257 ± 15	290 ± 30	460 ± 90	$13.6 +^{0.4}_{-0.3}$			
^{82}Kr	84 ± 6	$230^+ \pm 50^+$	1300 ± 400	$12.8 +^{0.4}_{-0.3}$			
^{83}Kr	251 ± 16	215 ± 50	95 ± 25	$11.5 +^{0.3}_{-0.3}$			
^{84}Kr	36.5 ± 4.5	$215^+ \pm 50^+$	4000 ± 1600	$11.6 +^{0.7}_{-0.5}$			

*This work, # Maguire et al. (1978), § Mughabghab and Garber (1973),
+ Assumed value

Table 7   Adopted level schemes of ^{79}Se up to
the excitation energy E_{cut} for calculating the
isomeric ratio IR*

Level Number	Energy (MeV)	Spin	Parity	Branching ratio (Level number, probability in %)		
				^{79}Se		
1	0.0	3.5	+			
2	0.096	0.5	−	(Isomeric state)		
3	0.130	4.5	(+)	(1,100)		
4	0.365	2.5	−	(1,100)		
5	0.499	1.5	(+)	(2,100)		
6	0.528	0.5	(−)	(2,100)		
7	0.572	2.5	−	(2,100)		
8	0.620	2.5	+	(1,34)	(3,33)	(4,33)
9	0.729	2.5	+	(1,100)		
10	0.790	4.5	−	(1,50)	(3,30)	(4,20)
11	0.819	3.5	+	(1,20)	(3,80)	
12	0.897	5.5	+	(1,10)	(3,90)	
13	0.974	1.5	−	(2,80)	(4,15)	(5,5)
14	0.982	1.5	+	(1,100)		
15	1.00	5.5	+	(1,10)	(3,90)	
16	1.06	3.5	+	(1,20)	(3,30)	(7,50)
17	1.071	6.5	+	(12,100)		
18	1.079	1.5	−	(4,100)		

*   The Jπ values between brackets and underlined gamma decay
probabilities have been assigned as described in the text.

Table 8   Comparison between calculated and experimental results for the average radiative width*

Target Isotope		ℓ = 0		ℓ = 1			
^{76}Se	Experimental	230 ± 50 (1/2$^+$, 5)					
	Calculated	254		230 (1/2$^-$)	217 (3/2$^-$)		
^{78}Se	Experimental	230 ± 55 (1/2$^+$, 4)					
	Calculated	243		223 (1/2$^-$)	210 (3/2$^-$)		
^{79}Se	Experimental						
	Calculated	132 (3$^+$)	124 (4$^+$)	334 (2$^-$)	303 (3$^-$)	233 (4$^-$)	199 (5$^-$)
^{80}Se	Experimental	230 ± 100 (1/2$^+$,2)					
	Calculated	236		236 (1/2$^-$)	200 (3/2$^-$)		
^{79}Br	Experimental	360 ± 40 (1$^-$, 2)	315+50(2$^-$,3)				
	Calculated	362	314	287 (0$^+$)	368 (1$^+$)	320 (2$^+$)	266 (3$^+$)
^{81}Br	Experimental	278 ± 50 (1$^-$,1)	275+45(2$^-$,1)				
	Calculated	272	247	278 (0$^+$)	272 (1$^+$)	247 (2$^+$)	218 (3$^+$)
^{78}Kr	Experimental	242 (1/2$^+$)					
	Calculated			231 (1/2$^-$)	220 (3/2$^-$)		
^{79}Kr	Experimental						
	Calculated	266 (0$^-$)	296 (1$^-$)	266 (0$^+$)	262 (1$^+$)	253 (2$^+$)	
^{80}Kr	Experimental	290 ± 30 (?,1)					
	Calculated	260 (1/2$^+$)		249 (1/2$^-$)	234 (3/2$^-$)		
^{81}Kr	Experimental						
	Calculated	226 (3$^+$)	105 (4$^+$)	259 (2$^-$)	241 (3$^-$)	208 (4$^-$)	185 (5$^-$)
^{82}Kr	Experimental	242 (1/2$^+$)					
	Calculated			187 (1/2$^-$)	184 (3/2$^-$)		
^{83}Kr	Experimental	215 ± 50 (?,2)					
	Calculated	211 (4$^+$)	179 (5$^+$)	285 (3$^-$)	215 (4$^-$)	194 (5$^-$)	159 (6$^-$)
^{84}Kr	Experimental						
	Calculated	266 (1/2$^+$)		242 (1/2$^-$)	239 (3/2$^-$)		

* The respective J^π values and the number of resonances taken for averaging are given in parenthesis. Experimental values are from Table 4.2 or from Mughabghab and Garber (1973).

§ Average experimental values for Γ_γ cannot be quoted in this context due to fluctuations; the calculated values represent only the contribution from statistical capture.

Table 9   The final parameter set used for the cross section calculations

Target Isotope	a (MeV^{-1})	U_x (MeV)	E_{cut} MeV	σ^2_{LVL}	β	E_1 MeV	Γ_1 MeV	σ_1 mb	E_2 MeV	Γ_2 MeV	σ_2 mb
^{76}Se	13.9*	7.3	.581	5.5	.32	14.85	3.45	75	17.6	4.85	103
^{78}Se	13.7	6.8	1.079	4.9	.25	14.8	3.45	78	17.5	4.8	106
^{79}Se	12.9	6.3	2.090	2.6,6.3§	.21	14.35	3.3	80	17.6	4.85	107
^{80}Se	13.0*	5.8	1.210	2.7	.17	15.8	3.65	74	17.15	4.7	111
^{79}Br	13.0	7.1	.400	2.2	.25	14.2	3.3	82	17.6	4.85	107
^{81}Br	12.4*	6.0	.100	4.0	.17	14.7	3.4	81	17.4	4.75	111
^{78}Kr	13.9	7.4	.907	6.1,12.2§	.32	14.8	3.4	78	17.5	4.8	106
^{79}Kr	13.0*	7.0	1.600	10.0	.29	14.7	3.4	79	17.5	4.8	108
^{80}Kr	13.6	7.0	.300	5.0	.25	14.7	3.4	80	17.4	4.8	110
^{81}Kr	12.8*	6.5	1.885	5.5§,16.0	.21	15.2	3.5	78	17.2	4.7	112
^{82}Kr	12.8	5.9	1.099	7.0	.17	15.7	3.6	77	17.1	4.7	114
^{83}Kr	11.5	5.2	3.300	6.3	.13	15.6	3.6	78	17.0	4.7	116
^{84}Kr	11.3*	4.5	2.160	4.3, 9.0§	.10	15.6	3.6	79	17.0	4.6	118

*   Value adopted from systematics of Fig. 12

§   Value adopted as being most plausible according to Fig. 13.

Table 10   Calculated neutron capture cross sections between 1 and 1000 keV

Neutron Energy (keV)	Capture Cross Section (mb)												
	^{76}Se	^{78}Se	^{79}Se	^{80}Se	^{79}Br	^{81}Br	^{78}Kr	^{79}Kr	^{80}Kr	^{81}Kr	^{82}Kr	^{83}Kr	^{84}Kr
1	1100	643	2800	362	5510	2850	2710	6640	1696	5900	766	2570	335
5	390	254	760	149	1770	950	878	2150	607	1930	301	880	135
10	273	173	470	95	1180	650	618	1440	435	1300	200	560	84
15	220	136	350	72	960	510	514	1170	356	1050	155	414	62
20	188	113	290	59	830	430	450	1025	307	910	128	332	51
25	165	98	250	51	740	375	406	927	272	810	110	278	43
30	149	88	218	45.5	672	333	372	855	245	738	98	241	38
35	164	80	196	41.5	620	301	345	800	225	679	88	213	35
40	127	74	180	38.4	576	275	323	755	209	631	81	192	32
60	103	61	139	31.5	461	211	265	630	167	459	65	140	27
80	92	54	117	27.8	392	176	232	550	146	360	58	113	23
100	85	50	103	25.2	347	154	212	500	133	300	54	97	21
150	75	43	66	21.4	283	124	186	410	116	223	47.5	74	18
200	69	39.5	50	19.4	249	108	174	290	108	185	44	63	16.7
400	61	35.5	28	17.4	92	61	160	121	98	113	41	46	15.2
600	41	36.6	20	17.6	56	39	94	71	103	56	43	42	15.1
800	28.6	16.4	17	8.0	42	27	81	47	55.6		35.3	39.5	15.8
1000	26.5	14.5	12	6.6	32	22.5	80	36	50.2		21.5	37.8	8.6

Table 11   Maxwellian average capture cross sections
for kT = 30 keV: comparison of present theoretical
and experimental values with previous results

Target Isotope	$\langle\sigma\rangle_{30}$ keV				This work	
	Holmes et al. (1976)	Leugers et al. (1979)	Prince (1979)	Harris (1981)	Calc.	Exp.
^{76}Se	83	138	–	126	149	
^{78}Se	49	80	–	89.5	90+18	
^{79}Se	260	274	–	514	218+50	
^{80}Se	41	41	–	34	47	
^{79}Br	520	661	–	749	657	
^{81}Br	460	360	–	596	322	
^{78}Kr	203	284	–	253	368	359 ± 44
^{79}Kr	1130	–	–	–	857	
^{80}Kr	148	228	185	156	242	265 ± 13
^{81}Kr	1030	800	–	994	682	
^{82}Kr	122	95	77	79	100	87 ± 6
^{83}Kr	571	345	295	259	237	350 ± 16
^{84}Kr	25	30	29	13	40	37.3 ± 4.3

Additional experimental cross sections $\langle\sigma\rangle_{30\ keV}$ (mb):

^{80}Se 35 ± 5

^{79}Br 800 ± 150   compilation by Benzi et al. (1973)

^{81}Br 360 ± 70

Table 12   Parameters for the decay of ^{79}Se under s-process conditions

Isotope	Level J^π, Energy (keV)	lg ft [+]	T_β-(yr)	λ_i^* [§] (yr^{-1})	$P_i \lambda_i$ [§] (yr^{-1})
^{79}Se	$7/2^+$, 0	10.17	6.5×10^4	1.4×10^{-5}	1.3×10^{-5}
	$1/2^-$, 96	5.4 (0.5)	6.0×10^{-2}	15.3	1.5×10^{-1}
	$9/2^+$, 130	5.4 (0.6)	2.1	0.75	9.5×10^{-3}
	$5/2^-$, 365	5.4 (0.6)	2.7×10^{-2}	26.5	9.7×10^{-5}
					$t_{1/2}^* = 4.3$ yr
^{79}Br	$9/2^+$, 207	5.4 (1.1)	9.4	2.1×10^{-2}	5.3×10^{-5}
					$t_{1/2}^* = 1.3 \times 10^4$ yr

[+] estimates from Conrad (1976)

[§] stellar rates from Conrad (1976) including effects due to almost complete ionization (bound state beta decay, modification of electron capture etc.)

Table 13   Decomposition of isotopic abundances into s- and
r-process contributions (p-process neglected)

Isotope	σN_s^+	N_s	$N^{\odot}$ §	$N^{\odot}-N_s \approx N_r$	$N_r/N^{\odot}$ (%)
^{75}As	845	1.72±0.44	6.79±0.75	5.1±1.4	75
^{76}Ge			9.20±0.86	9.2±0.9	100
^{76}Se	783	5.25±2.1	5.59±0.36	–	0
*^{77}Se	767	1.81±0.92	4.72±0.30	2.9±1.0	62
^{78}Se	693	7.70±1.9	14.6 ±0.93	6.9±2.1	47
^{79}Se	332		decayed to ^{79}Br		
^{80}Se	289	6.14±2.46	30.9±1.98	23.7±3.2	76
^{82}Se			5.70±0.36	5.7±0.4	100
^{79}Br	341	2.04±0.52	5.98±1.14	3.9±1.3	66
^{81}Br	281	2.22±0.72	5.82±1.10	4.5±1.7	77
^{80}Kr	329	1.28±0.33	1.28±0.14#	–	0
^{81}Kr	325		decayed to ^{81}Kr		
^{82}Kr	555	6.61±1.72	6.61±0.73#	–	0
^{83}Kr	540	2.15±0.56	6.56±1.04#	4.4±2.1	67
^{84}Kr	450	12.3 ±3.2	32.5 ±5.1#	20.2±5.7	61

+   Calculated from $\sigma N(78_{Se}) = \sigma N^1(78_{Se}) + \sigma N^2(78_{Se}) = (276 + 416)$ mb
(Käppeler et al.,1982)

§   Anders and Ebihara (1982)

*   σ taken from Woosley et al. (1978)

this work

Table 14   Estimates for the neutron density during the s-process

Branching point	temperature dependent	$B_{\beta-}$	n_n (in units of 10^7 cm^{-3})	Ref	Problems
^{85}Kr	no	0.5	(30 – 200)	(1)	overprocudtion of ^{86}Kr and ^{87}Rb, therefore n_n possibly too high
^{151}Sm	yes	$\sim$ 0.01	20 – 100	(2)	^{154}Gd cross section needs confirmation, temperature effects
^{170}Tm	yes	$\sim$ 0.9	1 – 4	(3)	$B_{\beta-}$ very large $\rightarrow$ systematic uncertainty
^{185}W	no	$\sim$ 0.95	20 – 60	(4)	same as for ^{170}Tm, but no temperature dependence
^{204}Tl	no	0.8	1 – 8	(5)	lead abundance uncertain

References: (1) Käppeler et al. (1982), (2) Beer et al. (1983), (3) Beer et al. (1981), (4) Käppeler (1983)   , (5) Macklin and Winters (1976)

- 47 -
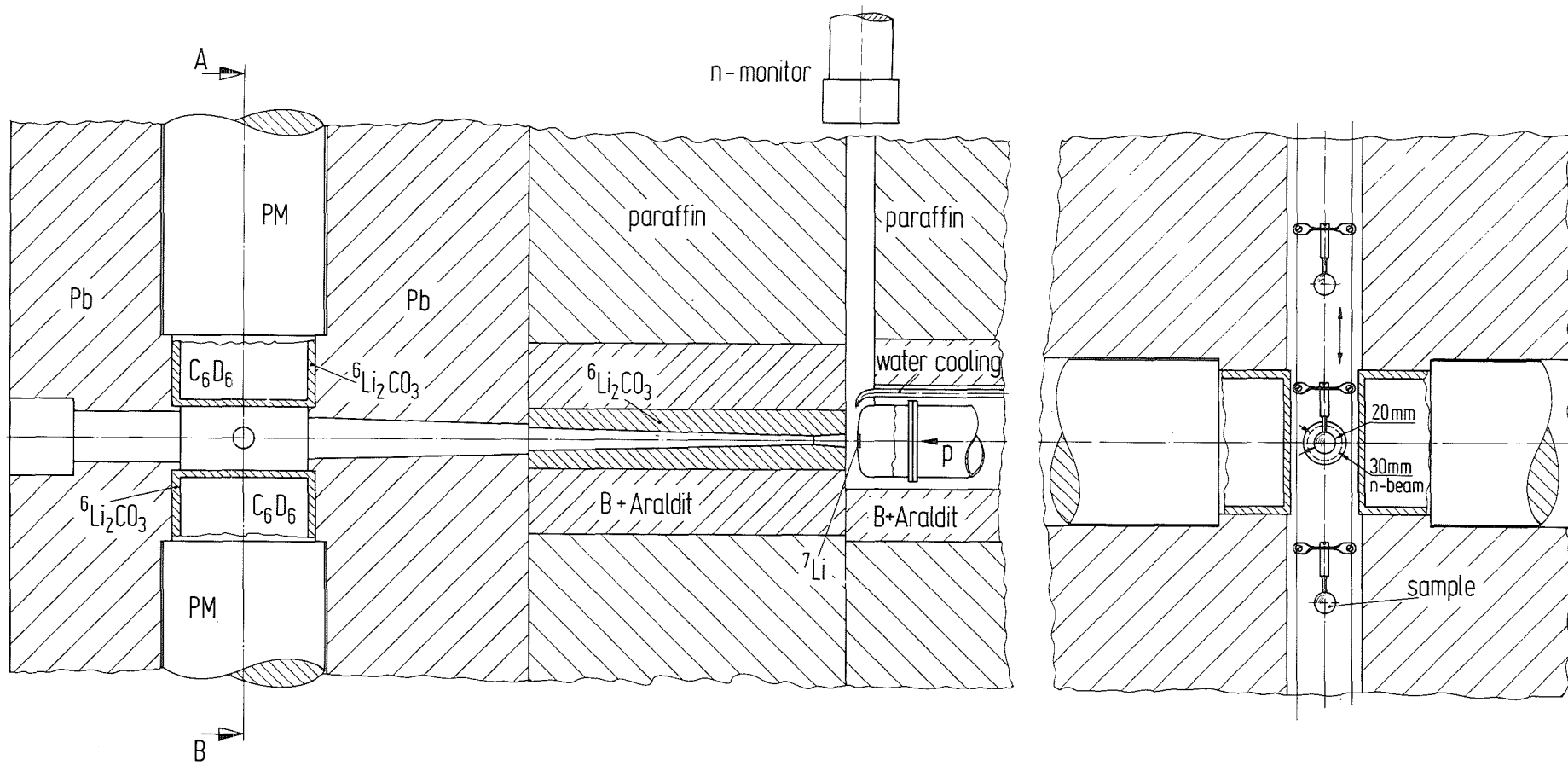
Fig. 1   Schematic experimental set-up

NEUTRON MONITOR
(^{6}Li–GLASS)

C_6D_6–SCINTILLATORS
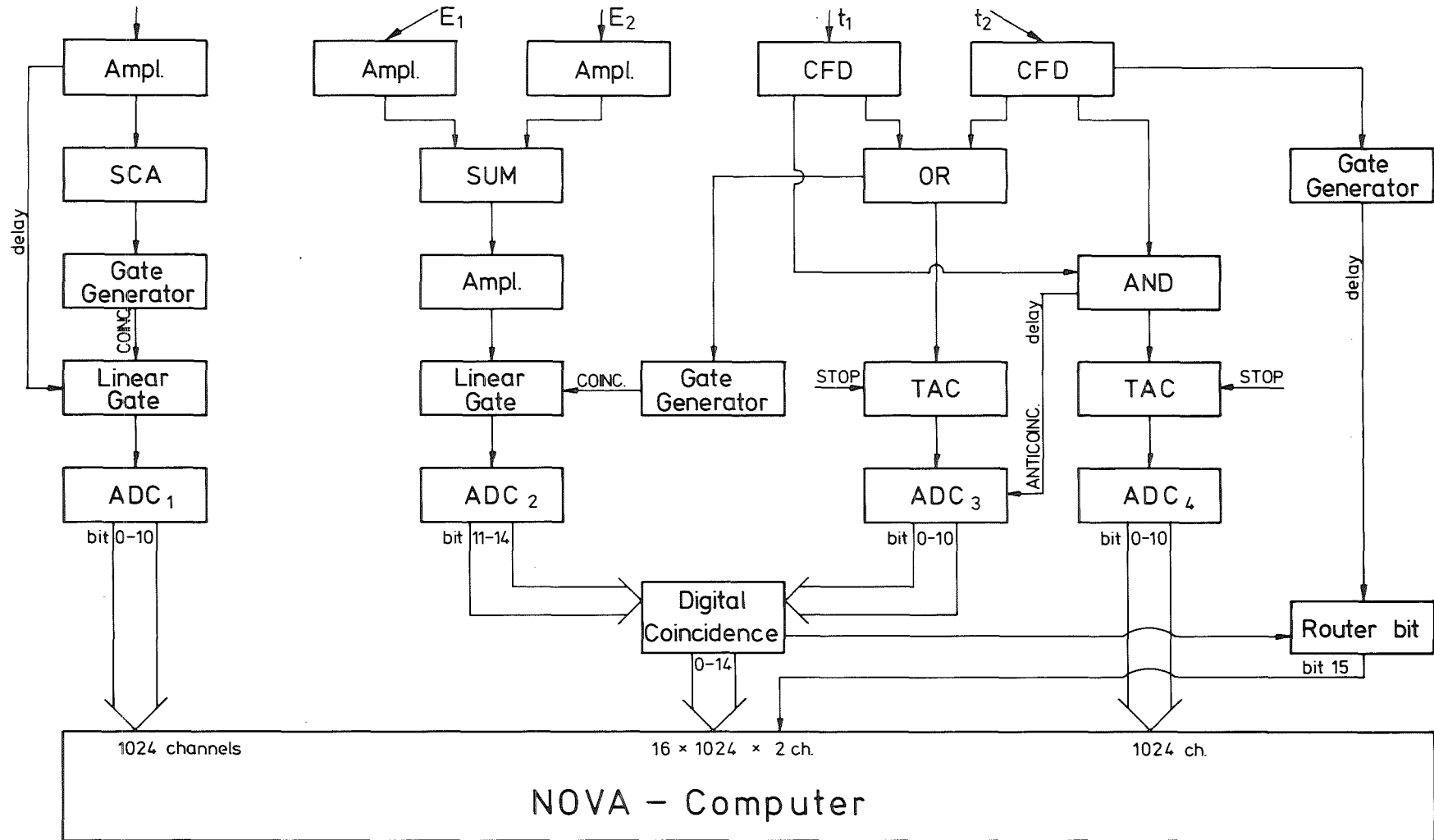
Fig. 2   Block diagram of the electronics and the data acquisition system
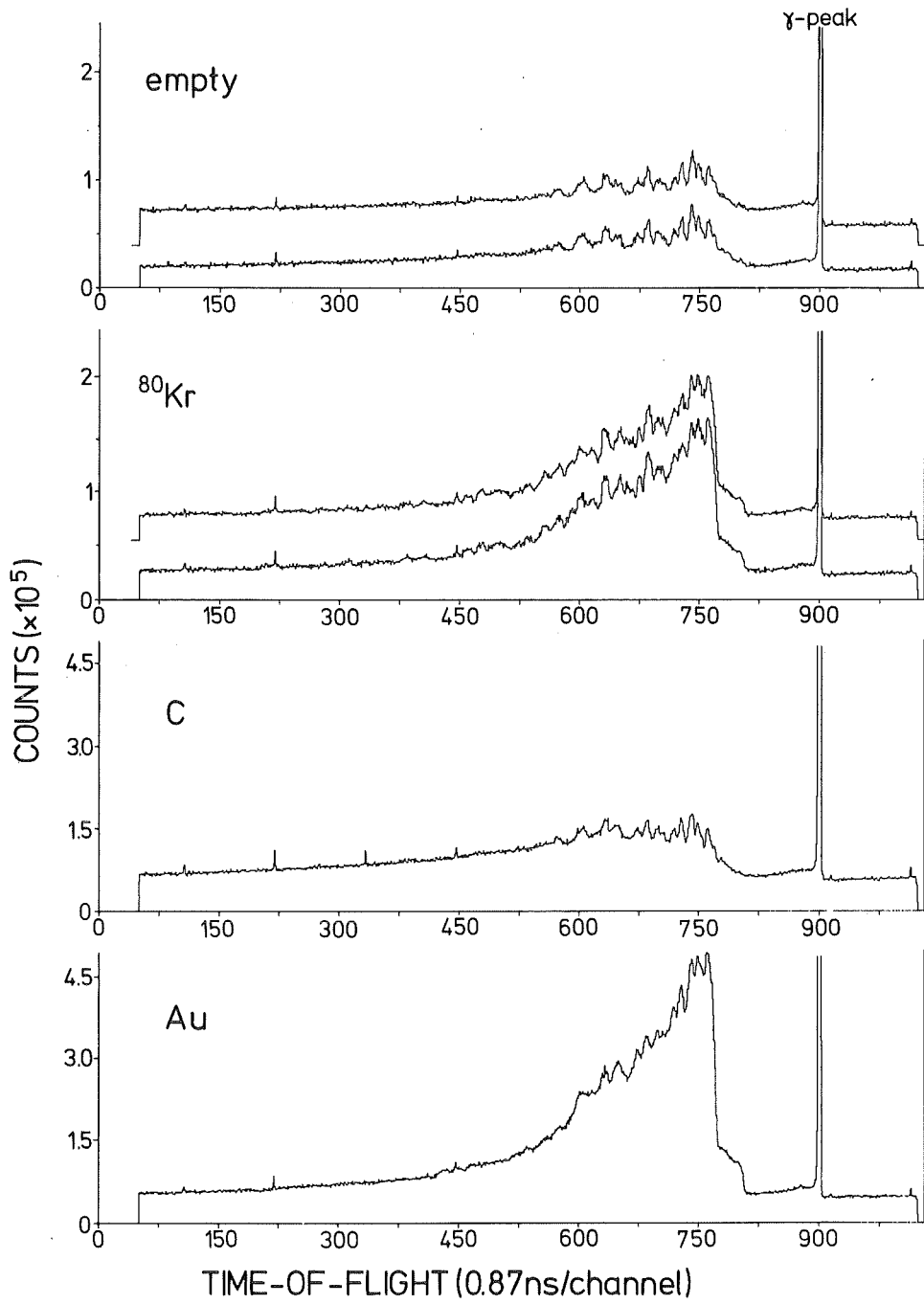
Fig. 3   Summed TOF-spectra (without corrections)
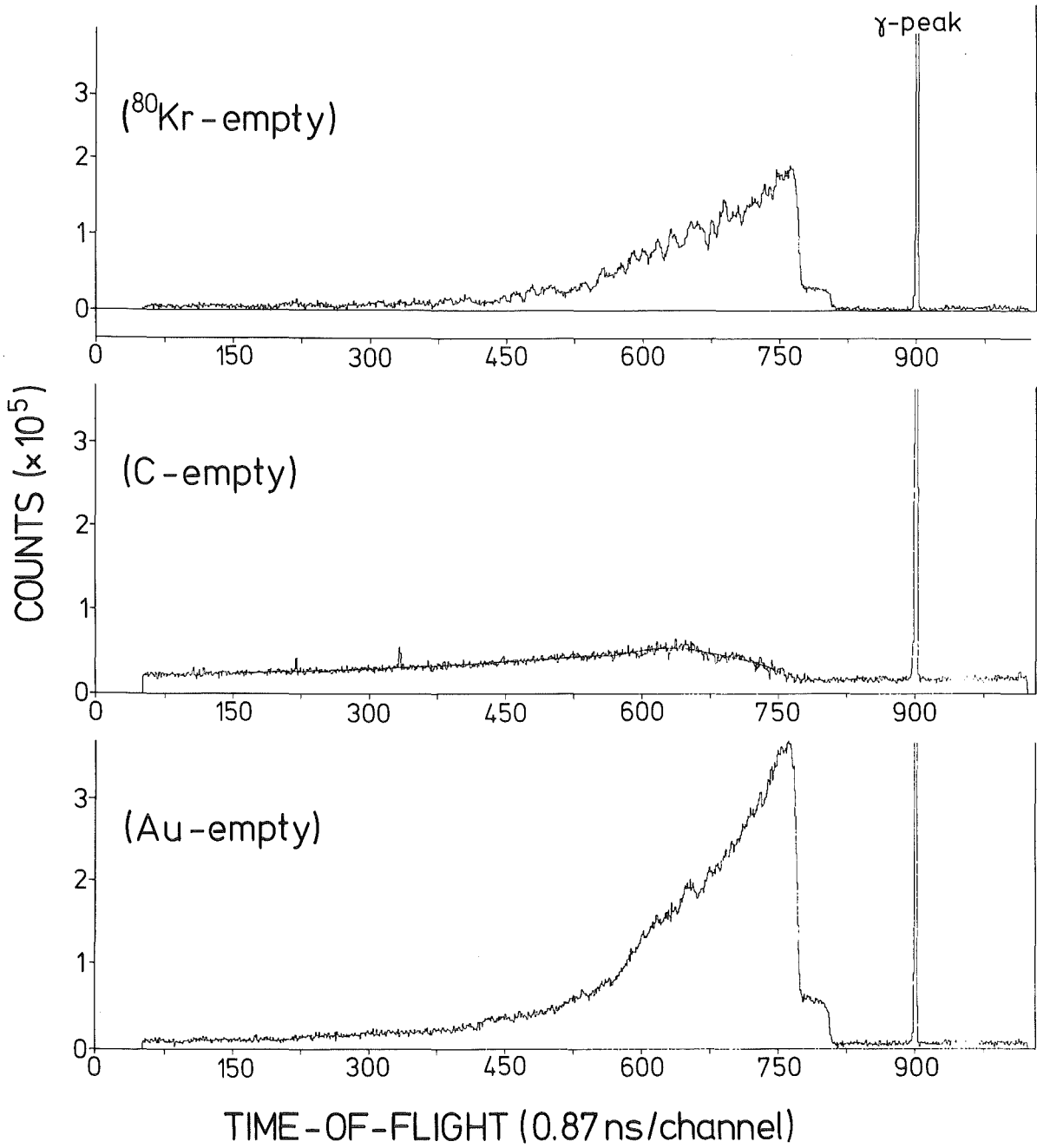
Fig. 4   TOF-spectra after subtraction of the
          spectrum for the empty canning
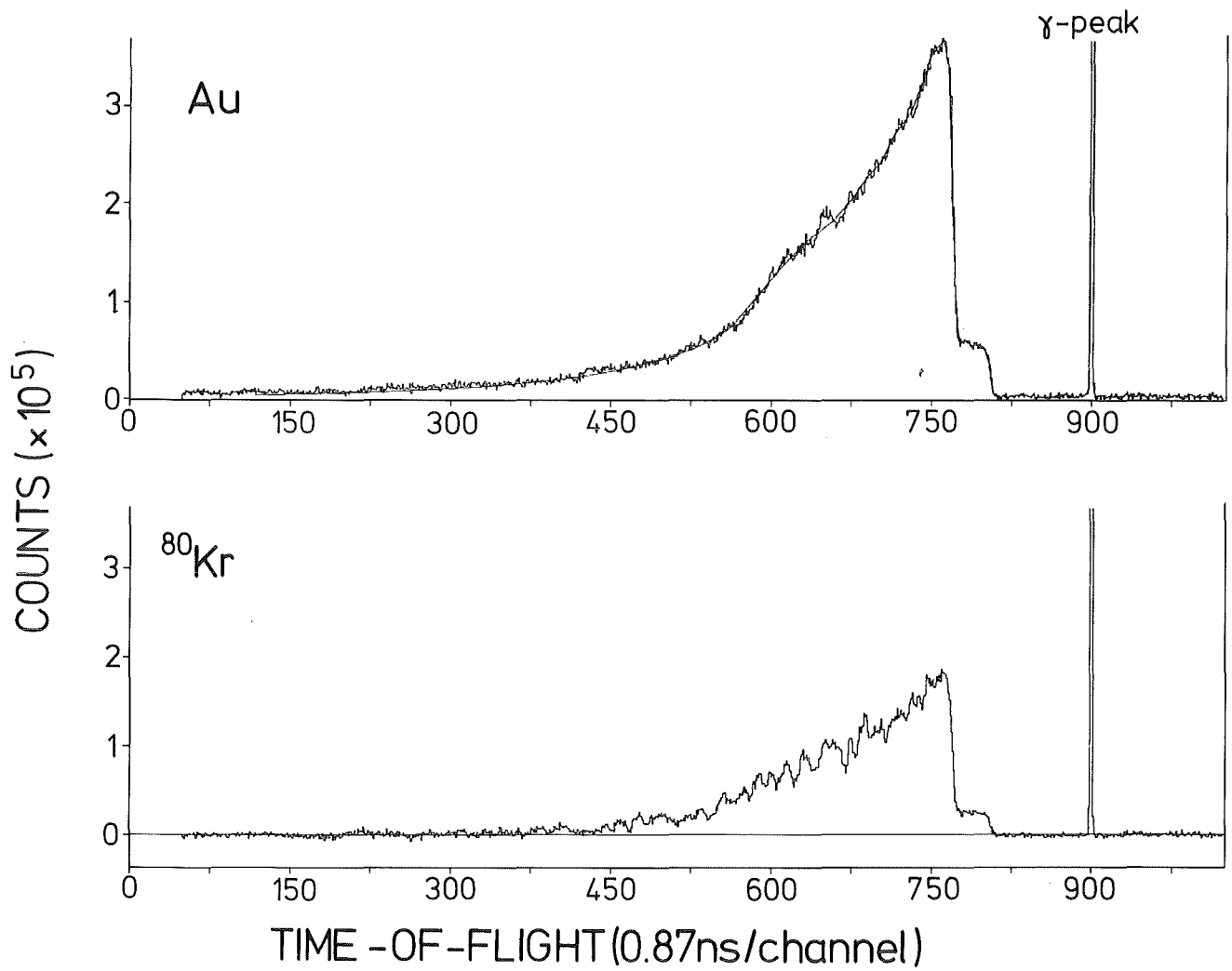
Fig. 5 Final TOF spectra corrected for neutron scattering
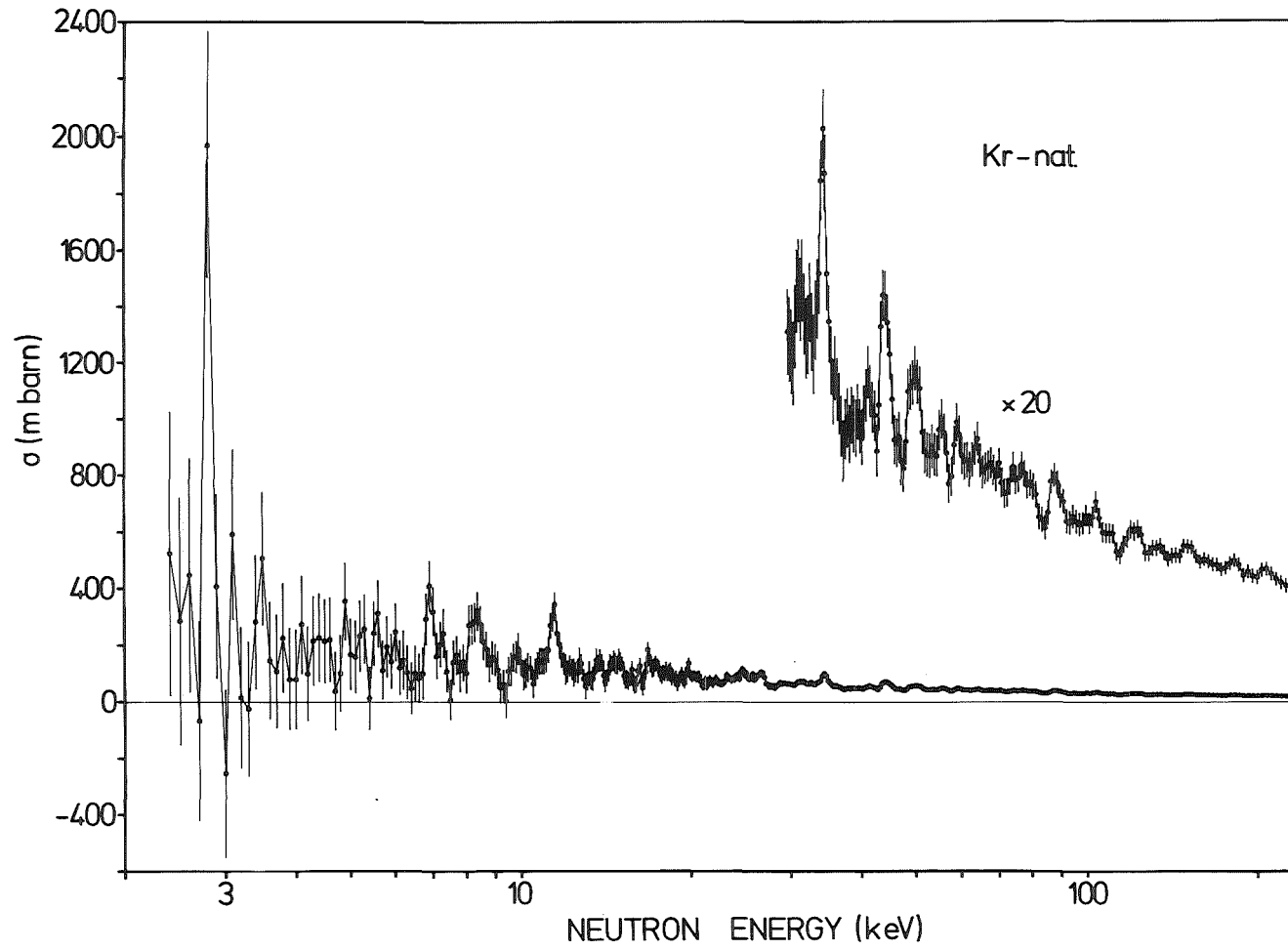
Fig. 6 Capture cross section for natural krypton
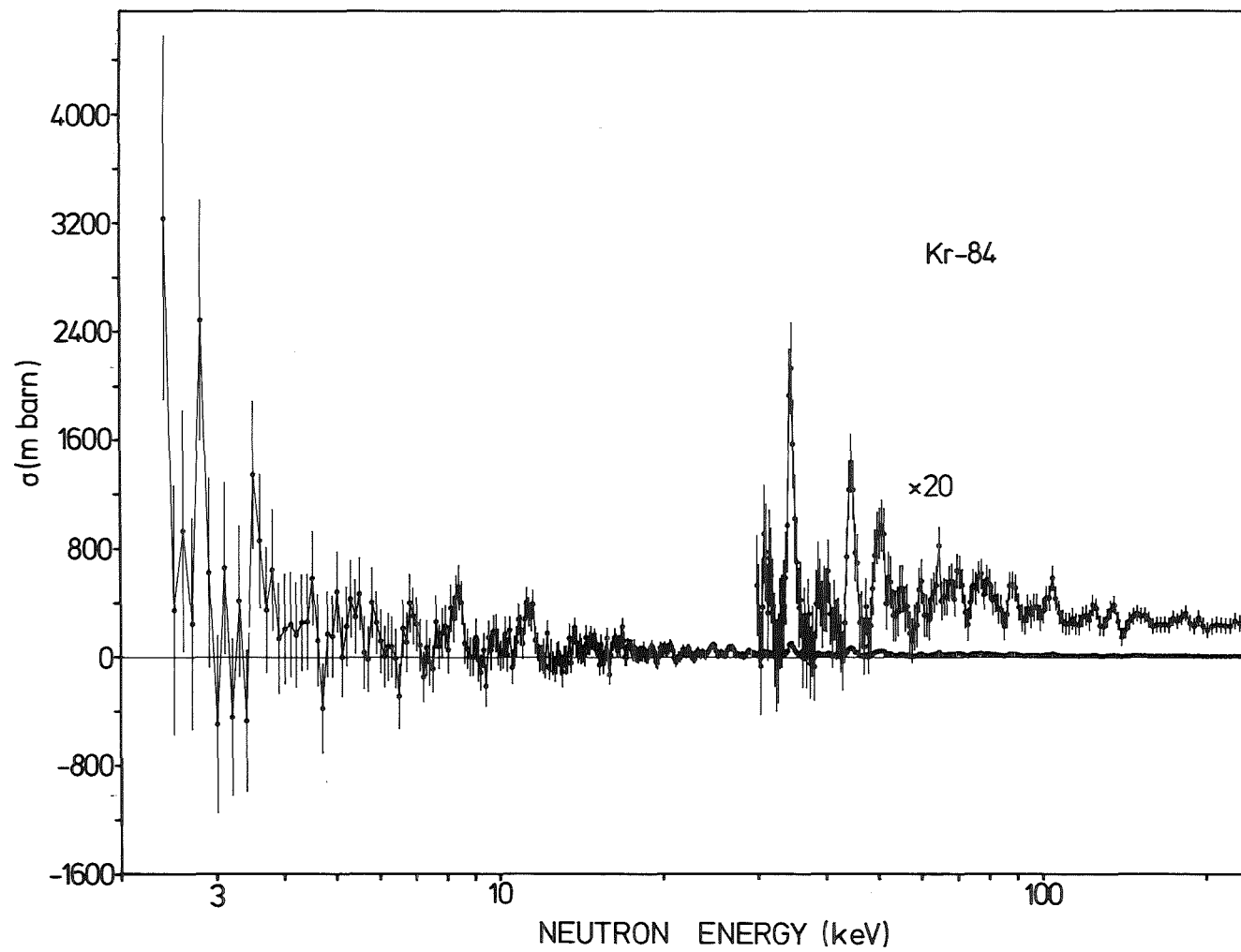
Fig. 7 Capture cross section for ^{84}Kr
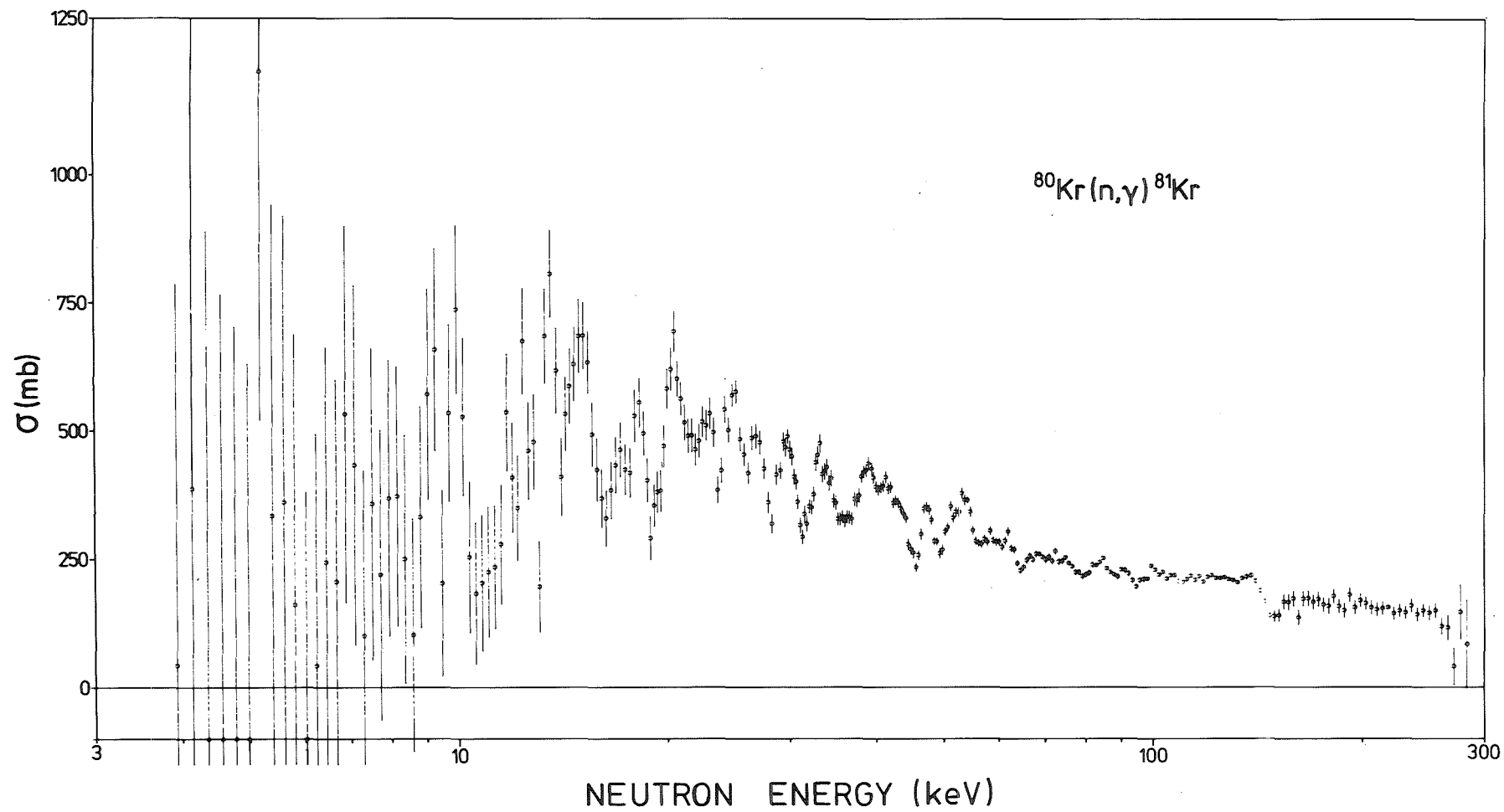
Fig. 8   Capture cross section for ^{80}Kr
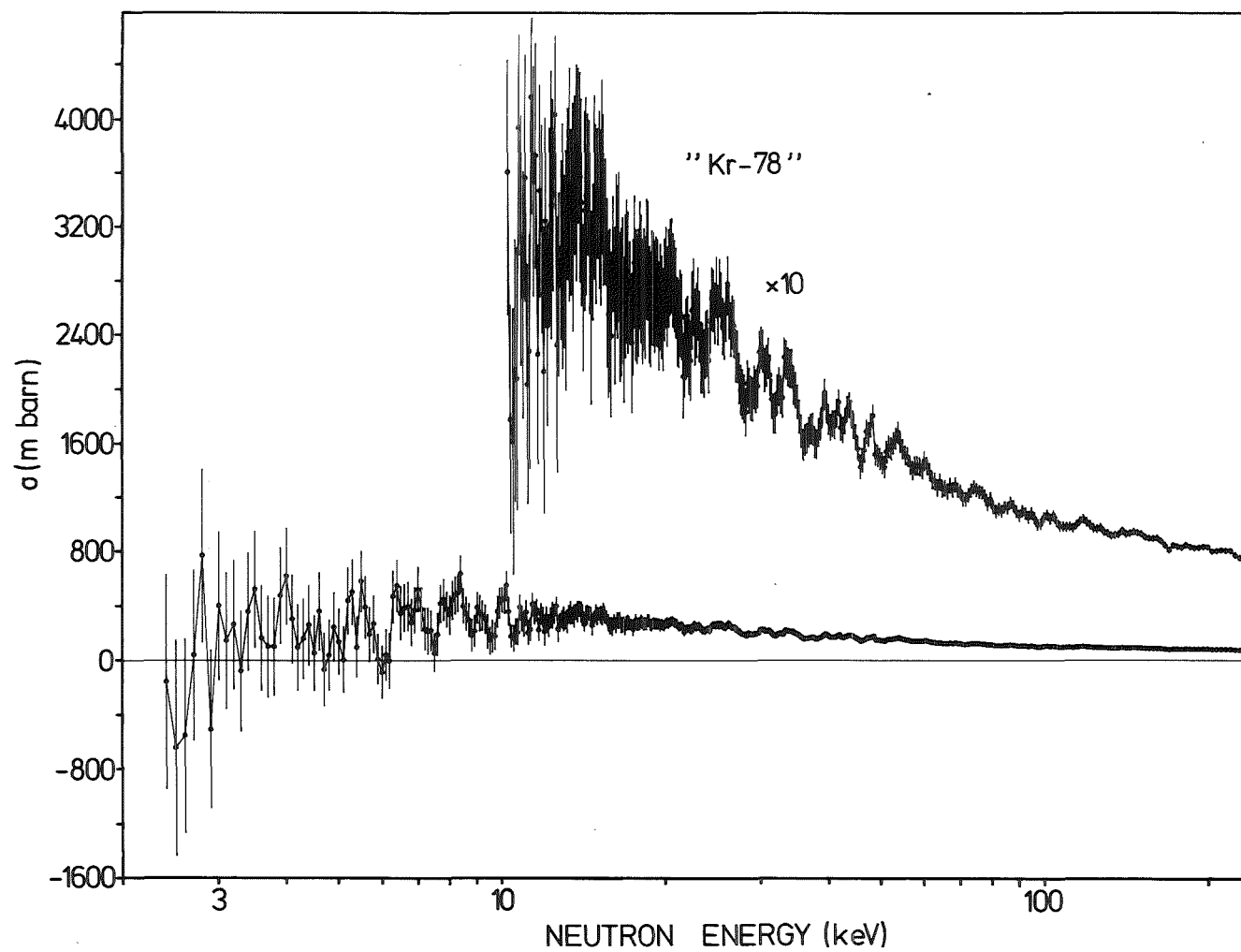
Fig. 9 Capture cross section for the mixture enriched in ^{78,80}Kr
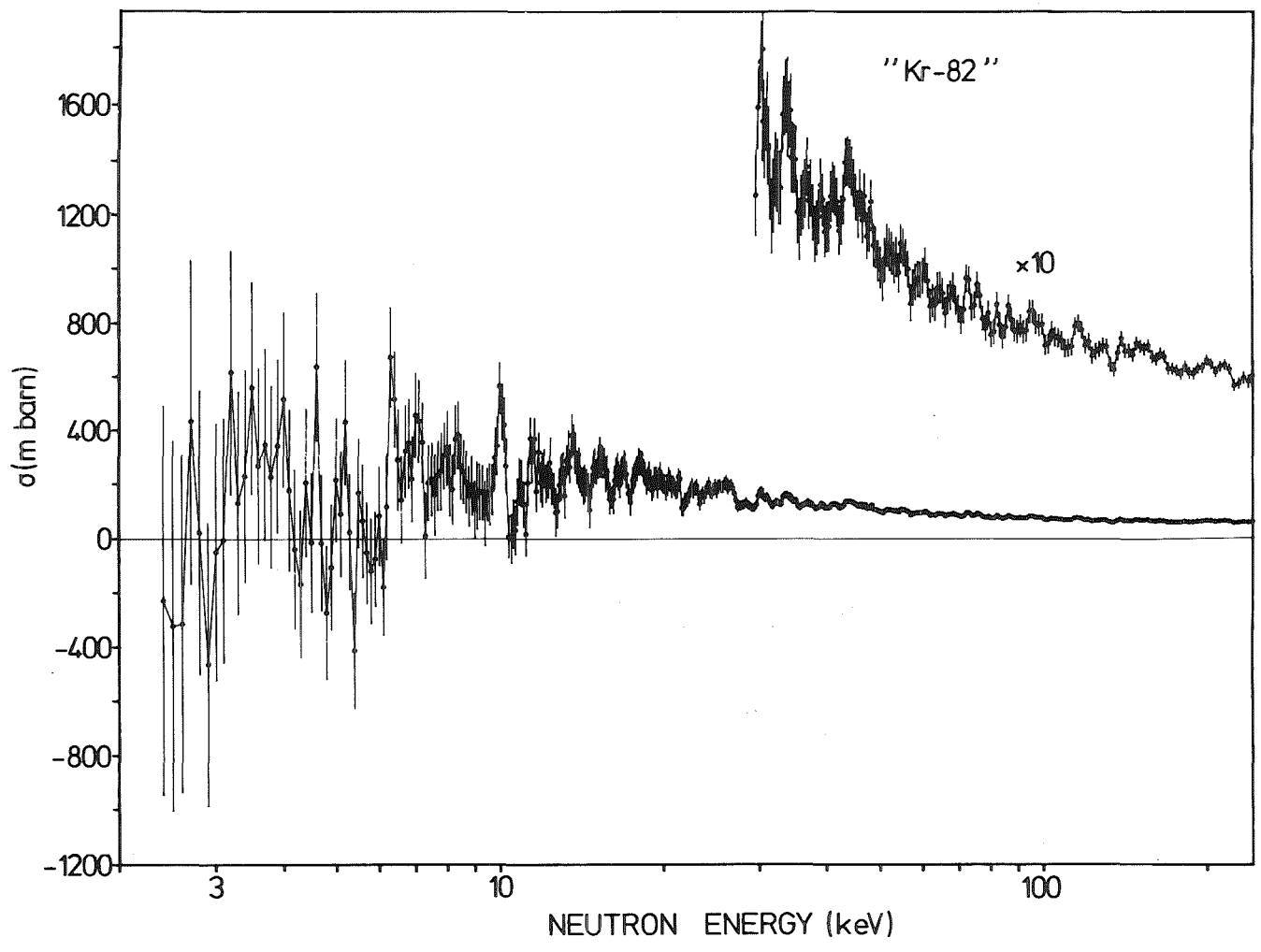
Fig. 10   Capture cross section for the mixture enriched in ^{82}Kr
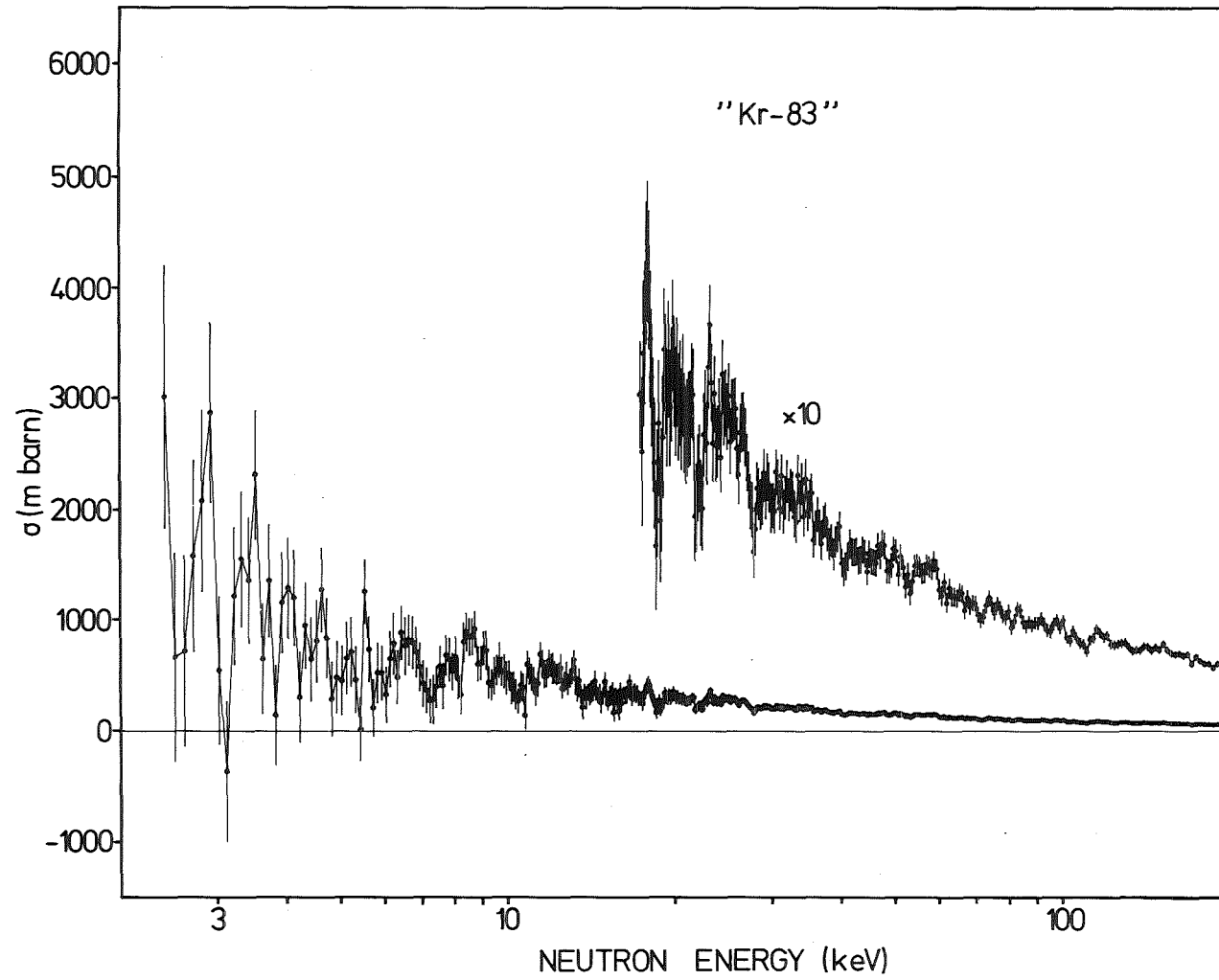
Fig. 11   Capture cross section for the mixture enriched in ^{83}Kr
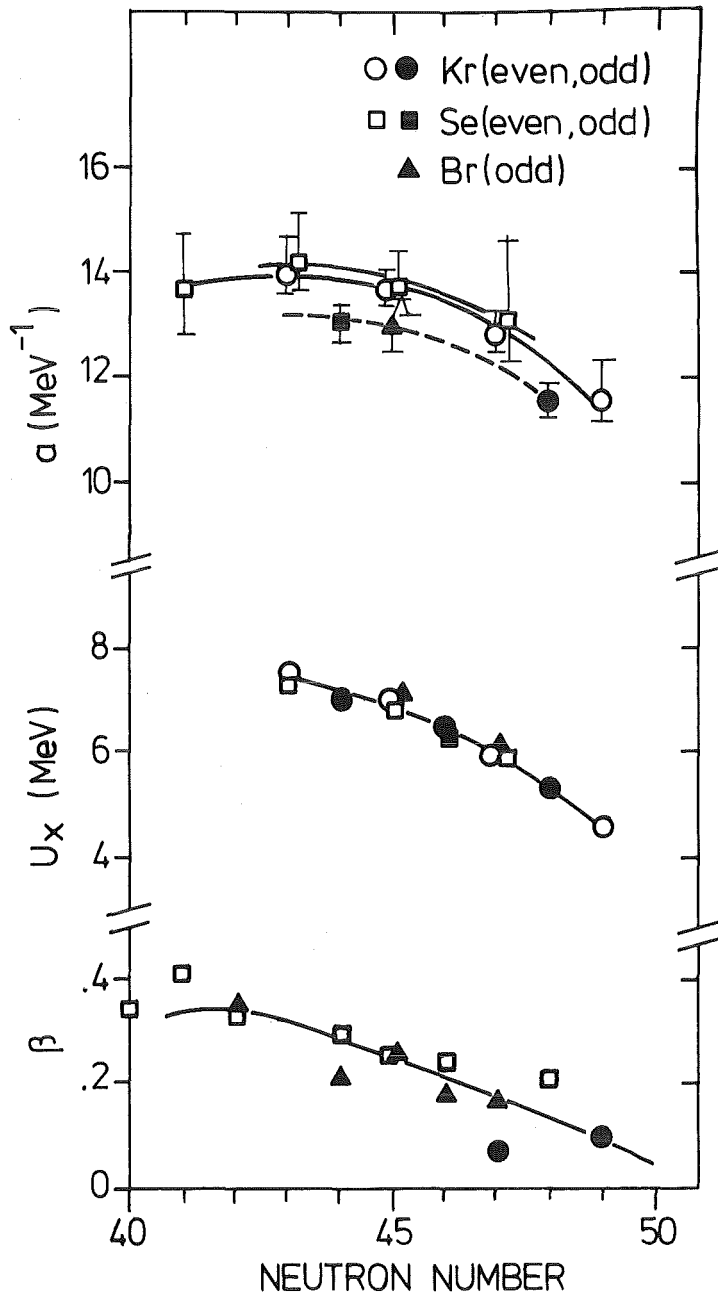
Fig. 12   Level density parameter $\underline{a}$, matching energy U_x
and deformation parameter ß as a function
of neutron number in the investigated compound
nuclei. While $\underline{a}$ shows a significant odd-even
effect this trend does not reproduce for U_x and ß.
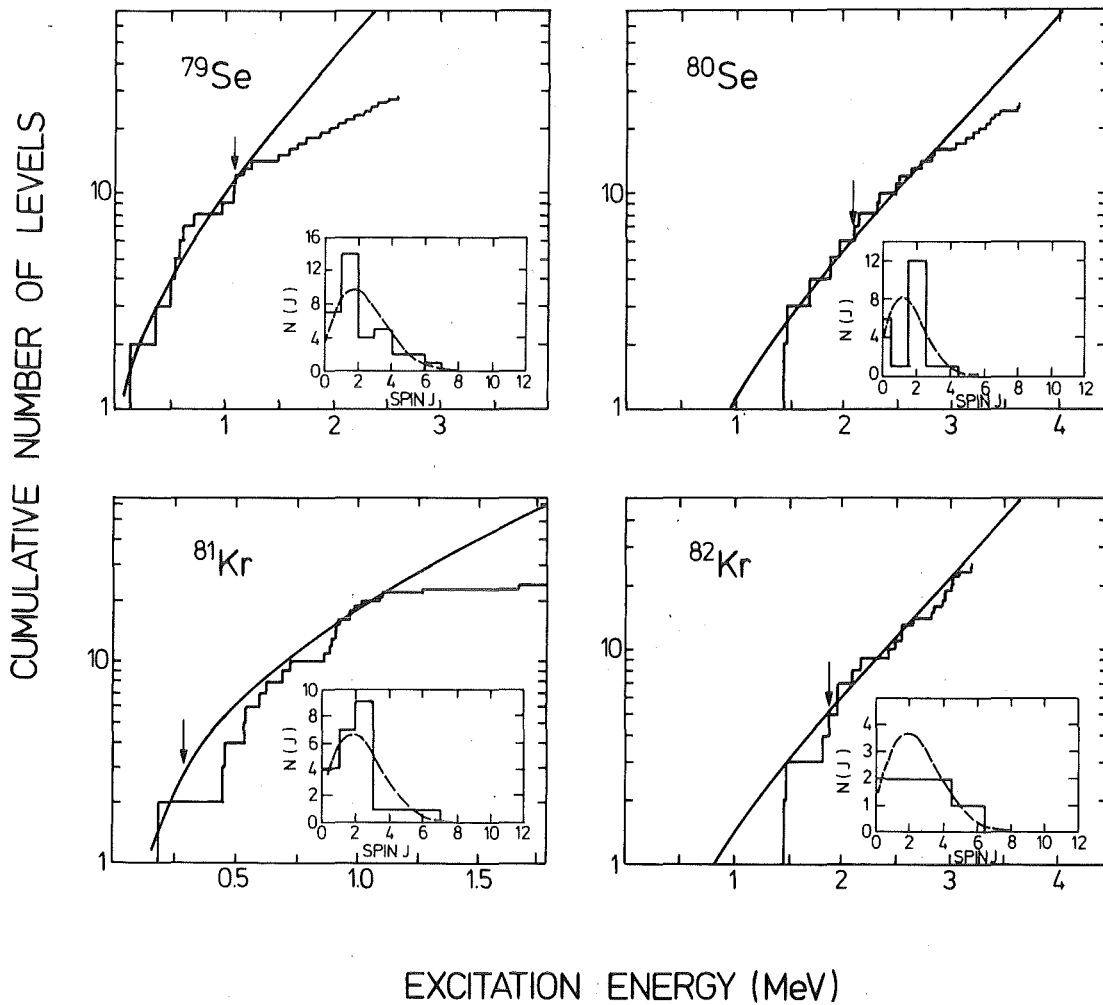
Fig. 13   Comparison between the calculated cumulative
number of levels (solid line) and known discrete
levels for some compound nuclei. The energy E_{cut}
where the level continuum was supposed to
start is marked by an arrow. In the respective
inserts the theoretical spin distribution
(dashed line) and the spin distribution of
discrete levels below E_{cut} is given.
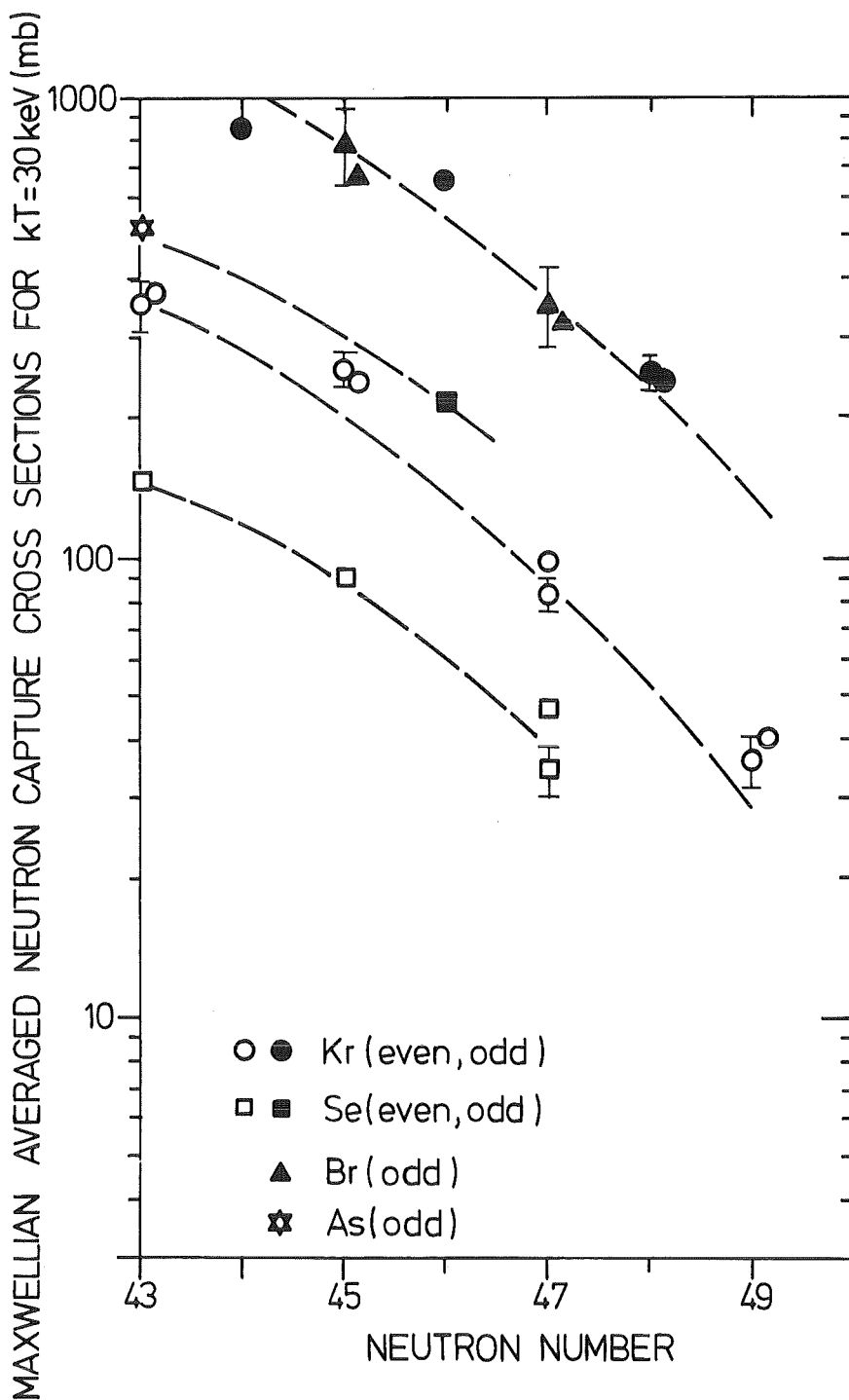
Fig. 14   Experimental and calculated Maxwellian averaged
           capture cross sections for kT=30 keV versus
           neutron number in the compound nuclei.
           The experimental points are plotted with error bars.
           For ^{75}As the calculated value of Benzi et al. (1973)
           was adopted.
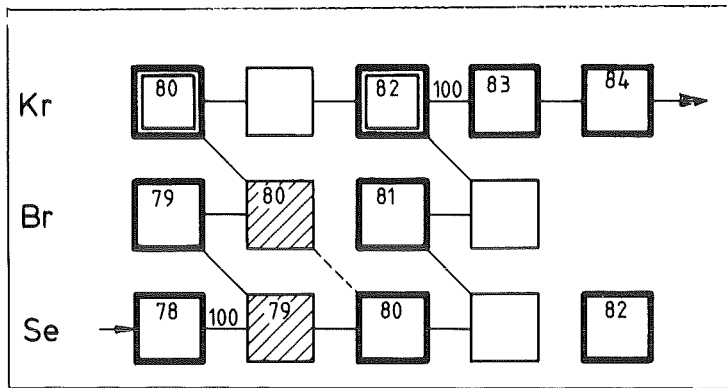
Fig. 15   The s-process flow through the mass region 78<A<84.
Branching points are shaded and s-only isotopes
are marked by double boxes.
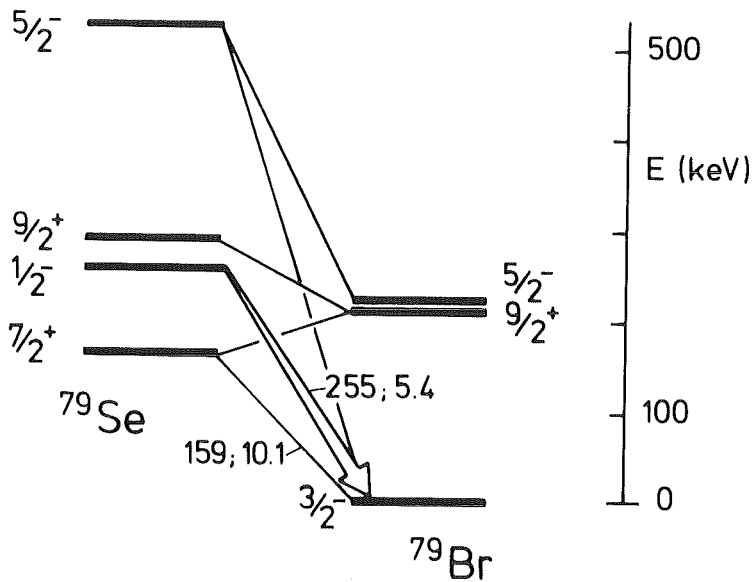
Fig. 16   Level schemes of ^{79}Se and ^{79}Br with the possible links
in a hot environment. The by far most important decay
of the 96 keV isomer in ^{79}Se is indicated by the white
arrow. The numbers correlated with the links designate
Q- and log ft-values of the transitions.
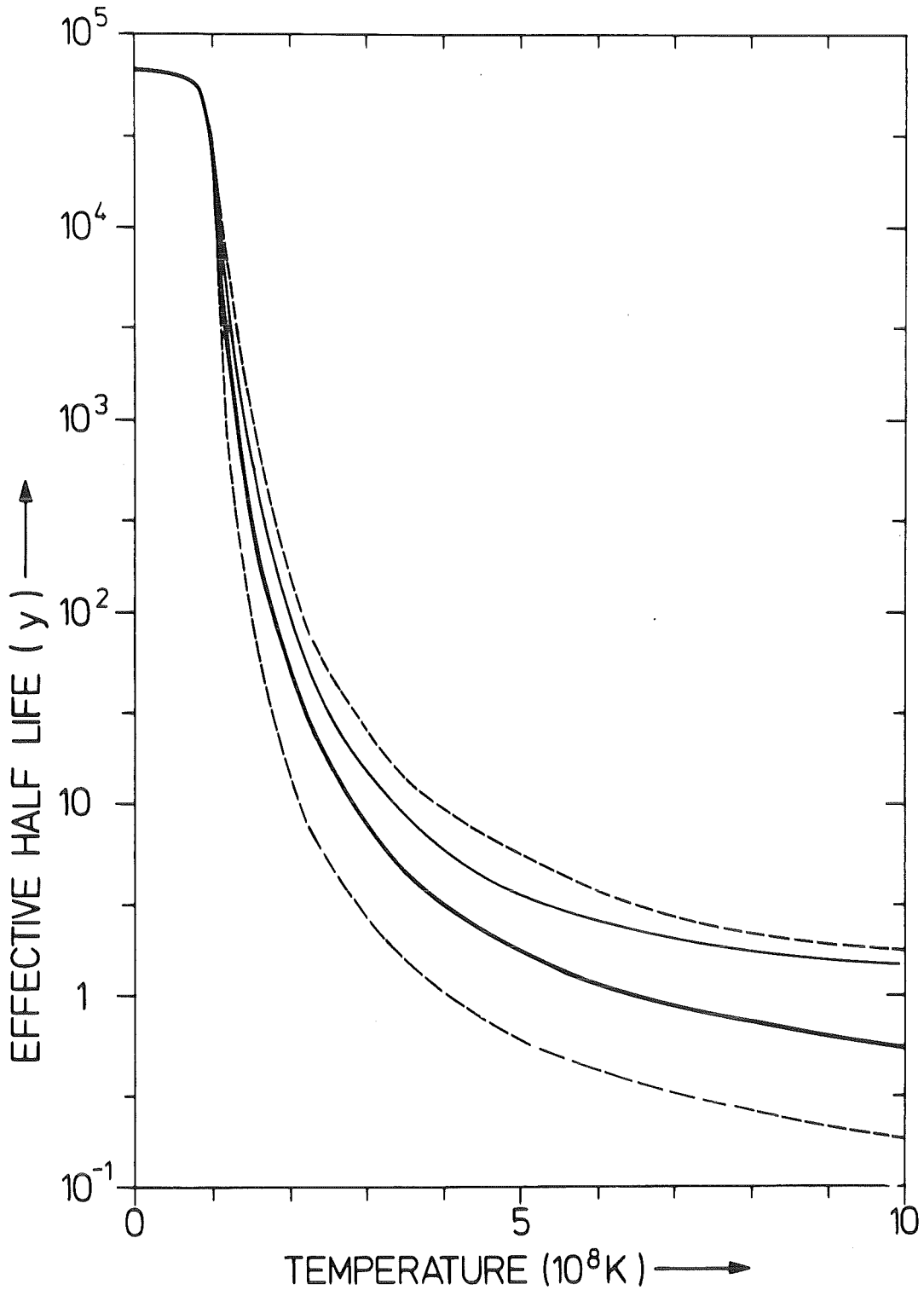
Fig. 17   Effective half life of ^{79}Se as a function of temperature.
The solid black line represents the result of this work.
The dashed lines indicate the range of uncertainty
which results from the 10 % uncertainty of the log ft-
value for the decay from the 96 keV state. For compari-
son the results of Newman (1973) and Cosner and Truran
(1981) are shown (thin solid line) who neglected the
effect of ionisation.
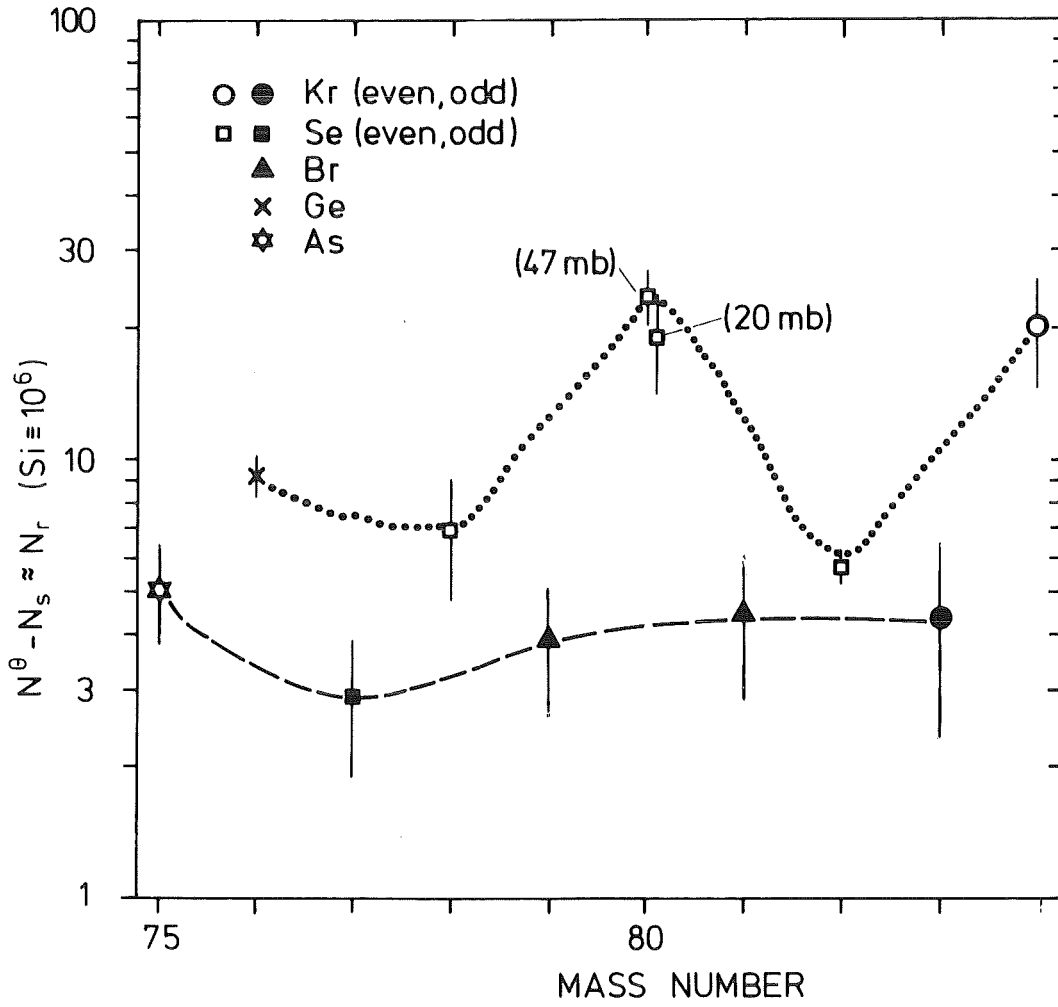
Fig. 18   The r-process abundances in the mass region
            78<A<84 as deduced from σN systematics.

REFERENCES

Almeida, J. 1982, KfK-Report 3347, Kernforschungszentrum Karlsruhe

Almeida, J., and Käppeler, F. 1983, _Ap. J._, 265, 417

Anders, E., and Ebihara, M. 1982, _Geochim. Cosmochim. Acta_, 46, 2363

Beer, H., Käppeler, F., Wisshak, K., and Ward, R.A. 1981, _Ap. J. Suppl._ 46, 295

Beer, H., and Käppeler, F.1982, "Neutron-Capture Gamma-Ray Spectroscopy and Related Topics 1981", The Institute of Physics, Bristol and London, Conference Series number 62, p. 558

Beer, H., Käppeler, F., Takahaski, K., and Yokoi, K. 1983, submitted to _Ap. J._

Benzi, V., D'Orazi, R., and Reffo, G. 1973, _Nuovo Cimento_, 13B, 226

Cameron, A.G.W. 1981, in "Essays in Nuclear Astrophysics", ed. C.A. Barnes, D.D. Clayton, and D.N. Schramm, Cambridge University Press, Cambridge, p. 23

Clayton, D.D., Fowler, W.A., Hull, and Zimmermann, B.A. 1961, _Ann. Phys._ 12, 331

Clayton, D.D. 1968, in "Principles of Stellar Evolution and Nucleosynthesis", McGraw-Hill, New York, p.552

Conrad, J.H. 1976, Ph.D. thesis, University of Heidelberg

Cosner, K., and Truran, J.W. 1981, _Astrophys. Space Sci_, 78, 85

Fuller, G.H., and Cohen, V.W. 1969, _Nuclear Data Tables_, A5, 433

Fröhner, F.H. 1968, Report GA-8380, Gulf General Atomic

Garber, D. 1975, ENDF/B-IV, Report BNL-17541 (ENDF-201) Brookhaven National Laboratory

Gilbert, A., and Cameron, A.G.W 1965, _Can.J.Phys._ 43, 1446

Harris, M.J. 1981, _Space Sci. Rev._, 77, 357

Hensley, F. 1980, KfK-Report 2918, Kernforschungszentrum Karlsruhe

Holmes, J.A., Woosley, S.E., Fowler, W.A., and Zimmerman, B.A. 1976, _Atomic Data and Nuclear Data Tables_, 18, 305

Käppeler, F., Beer, H., Wisshak, K., Clayton, D.D., Macklin, R.L., and Ward, R.A. 1982, Ap.J., 257, 821

Käppeler, F. 1983, unpublished

Lederer, C.A., and Shirley, V.S. 1978, "Table of Isotopes", John Wiley & Sons, New York

Leugers, B. 1979, KfK-Report 2895, Kernforschungszentrum Karlsruhe

Leugers, B., Käppeler, F. Reffo, G., and Fabbri, F. 1979, "Nuclear Reaction Mechanisms", CLUED, Milano, p. 309

Macklin, R.L., and Gibbons, J.H. 1967, Phys.Rev., 159, 1007

Macklin, R.L., Halperin, J., and Winters, R.R., 1975, Phys. Rev. C11, 1270

Macklin, R.L., and Winters, R.R. 1976, Ap.J. 208, 812

Macklin, R.L. 1982 (private communication)

Maguire, H.T. Jr., Fisher, H.M., and Block, R.C. 1978, "Neutron Physics and Nuclear Data for Reactors and other Applied Purposes", OECD/NEA, Paris, p. 472

Marti, K., Wilkening, L., and Suess, H.E. 1982, Ap. J., 173, 445

Mughabghab, S.F., and Garber, D.I. 1973, "Neutron Cross Section, Resonance Parameters", BNL-Report 325 3rd ed., Vol. 1, Brookhaven National Laboratory

Mughabghab, S.F., Divadeenam, M., and Holden, N.B. 1981, "Neutron Cross Sections", Vol. 1, Academic Press, New York

Newman, M. (1973), M.S. thesis, Rice University, Houston

Palme, H., Suess, H.E., and Zeh, H.D. 1981, in "Landolt-Börnstein", New Series VI/2, chaps. 3,4

Perey, F.G., and Buck, B. 1962, Nucl.Phys. 32, 353

Prince, A. 1979, BNL-Report NCS-51028, Brookhaven National Laboratory, Upton, New York

Rau, F. 1963, Nukleonik, 5, 191

Reffo, G. 1980a, IAEA Report SMR-43, p.205 Int. Atomic Energy Agency, Vienna and CNEN-Report RT/FI (78)11, Comitato per l'Energia Nucleare, Bologna

Reffo, G. 1980b, in "Theory and Applications of Moment Methods in Many Fermion Systems", B.J. Dalton et al. Eds. Plenum Press, New York

Reffo, G., and Fabbri, F. 1981, unpublished

Reffo, G., Fabbri, F., Wisshak, K., and Käppeler, F. 1982, Nucl. Sci. Eng., 80, 630

Stelson, P.H., and Grodzins, L. 1965, Nucl. Data A, 1, 21

Walter, G., and Beer, H. 1982, KfK-Report 3327, Kernforschungs-zentrum Karlsruhe

Walter, G., et al., 1983, to be published

Ward, R.A., Newman, M.J., and Clayton, D.D. 1976, Ap.J.Suppl. 31, 33

Wilmore, D. and Hodgson, P.E. 1964, Nucl.Phys., 55, 673

Winters, R.R., Käppeler, F., Wisshak, K., Reffo, G. and Mengoni A. 1983, private communication

Wisshak, K., Walter, G., and Käppeler, F. 1983, KfK-Report 3542, Kernforschungszentrum Karlsruhe and Nucl. Instr. Meth. (submitted)

Woosley, S.E., Fowler, W.A., Holmes, J.A., and Zimmerman, B.A. 1978, Atomic Data and Nuclear Data Tables, 22, 371.

Appendix I : Capture cross section of natural krypton as a function
of neutron energy

E(keV)	σ(mb)	Δσ(mb)	E(keV)	σ(mb)	Δσ(mb)
2.5	268.9	483.5	7.2	191.9	79.5
2.6	421.0	441.5	7.3	227.9	78.0
2.7	-62.3	392.7	7.4	103.0	76.5
2.8	1845.4	353.8	7.5	7.6	74.8
2.9	383.0	321.6	7.6	133.2	73.4
3.0	-236.4	295.4	7.7	156.9	71.9
3.1	555.9	274.0	7.8	106.1	70.5
3.2	14.8	255.7	7.9	133.4	69.1
3.3	-22.9	240.0	8.0	96.5	67.7
3.4	266.2	226.4	8.1	254.8	66.4
3.5	476.1	214.5	8.2	258.8	65.3
3.6	137.4	204.2	8.3	265.8	64.1
3.7	101.6	195.1	8.4	302.3	62.9
3.8	212.2	187.0	8.5	259.5	61.7
3.9	75.9	179.5	8.6	200.5	60.6
4.0	74.9	172.9	8.7	177.0	59.4
4.1	257.1	166.9	8.8	125.3	58.3
4.2	94.0	161.6	8.9	149.2	57.1
4.3	202.4	156.5	9.0	141.0	56.0
4.4	213.4	151.6	9.1	108.5	55.0
4.5	201.5	147.2	9.2	48.6	54.1
4.6	206.4	143.2	9.3	60.2	53.0
4.7	36.4	139.5	9.4	4.3	52.1
4.8	95.2	135.9	9.5	103.3	51.2
4.9	334.4	132.4	9.6	110.7	50.3
5.0	157.8	129.0	9.7	149.1	49.4
5.1	149.5	125.8	9.8	151.3	48.5
5.2	218.3	122.9	9.9	178.4	47.8
5.3	241.7	120.1	10.0	133.8	47.0
5.4	12.4	117.3	10.1	91.2	46.1
5.5	228.0	114.5	10.2	98.6	45.5
5.6	293.3	112.0	10.3	116.5	44.8
5.7	105.1	109.6	10.4	114.9	44.0
5.8	182.4	107.1	10.5	61.1	43.2
5.9	134.1	104.7	10.6	100.0	42.6
6.0	231.9	102.3	10.7	121.1	42.0
6.1	114.1	100.1	10.8	135.8	41.3
6.2	139.2	98.1	10.9	135.9	40.7
6.3	98.5	96.2	11.0	135.6	40.1
6.4	45.2	94.0	11.1	142.1	39.5
6.5	94.7	92.0	11.2	172.9	39.0
6.6	78.3	90.1	11.3	254.5	38.4
6.7	95.0	88.1	11.4	276.1	37.8
6.8	276.8	86.4	11.5	323.3	37.3
6.9	385.1	84.6	11.6	227.9	36.7
7.0	299.8	82.9	11.7	192.9	36.2
7.1	153.8	81.2	11.8	150.4	35.6

E(keV)	σ(mb)	Δσ(mb)	E(keV)	σ(mb)	Δσ(mb)
11.9	127.8	35.1	17.0	134.7	21.7
12.0	107.7	34.7	17.1	106.2	21.6
12.1	101.6	34.3	17.2	108.8	21.5
12.2	119.7	33.8	17.3	137.4	21.3
12.3	108.3	33.3	17.4	119.1	21.1
12.4	97.6	33.0	17.5	113.6	21.0
12.5	98.5	32.6	17.6	89.7	20.9
12.6	95.9	32.1	17.7	82.8	20.8
12.7	136.6	31.8	17.8	101.2	20.7
12.8	128.1	31.4	17.9	91.7	20.6
12.9	77.7	30.9	18.0	111.1	20.5
13.0	52.7	30.6	18.1	91.2	20.4
13.1	68.3	30.3	18.3	103.7	20.3
13.2	94.8	29.9	18.4	109.7	20.2
13.3	71.1	29.6	18.5	75.5	20.1
13.4	77.1	29.3	18.6	88.8	20.0
13.5	99.2	29.0	18.7	72.6	19.9
13.6	139.6	28.6	18.8	84.8	19.8
13.7	129.5	28.3	18.9	57.8	19.8
13.8	139.4	28.0	19.0	72.5	19.7
13.9	132.3	27.7	19.1	83.9	19.6
14.0	88.3	27.4	19.2	97.3	19.5
14.1	68.8	27.2	19.3	70.1	19.4
14.2	79.2	26.9	19.5	63.1	19.3
14.3	102.7	26.7	19.6	91.1	19.3
14.4	123.8	26.5	19.7	110.5	19.2
14.5	126.4	26.2	19.8	129.3	19.1
14.6	137.2	25.9	19.9	89.0	19.0
14.7	128.2	25.8	20.0	82.2	19.0
14.8	115.9	25.5	20.2	87.4	18.9
14.9	146.3	25.2	20.3	86.7	18.8
15.0	134.1	25.1	20.4	80.5	18.8
15.1	129.2	24.8	20.5	87.0	18.7
15.2	88.2	24.6	20.7	86.5	18.6
15.3	74.1	24.4	20.8	69.1	18.6
15.4	76.2	24.2	20.9	53.9	18.5
15.5	70.7	24.1	21.0	53.1	18.5
15.6	74.5	23.9	21.2	73.5	18.4
15.7	108.8	23.6	21.3	51.9	18.3
15.8	65.4	23.5	21.4	61.0	18.3
15.9	56.8	23.3	21.6	76.5	18.2
16.0	58.4	23.2	21.7	67.6	18.2
16.1	104.5	23.0	21.8	60.4	18.1
16.2	120.4	22.8	22.0	70.7	18.1
16.3	69.8	22.6	22.1	77.7	18.0
16.4	47.3	22.5	22.2	67.5	18.0
16.5	84.5	22.4	22.4	65.4	17.9
16.6	100.2	22.2	22.5	62.6	17.9
16.7	125.9	22.1	22.7	62.7	17.8
16.8	173.8	22.0	22.8	65.1	17.8
16.9	148.5	21.9	23.0	70.5	17.8

E(keV)	σ(mb)	Δσ(mb)	E(keV)	σ(mb)	Δσ(mb)
23.1	89.5	17.7	33.1	57.6	14.7
23.3	83.3	17.7	33.3	63.3	14.6
23.4	78.6	17.6	33.6	66.9	14.4
23.6	72.4	17.6	33.8	71.0	14.3
23.7	78.6	17.5	34.1	86.3	14.1
23.9	75.5	17.5	34.4	94.9	14.0
24.0	87.8	17.5	34.7	87.6	13.8
24.2	90.3	17.4	34.9	71.0	13.7
24.3	76.0	17.4	35.2	63.0	13.5
24.5	101.8	17.4	35.5	56.6	13.3
24.7	109.9	17.3	35.8	51.3	13.1
24.8	91.8	17.3	36.1	55.3	12.9
25.0	98.0	17.2	36.4	51.8	12.7
25.2	83.0	17.2	36.7	49.4	12.5
25.3	76.5	17.2	37.0	45.7	12.3
25.5	83.9	17.1	37.3	41.6	12.0
25.7	94.5	17.1	37.6	45.2	11.8
25.8	74.4	17.1	37.9	47.1	11.6
26.0	79.9	17.0	38.2	44.4	11.3
26.2	90.7	17.0	38.5	47.5	11.1
26.4	92.6	16.9	38.9	46.1	10.8
26.6	100.6	16.9	39.2	45.3	10.6
26.7	98.6	16.9	39.5	48.1	10.3
26.9	83.2	16.8	39.9	45.7	10.0
27.1	62.0	16.8	40.2	43.7	9.7
27.3	58.4	16.7	40.6	48.2	9.5
27.5	50.0	16.7	40.9	50.9	9.3
27.7	55.8	16.6	41.3	54.7	9.1
27.9	55.8	16.6	41.6	51.6	8.9
28.1	47.1	16.6	42.0	48.9	8.7
28.3	53.8	16.5	42.4	47.5	8.6
28.5	58.5	16.4	42.7	41.6	8.5
28.7	66.4	16.4	43.1	49.2	8.4
28.9	61.3	16.3	43.5	62.2	8.3
29.1	63.9	16.3	43.9	67.4	8.2
29.3	63.1	16.2	44.3	67.2	8.2
29.5	60.9	16.1	44.7	62.8	8.1
29.8	61.4	16.1	45.1	57.6	8.1
30.0	60.2	16.0	45.5	50.2	8.0
30.2	58.1	15.9	45.9	43.4	8.0
30.4	56.1	15.9	46.4	42.9	8.0
30.6	62.3	15.8	46.8	44.0	8.0
30.9	68.1	15.7	47.2	39.9	7.9
31.1	69.9	15.6	47.7	38.7	7.9
31.3	66.7	15.5	48.1	43.2	7.9
31.6	69.9	15.4	48.6	51.5	7.9
31.8	64.4	15.3	49.0	52.2	7.9
32.1	60.3	15.2	49.5	53.0	7.9
32.3	61.0	15.1	50.0	55.3	7.9
32.6	66.3	15.0	50.4	53.1	7.9
32.8	61.4	14.8	50.9	52.0	7.9

E(keV)	σ(mb)	Δσ(mb)	E(keV)	σ(mb)	Δσ(mb)
51.4	44.7	7.9	90.0	34.1	4.1
51.9	41.6	7.9	91.2	33.3	4.0
52.4	41.0	7.9	92.3	30.0	4.0
52.9	40.7	7.8	93.5	29.7	3.9
53.5	42.3	7.8	94.7	30.7	3.9
54.0	41.0	7.8	96.0	29.9	3.8
54.5	40.7	7.8	97.3	29.4	3.8
55.1	45.1	7.7	98.5	29.7	3.7
55.6	46.9	7.7	99.9	30.9	3.7
56.2	44.7	7.7	101.2	29.6	3.7
56.7	41.3	7.6	102.6	30.7	3.6
57.3	36.2	7.6	104.0	33.2	3.6
57.9	37.4	7.5	105.4	30.5	3.6
58.5	42.6	7.5	106.9	28.1	3.6
59.1	46.4	7.4	108.3	28.0	3.6
59.7	44.4	7.3	109.9	28.0	3.5
60.3	40.8	7.3	111.4	27.9	3.5
61.0	39.8	7.2	113.0	24.9	3.5
61.6	40.0	7.1	114.6	24.3	3.5
62.3	38.5	7.0	116.3	26.2	3.5
62.9	40.1	6.9	118.0	27.1	3.5
63.6	42.0	6.8	119.7	28.7	3.5
64.3	43.6	6.8	121.4	28.3	3.5
65.0	40.0	6.7	123.2	28.7	3.5
65.7	38.1	6.6	125.1	27.7	3.5
66.4	38.7	6.5	127.0	24.7	3.5
67.1	39.0	6.4	128.9	24.7	3.5
67.9	39.6	6.3	130.9	25.5	3.5
68.6	38.4	6.2	132.9	25.5	3.5
69.4	37.3	6.0	135.0	25.9	3.4
70.2	39.6	5.9	137.1	24.8	3.4
70.9	36.3	5.8	139.2	23.7	3.4
71.8	34.5	5.7	141.5	24.2	3.4
72.6	34.7	5.6	143.7	24.3	3.4
73.4	36.7	5.5	146.0	24.2	3.4
74.2	39.0	5.4	148.4	25.9	3.3
75.1	36.8	5.3	150.9	25.9	3.3
76.0	37.0	5.2	153.4	25.7	3.2
76.9	39.3	5.1	155.9	24.1	3.2
77.8	37.9	5.0	158.6	23.2	3.2
78.7	35.9	4.9	161.3	23.6	3.1
79.6	36.4	4.8	164.0	23.3	3.0
80.6	35.7	4.7	166.9	22.8	3.0
81.6	34.4	4.7	169.8	22.7	2.9
82.6	30.7	4.6	172.8	21.9	2.8
83.6	30.2	4.5	175.8	22.2	2.8
84.6	28.9	4.4	179.0	22.9	2.7
85.6	31.4	4.3	182.2	23.4	2.6
86.7	36.6	4.3	185.5	22.7	2.5
87.8	37.7	4.2	188.9	20.9	2.4
88.9	36.4	4.1	192.5	21.5	2.4

E(keV)	σ(mb)	Δσ(mb)	E(keV)	σ(mb)	Δσ(mb)
196.1	20.8	2.3	220.0	19.8	2.1
199.8	20.6	2.2	224.4	19.3	2.1
203.6	21.9	2.2	229.0	18.6	2.1
207.5	22.1	2.1	233.7	19.6	2.2
211.6	21.2	2.1	238.5	18.7	2.3
215.7	20.4	2.1	243.5	19.8	2.5

Appendix II : Capture cross section of Kr-78 as a function
            of neutron energy

E(keV)	σ(mb)	Δσ(mb)	E(keV)	σ(mb)	Δσ(mb)
10.0	-222.8	101.0	14.7	504.1	56.4
10.1	172.1	92.7	14.8	449.1	55.8
10.2	1779.9	91.8	14.9	461.6	55.1
10.3	893.9	90.8	15.0	260.4	54.7
10.4	421.8	89.6	15.1	619.0	54.0
10.5	513.7	88.4	15.2	286.2	53.4
10.6	745.2	87.4	15.3	-2.4	53.0
10.7	1075.2	86.4	15.4	807.7	52.5
10.8	2060.5	85.5	15.5	776.5	52.1
10.9	972.6	84.5	15.6	341.8	51.5
11.0	709.3	83.6	15.7	328.6	50.8
11.1	1705.2	82.7	15.8	130.7	50.4
11.2	353.2	81.7	15.9	308.4	50.0
11.3	-248.7	80.8	16.0	501.2	49.6
11.4	1116.0	79.9	16.1	1037.6	48.9
11.5	486.7	79.0	16.2	637.7	48.3
11.6	906.5	78.1	16.3	928.1	47.9
11.7	99.9	77.1	16.4	756.1	47.5
11.8	481.6	76.2	16.5	780.8	47.1
11.9	423.3	75.3	16.6	431.5	46.7
12.0	-986.2	74.6	16.7	533.5	46.2
12.1	559.4	74.0	16.8	265.3	45.8
12.2	70.5	73.1	16.9	-46.2	45.4
12.3	1145.6	72.2	17.0	437.9	45.0
12.4	542.4	71.5	17.1	587.2	44.6
12.5	1091.1	70.8	17.2	494.4	44.2
12.6	1612.1	69.9	17.3	665.2	43.6
12.7	-367.2	69.2	17.4	429.9	43.0
12.8	325.0	68.6	17.5	474.9	42.6
12.9	372.1	67.7	17.6	675.5	42.2
13.0	492.7	67.0	17.7	419.5	41.8
13.1	300.8	66.3	17.8	290.1	41.4
13.2	1452.5	65.7	17.9	230.2	41.0
13.3	1574.5	65.0	18.0	283.0	40.6
13.4	418.2	64.3	18.1	173.5	40.3
13.5	487.6	63.7	18.3	-26.0	39.9
13.6	-191.8	63.0	18.4	73.3	39.5
13.7	-84.0	62.3	18.5	232.9	39.1
13.8	-85.8	61.7	18.6	516.1	38.7
13.9	572.7	61.0	18.7	707.8	38.3
14.0	537.4	60.3	18.8	513.0	37.9
14.1	677.9	59.9	18.9	326.6	37.6
14.2	493.3	59.2	19.0	479.8	37.2
14.3	1216.6	58.6	19.1	1032.5	36.8
14.4	1122.3	58.2	19.2	904.5	36.4
14.5	1005.2	57.5	19.3	747.2	36.1
14.6	891.7	56.8	19.5	618.1	35.7

E(keV)	σ(mb)	Δσ(mb)	E(keV)	σ(mb)	Δσ(mb)
19.6	696.5	35.3	27.1	292.3	19.3
19.7	544.5	35.0	27.3	498.6	19.1
19.8	360.8	34.6	27.5	427.2	18.8
19.9	311.5	34.2	27.7	352.2	18.6
20.0	533.6	33.9	27.9	393.6	18.3
20.2	613.8	33.5	28.1	395.8	18.1
20.3	496.1	33.2	28.3	370.9	17.8
20.4	396.0	32.8	28.5	488.0	17.6
20.5	221.6	32.4	28.7	431.0	17.4
20.7	141.1	32.1	28.9	299.8	17.1
20.8	349.4	31.7	29.1	352.2	16.9
20.9	322.1	31.4	29.3	437.0	16.7
21.0	645.6	31.0	29.5	432.4	16.5
21.2	258.4	30.7	29.8	347.2	16.2
21.3	342.3	30.4	30.0	469.5	16.0
21.4	203.1	30.0	30.2	398.6	15.8
21.6	101.9	29.7	30.4	366.7	15.6
21.7	462.6	29.4	30.6	266.4	15.4
21.8	649.5	29.0	30.9	504.7	15.2
22.0	558.6	28.7	31.1	574.0	15.0
22.1	623.9	28.4	31.3	613.3	14.8
22.2	480.1	28.0	31.6	577.3	14.6
22.4	302.7	27.7	31.8	429.9	14.4
22.5	599.7	27.4	32.1	412.9	14.2
22.7	556.9	27.1	32.3	571.7	14.0
22.8	436.2	26.7	32.6	612.2	13.8
23.0	281.7	26.4	32.8	549.3	13.6
23.1	285.2	26.1	33.1	415.9	13.5
23.3	328.4	25.8	33.3	471.3	13.3
23.4	391.6	25.5	33.6	365.1	13.1
23.6	144.5	25.2	33.8	310.7	12.9
23.7	151.6	24.9	34.1	335.2	12.8
23.9	627.4	24.6	34.4	313.0	12.6
24.0	650.3	24.3	34.7	359.5	12.4
24.2	295.7	24.0	34.9	325.4	12.3
24.3	423.9	23.7	35.2	340.6	12.1
24.5	557.3	23.4	35.5	431.9	11.9
24.7	528.9	23.1	35.8	345.3	11.8
24.8	511.6	22.8	36.1	197.2	11.6
25.0	497.1	22.5	36.4	255.4	11.5
25.2	453.0	22.2	36.7	255.1	11.3
25.3	458.2	22.0	37.0	229.0	11.2
25.5	287.1	21.7	37.3	335.6	11.1
25.7	238.5	21.4	37.6	291.4	10.9
25.8	383.5	21.1	37.9	175.1	10.8
26.0	469.5	20.9	38.2	150.4	10.7
26.2	672.0	20.6	38.5	210.7	10.5
26.4	649.9	20.3	38.9	190.4	10.4
26.6	487.2	20.1	39.2	271.6	10.3
26.7	393.9	19.8	39.5	410.9	10.2
26.9	390.3	19.6	39.9	423.1	10.0

E(keV)	σ(mb)	Δσ(mb)	E(keV)	σ(mb)	Δσ(mb)
40.2	299.3	10.0	65.7	320.6	6.7
40.6	307.1	10.0	66.4	321.7	6.7
40.9	287.3	10.0	67.1	308.2	6.6
41.3	222.3	10.0	67.9	262.3	6.5
41.6	343.8	10.0	68.6	286.4	6.5
42.0	468.9	10.0	69.4	244.3	6.4
42.4	343.3	10.0	70.2	265.4	6.3
42.7	359.8	10.0	70.9	249.6	6.3
43.1	389.5	9.9	71.8	239.7	6.2
43.5	364.7	9.9	72.6	199.4	6.2
43.9	380.5	9.8	73.4	191.1	6.1
44.3	384.3	9.8	74.2	328.6	6.1
44.7	283.1	9.7	75.1	311.8	6.0
45.1	380.7	9.7	76.0	219.0	5.9
45.5	305.1	9.6	76.9	270.9	5.9
45.9	232.3	9.5	77.8	322.6	5.8
46.4	299.4	9.5	78.7	282.7	5.8
46.8	382.1	9.4	79.6	312.6	5.7
47.2	377.0	9.3	80.6	297.4	5.7
47.7	353.4	9.2	81.6	250.8	5.6
48.1	446.4	9.1	82.6	192.7	5.6
48.6	503.1	9.1	83.6	190.4	5.5
49.0	292.1	9.0	84.6	275.2	5.5
49.5	278.8	8.9	85.6	218.6	5.4
50.0	331.5	8.8	86.7	214.8	5.3
50.4	349.7	8.7	87.8	248.0	5.3
50.9	235.2	8.6	88.9	241.5	5.2
51.4	370.3	8.5	90.0	209.4	5.2
51.9	299.6	8.5	91.2	208.5	5.1
52.4	317.8	8.4	92.3	228.8	5.1
52.9	372.1	8.3	93.5	178.7	5.0
53.5	404.4	8.2	94.7	249.0	5.0
54.0	344.2	8.1	96.0	212.4	4.9
54.5	308.4	8.0	97.3	139.7	4.9
55.1	234.6	8.0	98.5	170.4	4.9
55.6	288.3	7.9	99.9	190.7	4.8
56.2	364.4	7.8	101.2	235.7	4.8
56.7	333.3	7.7	102.6	217.8	4.7
57.3	355.8	7.6	104.0	205.8	4.7
57.9	344.4	7.6	105.4	180.5	4.6
58.5	356.2	7.5	106.9	163.0	4.6
59.1	285.3	7.4	108.3	181.1	4.6
59.7	299.6	7.3	109.9	216.7	4.5
60.3	400.1	7.3	111.4	216.5	4.5
61.0	332.1	7.2	113.0	189.5	4.5
61.6	363.2	7.1	114.6	153.2	4.4
62.3	274.7	7.0	116.3	199.4	4.4
62.9	238.0	7.0	118.0	212.7	4.4
63.6	264.7	6.9	119.7	250.4	4.3
64.3	296.7	6.8	121.4	211.2	4.3
65.0	293.0	6.8	123.2	177.3	4.3

E(keV)	σ(mb)	Δσ(mb)	E(keV)	σ(mb)	Δσ(mb)
125.1	189.4	4.3	172.8	176.0	4.9
127.0	208.9	4.3	175.8	172.5	4.9
128.9	163.0	4.3	179.0	223.4	5.0
130.9	165.2	4.3	182.2	197.4	5.1
132.9	177.2	4.3	185.5	190.6	5.2
135.0	173.0	4.3	188.9	209.5	5.2
137.1	131.6	4.3	192.5	157.8	5.3
139.2	136.8	4.3	196.1	176.2	5.3
141.5	143.5	4.3	199.8	166.3	5.4
143.7	200.1	4.3	203.6	132.1	5.4
146.0	269.0	4.3	207.5	192.6	5.4
148.4	287.8	4.4	211.6	235.0	5.3
150.9	298.5	4.4	215.7	214.9	5.3
153.4	291.8	4.5	220.0	195.7	5.2
155.9	207.6	4.5	224.4	201.3	5.0
158.6	243.0	4.5	229.0	155.1	4.8
161.3	249.3	4.6	233.7	183.8	4.6
164.0	281.5	4.7	238.5	216.1	4.3
166.9	167.0	4.7	243.5	272.4	4.0
169.8	155.0	4.8			

Appendix III : Capture cross section of Kr-80 as a function
of neutron energy

E(keV)	σ(mb)	Δσ(mb)	E(keV)	σ(mb)	Δσ(mb)
4.0	858.1	253.9	8.7	45.5	94.7
4.1	1265.8	308.0	8.8	132.5	92.8
4.2	1190.1	304.9	8.9	225.0	99.5
4.3	798.9	293.8	9.0	391.6	101.7
4.4	346.0	286.0	9.1	497.7	99.6
4.5	156.9	270.9	9.2	533.4	98.2
4.6	-98.3	259.9	9.3	580.7	95.2
4.7	215.8	257.3	9.4	472.1	91.7
4.8	-673.8	247.4	9.5	427.0	89.1
4.9	-343.8	235.6	9.6	356.4	86.6
5.0	258.4	222.0	9.7	349.6	83.8
5.1	1188.3	228.3	9.8	526.0	82.1
5.2	1116.9	220.5	9.9	370.8	81.0
5.3	1299.0	217.6	10.0	596.7	80.3
5.4	1147.7	203.6	10.1	679.8	78.6
5.5	776.5	190.6	10.2	521.3	76.2
5.6	656.7	189.6	10.3	438.2	73.2
5.7	643.7	190.4	10.4	304.9	72.2
5.8	712.7	184.6	10.5	271.2	71.6
5.9	514.2	180.2	10.6	259.7	69.3
6.0	193.0	172.0	10.7	239.9	66.3
6.1	-191.7	164.2	10.8	166.0	66.4
6.2	125.8	161.5	10.9	166.4	65.3
6.3	290.7	168.1	11.0	178.8	63.8
6.4	583.2	164.6	11.1	223.1	61.8
6.5	546.6	157.8	11.2	303.2	61.6
6.6	434.1	151.8	11.3	288.4	60.5
6.7	236.6	148.1	11.4	154.8	58.4
6.8	607.9	143.6	11.5	270.6	58.8
6.9	576.3	139.2	11.6	213.2	65.5
7.0	421.0	136.1	11.7	274.1	68.7
7.1	949.5	133.4	11.8	335.2	68.0
7.2	627.9	129.0	11.9	441.5	68.8
7.3	467.3	137.4	12.0	530.0	67.2
7.4	263.6	135.5	12.1	381.4	64.1
7.5	424.4	129.6	12.2	274.8	62.0
7.6	632.4	126.5	12.3	248.6	61.0
7.7	596.0	123.3	12.4	354.7	60.1
7.8	354.8	117.4	12.5	429.6	61.4
7.9	301.7	114.7	12.6	486.4	60.4
8.0	469.6	113.2	12.7	610.9	59.5
8.1	478.1	109.8	12.8	550.7	58.4
8.2	363.0	108.4	12.9	481.9	58.4
8.3	439.9	104.6	13.0	398.0	57.1
8.4	339.1	103.6	13.1	291.1	53.9
8.5	400.8	100.6	13.2	118.3	52.6
8.6	323.9	95.6	13.3	138.3	52.5

E(keV)	σ(mb)	Δσ(mb)		E(keV)	σ(mb)	Δσ(mb)
13.4	390.1	52.6		18.6	426.9	39.3
13.5	495.5	53.0		18.7	390.6	38.4
13.6	513.6	53.2		18.8	339.6	39.9
13.7	518.6	51.5		18.9	335.5	38.1
13.8	666.9	51.6		19.0	356.4	36.8
13.9	620.0	50.4		19.1	203.0	.36.8
14.0	525.4	48.8		19.2	220.8	36.0
14.1	444.7	47.8		19.3	269.9	34.9
14.2	319.9	46.2		19.5	294.7	34.9
14.3	289.3	45.6		19.6	273.0	33.9
14.4	331.8	45.3		19.7	278.7	34.5
14.5	440.9	44.2		19.8	266.2	35.8
14.6	432.6	44.5		19.9	317.5	35.2
14.7	445.4	44.5		20.0	339.3	34.5
14.8	457.4	44.0		20.2	344.4	33.7
14.9	465.7	43.1		20.3	386.4	34.2
15.0	499.5	42.6		20.4	431.6	34.5
15.1	528.8	41.8		20.5	461.2	34.4
15.2	570.3	41.5		20.7	503.1	33.8
15.3	520.9	40.9		20.8	478.7	32.6
15.4	429.5	40.4		20.9	467.9	31.7
15.5	466.5	39.5		21.0	363.7	32.4
15.6	450.7	38.8		21.2	431.6	30.9
15.7	375.1	38.5		21.3	381.5	30.5
15.8	420.6	37.9		21.4	372.1	30.0
15.9	411.8	37.7		21.6	403.6	28.7
16.0	355.9	37.9		21.7	323.0	28.7
16.1	320.4	36.7		21.8	324.8	28.1
16.2	316.5	35.5		22.0	343.1	28.3
16.3	266.9	35.0		22.1	310.9	28.2
16.4	239.6	34.5		22.2	315.0	28.1
16.5	207.7	34.0		22.4	358.8	27.3
16.6	256.4	33.5		22.5	327.1	26.7
16.7	283.0	33.1		22.7	360.6	26.6
16.8	295.9	33.3		22.8	366.1	26.4
16.9	309.6	33.3		23.0	373.6	26.2
17.0	281.7	33.2		23.1	382.4	26.0
17.1	281.4	33.0		23.3	378.2	25.1
17.2	317.6	32.5		23.4	363.3	24.4
17.3	338.8	32.0		23.6	376.1	24.0
17.4	360.8	31.2		23.7	360.2	23.4
17.5	357.8	30.4		23.9	281.1	21.7
17.6	319.6	29.9		24.0	233.7	21.4
17.7	291.7	29.5		24.2	281.6	21.0
17.8	305.9	29.6		24.3	284.7	21.1
17.9	327.1	29.8		24.5	361.5	21.0
18.0	348.3	29.8		24.7	369.6	20.6
18.1	378.3	29.9		24.8	324.0	20.4
18.3	401.9	29.5		25.0	376.5	19.9
18.4	412.7	30.6		25.2	390.2	19.9
18.5	420.7	38.1		25.3	404.4	19.4

E(keV)	σ(mb)	Δσ(mb)		E(keV)	σ(mb)	Δσ(mb)
25.5	417.4	19.4		37.3	230.3	11.6
25.7	383.7	19.6		37.6	244.9	11.6
25.8	342.5	19.1		37.9	264.2	11.2
26.0	340.3	19.3		38.2	271.5	11.2
26.2	312.2	18.6		38.5	281.5	11.2
26.4	285.5	19.2		38.9	295.4	11.5
26.6	276.5	19.1		39.2	296.5	11.3
26.7	320.0	19.6		39.5	296.6	11.1
26.9	346.1	19.5		39.9	289.2	10.4
27.1	351.4	18.8		40.2	285.3	10.3
27.3	326.3	18.6		40.6	270.3	9.9
27.5	337.7	18.8		40.9	269.1	9.7
27.7	341.9	18.7		41.3	271.2	9.6
27.9	303.2	18.1		41.6	276.0	9.7
28.1	278.1	18.2		42.0	265.5	9.7
28.3	247.8	17.4		42.4	258.9	9.3
28.5	265.3	16.8		42.7	246.5	9.2
28.7	277.2	16.8		43.1	242.0	9.1
28.9	300.5	16.1		43.5	249.2	9.0
29.1	300.6	15.8		43.9	244.6	8.9
29.3	301.4	15.8		44.3	228.3	8.7
29.5	295.4	15.2		44.7	227.3	9.0
29.8	324.1	15.0		45.1	185.0	8.8
30.0	326.1	15.0		45.5	188.8	8.6
30.2	344.9	14.4		45.9	183.6	8.6
30.4	318.5	14.3		46.4	158.7	8.5
30.6	332.7	14.4		46.8	181.2	8.8
30.9	288.1	14.1		47.2	209.7	9.0
31.1	266.3	13.7		47.7	239.3	9.0
31.3	231.9	13.6		48.1	234.8	8.8
31.6	199.5	13.5		48.6	219.2	8.5
31.8	227.8	13.3		49.0	207.6	8.3
32.1	231.6	13.2		49.5	199.7	8.1
32.3	217.1	13.1		50.0	182.0	7.9
32.6	227.2	13.2		50.4	176.3	8.4
32.8	238.1	13.3		50.9	205.7	8.5
33.1	275.3	14.4		51.4	203.3	8.5
33.3	303.8	14.8		51.9	236.1	8.8
33.6	328.3	14.7		52.4	223.1	8.9
33.8	313.4	14.7		52.9	233.2	8.8
34.1	308.7	14.5		53.5	236.1	8.6
34.4	296.6	14.4		54.0	262.9	8.1
34.7	279.1	13.8		54.5	254.1	7.9
34.9	286.6	13.8		55.1	245.0	7.6
35.2	254.3	13.1		55.6	217.8	7.1
35.5	238.8	12.1		56.2	193.5	6.9
35.8	232.6	11.7		56.7	189.0	7.0
36.1	234.7	11.6		57.3	188.8	7.2
36.4	225.8	11.3		57.9	195.2	7.4
36.7	234.2	11.3		58.5	185.0	7.2
37.0	232.6	11.4		59.1	202.7	7.3

E(keV)	σ(mb)	Δσ(mb)	E(keV)	σ(mb)	Δσ(mb)
59.7	196.5	7.1	108.3	146.2	4.2
60.3	191.1	7.0	109.9	139.2	4.0
61.0	189.1	6.9	111.4	136.1	3.8
61.6	179.6	6.6	113.0	139.6	3.8
62.3	194.4	6.5	114.6	145.8	3.8
62.9	202.8	6.4	116.3	139.5	3.7
63.6	177.7	6.2	118.0	146.2	3.7
64.3	169.2	6.1	119.7	132.8	3.8
65.0	154.7	6.0	121.4	140.8	3.9
65.7	152.2	5.7	123.2	149.5	4.0
66.4	160.7	5.6	125.1	140.9	4.0
67.1	166.4	5.6	127.0	139.4	4.0
67.9	171.2	5.5	128.9	140.7	3.9
68.6	172.9	5.5	130.9	137.4	3.8
69.4	177.6	5.4	132.9	137.7	3.9
70.2	175.1	5.4	135.0	143.2	4.0
70.9	169.0	5.7	137.1	151.2	4.4
71.8	168.3	5.8	139.2	152.9	4.7
72.6	172.7	5.8	141.5	146.2	4.9
73.4	183.2	5.7	143.7	130.0	5.3
74.2	161.0	5.6	146.0	111.6	5.5
75.1	161.6	5.4	148.4	95.7	5.9
76.0	171.1	5.3	150.9	88.9	7.3
76.9	158.5	5.1	153.4	86.3	8.7
77.8	153.1	5.0	155.9	111.7	10.9
78.7	148.5	5.2	158.6	107.1	11.7
79.6	142.0	5.2	161.3	107.2	11.5
80.6	145.3	5.2	164.0	86.1	11.7
81.6	144.9	5.3	166.9	113.9	12.0
82.6	151.8	5.2	169.8	115.7	11.4
83.6	159.9	5.0	172.8	119.4	11.3
84.6	155.7	4.7	175.8	119.8	11.2
85.6	166.4	4.7	179.0	102.2	11.2
86.7	164.5	4.5	182.2	113.0	11.8
87.8	153.1	4.5	185.5	116.9	12.0
88.9	146.9	4.5	188.9	106.8	11.9
90.0	150.1	4.8	192.5	120.2	12.0
91.2	159.0	4.9	196.1	117.6	11.6
92.3	152.4	5.0	199.8	115.4	11.0
93.5	158.2	5.2	203.6	119.2	10.8
94.7	136.1	5.1	207.5	104.2	10.9
96.0	131.0	4.9	211.6	89.0	10.9
97.3	143.2	4.7	215.7	92.0	10.6
98.5	140.5	4.5	220.0	104.1	10.9
99.9	148.4	4.2	224.4	99.5	10.7
101.2	157.0	4.3	229.0	105.5	11.0
102.6	151.2	4.4	233.7	97.9	11.3
104.0	151.6	4.5	238.5	95.7	11.5
105.4	151.4	4.5	243.5	96.2	11.8
106.9	148.9	4.3			

Appendix IV : Capture cross section of Kr-82 as a function
of neutron energy

E(keV)	σ(mb)	Δσ(mb)	E(keV)	σ(mb)	Δσ(mb)
2.5	-608.7	743.7	7.2	259.4	144.8
2.6	-595.5	641.0	7.3	-132.3	142.6
2.7	311.9	583.7	7.4	159.8	140.5
2.8	-150.0	539.0	7.5	126.3	138.2
2.9	-941.9	502.2	7.6	10.1	136.2
3.0	-139.4	472.3	7.7	83.1	134.2
3.1	-51.4	447.6	7.8	168.6	132.3
3.2	592.8	426.0	7.9	265.2	130.4
3.3	-63.6	406.9	8.0	249.3	128.6
3.4	127.9	389.8	8.1	109.1	127.1
3.5	456.7	374.4	8.2	103.6	125.6
3.6	200.2	360.3	8.3	287.1	124.1
3.7	233.4	347.4	8.4	325.2	122.6
3.8	185.5	335.5	8.5	169.4	121.2
3.9	288.3	323.9	8.6	164.2	119.8
4.0	328.7	313.3	8.7	186.1	118.4
4.1	-190.1	303.4	8.8	120.5	117.0
4.2	-382.4	294.2	8.9	145.0	115.6
4.3	-483.5	285.2	9.0	-22.1	114.3
4.4	125.8	276.3	9.1	15.5	113.2
4.5	-105.6	268.1	9.2	41.9	112.1
4.6	740.8	260.5	9.3	28.4	110.9
4.7	-130.7	253.5	9.4	-44.6	109.8
4.8	-183.9	246.5	9.5	57.4	108.8
4.9	-77.6	239.7	9.6	68.6	107.8
5.0	179.0	232.9	9.7	100.0	106.8
5.1	-238.9	226.7	9.8	198.0	105.8
5.2	195.6	221.1	9.9	295.0	105.0
5.3	-350.2	215.5	10.0	511.4	104.0
5.4	-824.6	210.1	10.1	374.2	103.0
5.5	-81.3	204.8	10.2	354.6	102.3
5.6	-145.8	200.0	10.3	194.0	101.5
5.7	-252.0	195.4	10.4	-89.1	100.6
5.8	-374.0	190.8	10.5	-102.2	99.6
5.9	-259.6	186.3	10.6	-28.3	98.9
6.0	39.5	182.0	10.7	-35.8	98.2
6.1	-216.1	178.1	10.8	84.8	97.4
6.2	67.3	174.6	10.9	183.7	96.7
6.3	729.8	171.3	11.0	176.1	96.0
6.4	426.7	167.6	11.1	65.9	95.3
6.5	162.5	164.3	11.2	-81.2	94.6
6.6	6.2	161.1	11.3	154.2	93.9
6.7	285.8	157.9	11.4	375.1	93.1
6.8	235.2	155.2	11.5	243.4	92.4
6.9	83.1	152.5	11.6	370.4	91.7
7.0	426.4	149.9	11.7	112.6	91.0
7.1	265.6	147.3	11.8	266.4	90.3

E(keV)	σ(mb)	Δσ(mb)	E(keV)	σ(mb)	Δσ(mb)
11.9	100.2	89.6	17.0	248.6	60.5
12.0	91.8	89.1	17.1	234.1	59.9
12.1	183.6	88.5	17.2	191.6	59.4
12.2	146.9	87.8	17.3	97.1	58.7
12.3	166.7	87.1	17.4	53.8	57.9
12.4	216.3	86.6	17.5	97.8	57.4
12.5	96.7	86.0	17.6	160.4	56.8
12.6	57.5	85.3	17.7	182.2	56.3
12.7	-74.8	84.7	17.8	187.2	55.8
12.8	-49.4	84.2	17.9	207.2	55.2
12.9	86.1	83.4	18.0	244.1	54.7
13.0	141.8	82.9	18.1	225.0	54.2
13.1	204.6	82.3	18.3	223.8	53.6
13.2	132.0	81.7	18.4	213.8	53.1
13.3	295.0	81.1	18.5	186.1	52.5
13.4	263.5	80.6	18.6	169.9	52.0
13.5	174.6	80.0	18.7	129.5	51.4
13.6	325.2	79.4	18.8	170.3	50.9
13.7	298.5	78.8	18.9	198.7	50.3
13.8	197.8	78.2	19.0	155.2	49.8
13.9	131.5	77.6	19.1	144.4	49.2
14.0	165.4	77.0	19.2	156.8	48.7
14.1	161.2	76.6	19.3	188.1	48.1
14.2	152.8	75.9	19.5	180.0	47.6
14.3	136.3	75.3	19.6	139.2	47.0
14.4	141.2	74.9	19.7	185.7	46.5
14.5	119.2	74.3	19.8	213.4	45.9
14.6	78.9	73.6	19.9	159.2	45.4
14.7	-4.4	73.2	20.0	143.7	44.8
14.8	97.9	72.5	20.2	137.4	44.2
14.9	173.3	71.9	20.3	96.7	43.7
15.0	182.5	71.4	20.4	105.9	43.1
15.1	149.3	70.8	20.5	146.4	42.6
15.2	181.0	70.1	20.7	119.2	42.0
15.3	233.0	69.6	20.8	79.3	41.5
15.4	219.9	69.2	20.9	106.1	40.9
15.5	217.7	68.7	21.0	119.8	40.3
15.6	223.2	68.0	21.2	84.3	39.8
15.7	172.8	67.3	21.3	103.6	39.2
15.8	183.6	66.8	21.4	165.5	38.7
15.9	115.1	66.4	21.6	146.6	38.1
16.0	70.6	65.9	21.7	41.6	37.6
16.1	78.0	65.2	21.8	35.6	37.0
16.2	74.5	64.4	22.0	68.2	36.5
16.3	174.4	64.0	22.1	77.8	36.0
16.4	215.7	63.5	22.2	85.3	35.4
16.5	245.4	63.0	22.4	88.2	34.9
16.6	198.1	62.5	22.5	124.7	34.3
16.7	158.7	62.0	22.7	128.3	33.8
16.8	203.6	61.5	22.8	102.2	33.3
16.9	209.9	61.0	23.0	111.2	32.7

E(keV)	σ(mb)	Δσ(mb)	E(keV)	σ(mb)	Δσ(mb)
23.1	117.4	32.2	33.1	74.2	12.8
23.3	86.5	31.7	33.3	97.5	12.6
23.4	44.7	31.2	33.6	100.5	12.4
23.6	74.3	30.7	33.8	104.9	12.2
23.7	97.9	30.2	34.1	97.2	12.1
23.9	97.3	29.7	34.4	102.3	11.9
24.0	130.6	29.1	34.7	87.2	11.8
24.2	147.6	28.7	34.9	83.7	11.6
24.3	158.5	28.2	35.2	91.8	11.5
24.5	96.0	27.7	35.5	74.2	11.4
24.7	87.2	27.2	35.8	67.2	11.3
24.8	119.2	26.7	36.1	77.1	11.2
25.0	125.8	26.2	36.4	82.7	11.1
25.2	89.9	25.8	36.7	86.6	11.0
25.3	118.1	25.3	37.0	96.0	11.0
25.5	118.1	24.8	37.3	80.5	10.9
25.7	114.8	24.4	37.6	83.4	10.9
25.8	128.2	23.9	37.9	67.5	10.8
26.0	152.3	23.5	38.2	55.8	10.8
26.2	166.0	23.1	38.5	56.8	10.8
26.4	132.2	22.6	38.9	57.4	10.8
26.6	147.6	22.2	39.2	71.4	10.9
26.7	145.7	21.8	39.5	63.5	10.9
26.9	125.0	21.4	39.9	52.9	11.0
27.1	98.9	21.0	40.2	56.9	10.7
27.3	73.7	20.6	40.6	60.8	10.3
27.5	39.3	20.2	40.9	74.7	9.9
27.7	47.6	19.8	41.3	77.8	9.6
27.9	57.5	19.4	41.6	75.2	9.3
28.1	66.2	19.0	42.0	72.3	9.1
28.3	75.5	18.7	42.4	61.1	8.9
28.5	83.7	18.3	42.7	69.6	8.7
28.7	66.0	18.0	43.1	80.5	8.5
28.9	55.3	17.6	43.5	95.4	8.4
29.1	48.1	17.3	43.9	97.7	8.3
29.3	42.9	17.0	44.3	102.0	8.2
29.5	48.2	16.6	44.7	98.0	8.2
29.8	57.0	16.3	45.1	104.0	8.1
30.0	96.3	16.0	45.5	96.5	8.1
30.2	112.1	15.7	45.9	90.2	8.0
30.4	122.7	15.4	46.4	105.6	8.0
30.6	87.4	15.2	46.8	87.2	8.0
30.9	92.4	14.9	47.2	89.9	8.0
31.1	108.5	14.6	47.7	63.5	8.0
31.3	104.5	14.4	48.1	69.3	8.0
31.6	95.9	14.1	48.6	86.2	8.0
31.8	71.4	13.9	49.0	69.4	8.0
32.1	81.0	13.6	49.5	69.5	8.0
32.3	96.1	13.4	50.0	68.1	8.0
32.6	90.6	13.2	50.4	67.9	8.0
32.8	83.6	13.0	50.9	53.2	8.0

E(keV)	σ(mb)	Δσ(mb)	E(keV)	σ(mb)	Δσ(mb)
51.4	64.3	8.0	90.0	48.3	4.4
51.9	63.0	8.0	91.2	48.2	4.4
52.4	63.9	8.0	92.3	47.4	4.3
52.9	60.3	8.0	93.5	47.2	4.3
53.5	54.4	8.0	94.7	61.8	4.3
54.0	48.9	8.0	96.0	62.9	4.3
54.5	44.1	8.0	97.3	53.9	4.3
55.1	60.4	7.9	98.5	54.0	4.3
55.6	66.1	7.9	99.9	51.8	4.3
56.2	67.8	7.9	101.2	40.9	4.3
56.7	63.2	7.8	102.6	43.2	4.3
57.3	47.4	7.8	104.0	48.4	4.3
57.9	53.1	7.7	105.4	46.4	4.4
58.5	57.9	7.7	106.9	46.9	4.4
59.1	55.2	7.6	108.3	46.3	4.4
59.7	57.8	7.5	109.9	45.1	4.4
60.3	61.2	7.5	111.4	45.3	4.5
61.0	65.9	7.4	113.0	44.8	4.5
61.6	62.6	7.3	114.6	52.1	4.5
62.3	46.2	7.2	116.3	55.2	4.6
62.9	47.0	7.1	118.0	50.5	4.6
63.6	51.8	7.0	119.7	46.8	4.6
64.3	62.1	6.9	121.4	46.9	4.6
65.0	65.9	6.8	123.2	38.3	4.6
65.7	63.8	6.7	125.1	42.4	4.6
66.4	53.5	6.6	127.0	43.7	4.6
67.1	57.4	6.5	128.9	44.9	4.6
67.9	58.4	6.3	130.9	45.7	4.6
68.6	61.6	6.2	132.9	37.5	4.6
69.4	54.3	6.1	135.0	33.7	4.5
70.2	51.8	6.0	137.1	39.4	4.5
70.9	48.6	5.9	139.2	45.4	4.4
71.8	53.3	5.8	141.5	41.4	4.3
72.6	66.1	5.7	143.7	45.9	4.2
73.4	62.0	5.6	146.0	48.7	4.1
74.2	55.4	5.5	148.4	58.7	4.0
75.1	56.8	5.4	150.9	58.7	3.8
76.0	63.5	5.3	153.4	58.6	3.7
76.9	61.8	5.2	155.9	53.5	3.5
77.8	53.1	5.1	158.6	49.4	3.4
78.7	50.1	5.0	161.3	48.2	3.2
79.6	58.4	4.9	164.0	56.5	3.0
80.6	48.6	4.9	166.9	47.9	2.8
81.6	49.6	4.8	169.8	42.4	2.6
82.6	59.6	4.7	172.8	40.8	2.5
83.6	48.3	4.7	175.8	40.2	2.3
84.6	44.3	4.6	179.0	43.4	2.1
85.6	46.3	4.5	182.2	44.3	1.9
86.7	56.5	4.5	185.5	40.2	1.8
87.8	53.3	4.5	188.9	42.4	1.7
88.9	49.8	4.4	192.5	41.6	1.5

E(keV)	σ(mb)	Δσ(mb)	E(keV)	σ(mb)	Δσ(mb)
196.1	42.4	1.4	220.0	45.7	1.2
199.8	46.4	1.3	224.4	39.5	1.2
203.6	43.9	1.3	229.0	38.7	1.3
207.5	44.1	1.2	233.7	43.5	1.5
211.6	50.7	1.2	238.5	42.1	1.7
215.7	50.5	1.2	243.5	47.8	2.1

Appendix V : Capture cross section of Kr-83 as a function
            of neutron energy

E(keV)	σ(mb)	Δσ(mb)	E(keV)	σ(mb)	Δσ(mb)
2.5	961.2	1123.2	7.2	327.5	220.7
2.6	927.9	1017.0	7.3	396.7	217.8
2.7	1976.0	890.6	7.4	498.1	214.8
2.8	2355.1	796.0	7.5	756.9	211.5
2.9	3901.3	721.5	7.6	494.7	208.7
3.0	839.3	663.7	7.7	871.6	205.8
3.1	-576.3	618.0	7.8	788.1	203.0
3.2	1552.2	579.9	7.9	615.3	200.3
3.3	1994.5	547.9	8.0	818.1	197.5
3.4	1850.1	520.5	8.1	538.2	195.2
3.5	2718.3	497.0	8.2	364.2	192.8
3.6	666.4	476.4	8.3	925.7	190.5
3.7	1680.2	458.5	8.4	1023.6	188.2
3.8	36.5	442.6	8.5	1017.2	185.9
3.9	1445.8	427.8	8.6	1076.4	183.6
4.0	1595.3	414.5	8.7	1165.5	181.3
4.1	1591.8	402.6	8.8	773.2	179.0
4.2	462.6	391.8	8.9	778.8	176.8
4.3	1325.1	381.4	9.0	970.2	174.5
4.4	786.7	371.4	9.1	963.0	172.6
4.5	1000.6	362.3	9.2	590.5	170.8
4.6	1498.1	353.9	9.3	531.1	168.5
4.7	1202.7	346.2	9.4	701.1	166.7
4.8	395.7	338.7	9.5	686.3	164.8
4.9	628.0	331.2	9.6	818.5	163.0
5.0	476.9	323.9	9.7	650.1	161.1
5.1	920.3	317.2	9.8	632.6	159.3
5.2	859.6	311.1	9.9	549.6	157.8
5.3	617.3	305.0	10.0	560.7	156.0
5.4	157.2	299.1	10.1	409.9	154.2
5.5	1603.3	293.2	10.2	417.7	152.7
5.6	1000.3	287.9	10.3	388.1	151.3
5.7	336.3	282.6	10.4	344.3	149.5
5.8	712.9	277.4	10.5	583.2	147.7
5.9	711.1	272.3	10.6	523.0	146.2
6.0	408.3	267.2	10.7	176.5	144.8
6.1	912.7	262.7	10.8	729.3	143.4
6.2	1017.7	258.6	10.9	643.5	142.0
6.3	465.0	254.5	11.0	587.4	140.6
6.4	1079.8	250.0	11.1	548.3	139.1
6.5	1030.4	246.0	11.2	407.4	137.7
6.6	1051.7	242.0	11.3	474.4	136.3
6.7	970.8	238.0	11.4	782.8	134.9
6.8	820.6	234.5	11.5	702.4	133.5
6.9	695.3	231.0	11.6	550.3	132.1
7.0	429.2	227.6	11.7	623.2	130.7
7.1	411.6	224.1	11.8	781.1	129.3

E(keV)	σ(mb)	Δσ(mb)	E(keV)	σ(mb)	Δσ(mb)
11.9	767.5	127.9	17.0	370.9	76.4
12.0	730.9	126.8	17.1	400.7	75.6
12.1	679.0	125.7	17.2	334.6	74.9
12.2	618.7	124.3	17.3	363.1	73.7
12.3	671.1	122.9	17.4	308.2	72.6
12.4	701.5	121.8	17.5	422.2	71.8
12.5	496.8	120.7	17.6	425.0	71.1
12.6	591.3	119.3	17.7	499.2	70.3
12.7	679.2	118.2	17.8	524.9	69.6
12.8	552.4	117.2	17.9	487.9	68.8
12.9	617.1	115.7	18.0	405.9	68.1
13.0	700.0	114.6	18.1	364.0	67.3
13.1	799.2	113.5	18.3	309.6	66.6
13.2	598.7	112.5	18.4	259.8	65.8
13.3	395.0	111.4	18.5	174.5	65.1
13.4	515.2	110.3	18.6	242.3	64.3
13.5	398.2	109.2	18.7	335.6	63.6
13.6	189.6	108.1	18.8	206.2	62.8
13.7	361.0	107.0	18.9	232.3	62.1
13.8	333.3	105.9	19.0	300.5	61.3
13.9	430.2	104.7	19.1	413.0	60.6
14.0	394.3	103.6	19.2	383.5	59.8
14.1	431.2	102.9	19.3	346.7	59.1
14.2	414.2	101.8	19.5	409.4	58.4
14.3	559.4	100.6	19.6	353.5	57.6
14.4	439.7	99.9	19.7	359.0	56.9
14.5	382.6	98.8	19.8	412.9	56.2
14.6	410.0	97.7	19.9	383.0	55.5
14.7	316.5	96.9	20.0	347.8	54.7
14.8	387.0	95.8	20.2	386.9	54.0
14.9	529.3	94.6	20.3	354.5	53.3
15.0	398.0	93.9	20.4	367.5	52.6
15.1	280.6	92.8	20.5	322.7	51.9
15.2	397.8	91.6	20.7	371.8	51.2
15.3	361.3	90.9	20.8	341.3	50.5
15.4	422.0	90.1	20.9	330.1	49.8
15.5	179.8	89.3	21.0	339.6	49.1
15.6	390.6	88.2	21.2	355.0	48.4
15.7	271.7	87.1	21.3	348.4	47.7
15.8	196.6	86.3	21.4	368.5	47.0
15.9	474.2	85.5	21.6	363.8	46.3
16.0	311.4	84.8	21.7	236.9	45.7
16.1	424.3	83.6	21.8	251.1	45.0
16.2	392.5	82.5	22.0	281.4	44.3
16.3	373.6	81.7	22.1	284.7	43.6
16.4	445.7	81.0	22.2	241.3	43.0
16.5	516.3	80.2	22.4	242.5	42.3
16.6	419.6	79.4	22.5	322.3	41.7
16.7	333.5	78.7	22.7	354.4	41.0
16.8	359.2	77.9	22.8	321.4	40.4
16.9	406.4	77.2	23.0	402.5	39.8

E(keV)	σ(mb)	Δσ(mb)	E(keV)	σ(mb)	Δσ(mb)
23.1	449.2	39.1	33.1	230.2	16.1
23.3	389.9	38.5	33.3	279.3	15.8
23.4	329.5	37.9	33.6	246.2	15.6
23.6	378.6	37.3	33.8	262.4	15.4
23.7	313.7	36.7	34.1	217.3	15.2
23.9	320.9	36.1	34.4	258.7	15.0
24.0	342.7	35.5	34.7	228.4	14.8
24.2	284.7	34.9	34.9	248.0	14.6
24.3	378.1	34.3	35.2	256.8	14.4
24.5	344.3	33.7	35.5	207.7	14.2
24.7	355.0	33.1	35.8	223.0	14.1
24.8	331.8	32.6	36.1	239.9	13.9
25.0	361.9	32.0	36.4	222.7	13.8
25.2	321.6	31.5	36.7	203.2	13.6
25.3	350.5	30.9	37.0	224.6	13.5
25.5	347.6	30.4	37.3	235.3	13.4
25.7	352.3	29.9	37.6	213.3	13.3
25.8	305.3	29.3	37.9	207.7	13.2
26.0	267.8	28.8	38.2	211.7	13.2
26.2	308.2	28.3	38.5	191.8	13.1
26.4	324.6	27.8	38.9	208.5	13.1
26.6	322.9	27.3	39.2	212.3	13.0
26.7	303.6	26.8	39.5	225.8	13.0
26.9	282.0	26.3	39.9	184.8	13.0
27.1	273.7	25.9	40.2	171.1	13.0
27.3	252.6	25.4	40.6	179.7	12.9
27.5	251.3	24.9	40.9	189.2	12.9
27.7	201.1	24.5	41.3	202.8	12.8
27.9	223.4	24.0	41.6	194.5	12.7
28.1	273.8	23.6	42.0	194.1	12.7
28.3	263.1	23.2	42.4	199.5	12.6
28.5	245.0	22.8	42.7	187.4	12.5
28.7	251.2	22.3	43.1	184.0	12.4
28.9	287.9	21.9	43.5	188.1	12.3
29.1	264.6	21.5	43.9	179.2	12.3
29.3	286.8	21.2	44.3	155.1	12.2
29.5	277.7	20.8	44.7	179.2	12.1
29.8	245.8	20.4	45.1	173.0	12.0
30.0	244.1	20.0	45.5	174.6	11.9
30.2	237.0	19.7	45.9	178.1	11.8
30.4	277.8	19.3	46.4	195.0	11.7
30.6	269.4	19.0	46.8	189.2	11.6
30.9	238.3	18.7	47.2	201.2	11.6
31.1	276.7	18.3	47.7	205.9	11.5
31.3	231.5	18.0	48.1	173.2	11.4
31.6	250.8	17.7	48.6	166.2	11.3
31.8	277.9	17.4	49.0	175.0	11.2
32.1	256.0	17.1	49.5	194.3	11.1
32.3	265.9	16.9	50.0	191.5	11.0
32.6	263.6	16.6	50.4	163.0	10.9
32.8	234.5	16.3	50.9	188.7	10.8

E(keV)	σ(mb)	Δσ(mb)	E(keV)	σ(mb)	Δσ(mb)
51.4	177.3	10.7	90.0	114.3	5.9
51.9	152.8	10.7	91.2	120.2	5.8
52.4	167.5	10.6	92.3	113.9	5.7
52.9	147.8	10.5	93.5	105.7	5.6
53.5	163.8	10.4	94.7	101.3	5.5
54.0	183.4	10.3	96.0	110.8	5.4
54.5	184.3	10.2	97.3	117.3	5.3
55.1	178.1	10.1	98.5	107.9	5.2
55.6	170.5	10.0	99.9	117.2	5.1
56.2	170.9	10.0	101.2	97.9	5.0
56.7	183.2	9.9	102.6	93.9	4.9
57.3	184.7	9.8	104.0	103.6	4.9
57.9	179.6	9.7	105.4	96.8	4.8
58.5	187.6	9.6	106.9	91.1	4.7
59.1	176.7	9.5	108.3	90.5	4.6
59.7	150.9	9.4	109.9	82.3	4.6
60.3	144.8	9.4	111.4	96.9	4.5
61.0	160.0	9.3	113.0	98.8	4.5
61.6	136.1	9.2	114.6	108.4	4.4
62.3	156.8	9.1	116.3	103.0	4.4
62.9	145.5	9.0	118.0	98.0	4.3
63.6	144.5	8.9	119.7	101.1	4.3
64.3	137.7	8.8	121.4	90.4	4.2
65.0	147.8	8.7	123.2	90.3	4.2
65.7	145.4	8.6	125.1	91.0	4.2
66.4	127.7	8.5	127.0	92.3	4.2
67.1	140.8	8.5	128.9	93.1	4.2
67.9	130.2	8.4	130.9	86.7	4.2
68.6	135.0	8.3	132.9	83.5	4.2
69.4	133.7	8.2	135.0	85.3	4.2
70.2	121.6	8.1	137.1	84.7	4.2
70.9	116.3	8.0	139.2	89.6	4.2
71.8	121.2	7.9	141.5	89.6	4.3
72.6	132.7	7.8	143.7	83.0	4.3
73.4	141.8	7.7	146.0	86.4	4.4
74.2	134.5	7.6	148.4	80.6	4.5
75.1	123.5	7.5	150.9	88.4	4.5
76.0	132.8	7.4	153.4	80.5	4.6
76.9	128.1	7.3	155.9	78.0	4.7
77.8	120.9	7.2	158.6	77.8	4.8
78.7	118.5	7.0	161.3	79.1	4.9
79.6	124.8	6.9	164.0	74.4	5.1
80.6	108.8	6.8	166.9	78.6	5.2
81.6	115.8	6.7	169.8	68.3	5.4
82.6	129.6	6.6	172.8	77.3	5.5
83.6	130.1	6.5	175.8	71.7	5.7
84.6	117.8	6.4	179.0	67.3	5.9
85.6	111.5	6.3	182.2	67.1	6.1
86.7	112.7	6.2	185.5	63.9	6.3
87.8	109.0	6.1	188.9	68.7	6.4
88.9	113.4	6.0	192.5	68.7	6.6

E(keV)	σ(mb)	Δσ(mb)	E(keV)	σ(mb)	Δσ(mb)
196.1	68.0	6.8	220.0	57.9	6.8
199.8	70.6	6.9	224.4	55.3	6.6
203.6	63.9	7.0	229.0	59.0	6.3
207.5	64.8	7.0	233.7	56.4	5.9
211.6	63.2	7.0	238.5	61.4	5.4
215.7	68.1	7.0	243.5	59.5	4.8

Appendix VI : Capture cross section of Kr-84 as a function
of neutron energy

E(keV)	σ(mb)	Δσ(mb)	E(keV)	σ(mb)	Δσ(mb)
2.5	324.8	1275.0	7.2	-135.2	219.2
2.6	871.2	1115.5	7.3	66.9	216.2
2.7	229.8	949.7	7.4	-30.4	213.2
2.8	2330.1	825.7	7.5	-78.0	209.7
2.9	583.2	728.7	7.6	245.5	206.6
3.0	-461.1	654.3	7.7	74.7	203.5
3.1	616.9	596.5	7.8	167.2	200.4
3.2	-412.8	549.3	7.9	213.6	197.2
3.3	388.7	510.6	8.0	51.8	194.0
3.4	-438.0	478.5	8.1	340.8	191.2
3.5	1261.2	451.7	8.2	266.5	188.5
3.6	804.6	429.2	8.3	412.3	185.7
3.7	326.3	410.3	8.4	482.8	182.8
3.8	602.7	394.3	8.5	378.7	180.0
3.9	129.4	379.9	8.6	96.7	177.1
4.0	194.7	367.6	8.7	60.5	174.2
4.1	227.3	357.1	8.8	5.0	171.3
4.2	153.8	347.9	8.9	2.3	168.4
4.3	240.3	339.5	9.0	140.5	165.5
4.4	245.3	331.6	9.1	-17.2	163.1
4.5	546.1	324.7	9.2	-104.0	160.6
4.6	117.3	318.6	9.3	51.2	157.6
4.7	-351.8	313.2	9.4	-197.5	155.2
4.8	162.4	307.9	9.5	140.6	152.7
4.9	145.3	302.9	9.6	50.9	150.3
5.0	453.4	297.9	9.7	182.4	147.8
5.1	2.5	293.5	9.8	169.6	145.4
5.2	215.0	289.4	9.9	74.8	143.4
5.3	401.6	285.4	10.0	15.3	141.0
5.4	280.2	281.4	10.1	45.0	138.6
5.5	437.8	277.5	10.2	159.2	136.6
5.6	32.5	273.9	10.3	17.1	134.7
5.7	-13.6	270.2	10.4	186.8	132.3
5.8	377.7	266.6	10.5	-70.6	.130.0
5.9	240.6	262.9	10.6	38.2	128.1
6.0	111.8	259.2	10.7	104.1	126.2
6.1	6.1	255.8	10.8	261.9	124.4
6.2	73.3	252.6	10.9	187.5	122.6
6.3	73.6	249.4	11.0	94.9	120.7
6.4	-7.0	245.8	11.1	264.6	118.9
6.5	-270.3	242.4	11.2	378.5	117.1
6.6	199.9	239.0	11.3	313.4	115.4
6.7	104.9	235.5	11.4	278.3	113.6
6.8	375.2	232.4	11.5	368.4	111.9
6.9	286.9	229.2	11.6	117.6	110.1
7.0	229.8	225.9	11.7	77.7	108.4
7.1	86.0	222.6	11.8	-11.3	106.7

E(keV)	σ(mb)	Δσ(mb)	E(keV)	σ(mb)	Δσ(mb)
11.9	-3.9	105.0	17.0	4.0	59.5
12.0	6.5	103.8	17.1	-0.3	59.0
12.1	-58.2	102.6	17.2	76.9	58.6
12.2	167.2	100.9	17.3	87.3	57.9
12.3	-73.0	99.3	17.4	68.8	57.3
12.4	14.6	98.1	17.5	31.8	56.9
12.5	-39.9	96.9	17.6	72.4	56.5
12.6	-87.1	95.3	17.7	27.0	56.1
12.7	-6.1	94.2	17.8	20.8	55.7
12.8	35.5	93.0	17.9	13.5	55.3
12.9	-49.2	91.5	18.0	29.8	54.9
13.0	-100.0	90.3	18.1	31.9	54.5
13.1	3.5	89.2	18.3	26.1	54.1
13.2	-19.6	88.1	18.4	61.1	53.8
13.3	-41.0	87.0	18.5	21.9	53.4
13.4	132.0	85.9	18.6	9.8	53.0
13.5	-37.7	84.9	18.7	7.5	52.7
13.6	113.4	83.8	18.8	32.7	52.3
13.7	206.5	82.7	18.9	51.4	52.0
13.8	101.8	81.7	19.0	75.7	51.7
13.9	22.5	80.7	19.1	47.7	51.3
14.0	74.2	79.7	19.2	33.5	51.0
14.1	41.3	79.0	19.3	-25.4	50.7
14.2	26.1	78.0	19.5	-40.4	50.4
14.3	22.2	77.0	19.6	-1.3	50.1
14.4	137.4	76.4	19.7	65.4	49.8
14.5	81.2	75.4	19.8	53.7	49.5
14.6	96.8	74.5	19.9	51.0	49.2
14.7	137.5	73.9	20.0	68.5	48.9
14.8	111.6	72.9	20.2	52.6	48.6
14.9	119.9	72.0	20.3	50.8	48.3
15.0	91.3	71.4	20.4	61.1	48.1
15.1	51.2	70.6	20.5	86.5	47.8
15.2	-50.6	69.7	20.7	73.0	47.5
15.3	85.1	69.1	20.8	44.9	47.3
15.4	35.7	68.5	20.9	-5.9	47.0
15.5	-41.9	68.0	21.0	-30.4	46.8
15.6	25.2	67.2	21.2	-16.3	46.5
15.7	134.2	66.4	21.3	6.0	46.3
15.8	-12.3	65.8	21.4	-0.4	46.1
15.9	-117.4	65.3	21.6	20.1	45.8
16.0	16.8	64.8	21.7	55.4	45.6
16.1	95.2	64.0	21.8	34.6	45.4
16.2	138.5	63.3	22.0	26.5	45.2
16.3	101.6	62.8	22.1	58.5	45.0
16.4	68.6	62.3	22.2	60.6	44.8
16.5	91.6	61.8	22.4	16.5	44.5
16.6	72.7	61.3	22.5	13.5	44.3
16.7	135.1	60.8	22.7	-11.5	44.2
16.8	212.2	60.4	22.8	-10.0	44.0
16.9	115.2	59.9	23.0	32.8	43.8

E(keV)	σ(mb)	Δσ(mb)	E(keV)	σ(mb)	Δσ(mb)
23.1	44.3	43.6	33.1	12.6	35.4
23.3	28.7	43.4	33.3	17.7	35.2
23.4	17.1	43.2	33.6	27.5	34.9
23.6	35.2	43.1	33.8	45.7	34.6
23.7	24.5	42.9	34.1	90.6	34.4
23.9	9.7	42.7	34.4	100.0	34.1
24.0	28.6	42.6	34.7	73.8	33.7
24.2	42.7	42.4	34.9	48.0	33.4
24.3	61.4	42.2	35.2	33.0	33.1
24.5	80.1	42.1	35.5	17.3	32.7
24.7	83.7	41.9	35.8	19.9	32.4
24.8	81.5	41.8	36.1	2.4	32.0
25.0	45.4	41.6	36.4	11.4	31.6
25.2	12.7	41.5	36.7	1.8	31.2
25.3	19.8	41.3	37.0	14.9	30.8
25.5	36.3	41.2	37.3	-1.9	30.3
25.7	27.9	41.1	37.6	5.4	29.9
25.8	11.5	40.9	37.9	-3.2	29.4
26.0	15.4	40.8	38.2	18.4	28.9
26.2	51.0	40.6	38.5	28.3	28.4
26.4	71.4	40.5	38.9	22.3	27.9
26.6	68.0	40.4	39.2	14.8	27.3
26.7	73.9	40.2	39.5	20.3	26.8
26.9	54.3	40.1	39.9	19.8	26.2
27.1	18.9	40.0	40.2	29.8	25.6
27.3	23.9	39.9	40.6	15.0	25.0
27.5	20.9	39.7	40.9	6.8	24.4
27.7	12.5	39.6	41.3	16.2	23.9
27.9	23.9	39.5	41.6	9.4	23.5
28.1	3.4	39.3	42.0	10.4	23.1
28.3	13.8	39.2	42.4	4.8	22.8
28.5	34.5	39.0	42.7	-1.2	22.5
28.7	51.0	38.9	43.1	11.9	22.2
28.9	37.1	38.8	43.5	34.7	22.0
29.1	28.3	38.6	43.9	57.9	21.7
29.3	33.7	38.5	44.3	67.2	21.5
29.5	21.6	38.3	44.7	57.9	21.4
29.8	24.9	38.2	45.1	36.1	21.2
30.0	15.2	38.0	45.5	32.5	21.1
30.2	-2.9	37.9	45.9	12.0	20.9
30.4	17.4	37.7	46.4	13.1	20.8
30.6	42.7	37.5	46.8	3.7	20.7
30.9	36.3	37.3	47.2	17.5	20.6
31.1	15.4	37.2	47.7	3.9	20.5
31.3	34.3	37.0	48.1	11.1	20.4
31.6	28.4	36.8	48.6	23.7	20.3
31.8	17.8	36.6	49.0	35.1	20.2
32.1	6.2	36.4	49.5	41.3	20.1
32.3	-2.6	36.1	50.0	42.9	20.0
32.6	-0.2	35.9	50.4	45.5	19.9
32.8	11.8	35.7	50.9	42.6	19.8

E(keV)	σ(mb)	Δσ(mb)	E(keV)	σ(mb)	Δσ(mb)
51.4	18.5	19.7	90.0	17.3	9.8
51.9	27.5	19.6	91.2	13.6	9.7
52.4	26.0	19.4	92.3	12.7	9.6
52.9	14.5	19.3	93.5	16.8	9.5
53.5	14.3	19.2	94.7	14.8	9.5
54.0	15.8	19.0	96.0	17.2	9.4
54.5	23.4	18.9	97.3	17.4	9.4
55.1	23.7	18.7	98.5	13.6	9.3
55.6	16.7	18.5	99.9	16.0	9.3
56.2	17.6	18.4	101.2	20.4	9.3
56.7	8.4	18.2	102.6	20.5	9.3
57.3	5.7	18.0	104.0	27.4	9.2
57.9	10.2	17.8	105.4	20.3	9.2
58.5	11.2	17.5	106.9	15.4	9.2
59.1	23.3	17.3	108.3	12.5	9.2
59.7	26.4	17.1	109.9	11.6	9.2
60.3	14.7	16.9	111.4	11.7	9.2
61.0	14.4	16.6	113.0	13.4	9.2
61.6	13.1	16.4	114.6	11.5	9.2
62.3	20.2	16.2	116.3	11.3	9.2
62.9	22.5	15.9	118.0	14.1	9.2
63.6	24.9	15.7	119.7	14.6	9.2
64.3	38.6	15.4	121.4	12.9	9.2
65.0	19.5	15.1	123.2	18.1	9.2
65.7	20.9	14.9	125.1	16.9	9.1
66.4	20.7	14.6	127.0	11.0	9.1
67.1	25.5	14.4	128.9	10.7	9.1
67.9	26.3	14.1	130.9	13.6	9.0
68.6	20.1	13.9	132.9	16.4	8.9
69.4	30.0	13.6	135.0	18.2	8.8
70.2	29.5	13.4	137.1	12.5	8.7
70.9	24.8	13.1	139.2	7.0	8.6
71.8	15.6	12.9	141.5	9.6	8.5
72.6	11.3	12.7	143.7	12.5	8.3
73.4	19.0	12.5	146.0	14.1	8.1
74.2	24.8	12.2	148.4	15.2	7.9
75.1	23.7	12.0	150.9	14.3	7.7
76.0	27.7	11.8	153.4	14.6	7.5
76.9	28.9	11.6	155.9	13.0	7.3
77.8	21.6	11.4	158.6	10.7	7.0
78.7	26.7	11.2	161.3	11.3	6.7
79.6	25.3	11.1	164.0	11.2	6.5
80.6	19.7	10.9	166.9	11.4	6.2
81.6	20.8	10.7	169.8	11.1	5.9
82.6	16.8	10.6	172.8	13.5	5.6
83.6	16.4	10.4	175.8	12.5	5.3
84.6	10.7	10.3	179.0	13.9	5.1
85.6	14.9	10.2	182.2	15.2	4.8
86.7	24.7	10.1	185.5	11.9	4.5
87.8	25.0	10.0	188.9	10.8	4.3
88.9	24.0	9.9	192.5	13.7	4.1

E(keV)	σ(mb)	Δσ(mb)	E(keV)	σ(mb)	Δσ(mb)
196.1	10.9	3.9	220.0	10.9	3.4
199.8	9.4	3.7	224.4	12.7	3.4
203.6	10.8	3.6	229.0	11.8	3.6
207.5	11.4	3.5	233.7	11.8	3.9
211.6	11.2	3.4	238.5	11.3	4.3
215.7	10.9	3.3	243.5	8.7	4.9